Design and Development of Gas Diffusion Layers for Proton Exchange Membrane Fuel Cells at Various Relative Humidity Conditions

by

Grigoria Athanasaki

A Dissertation Presented in Partial Fulfillment
of the Requirements for the Degree
Doctor of Philosophy

Approved April 2021 by the
Graduate Supervisory Committee:

Arunachala Mada Kannan, Chair
Changho Nam
Xihong Peng

ARIZONA STATE UNIVERSITY

May 2021

ABSTRACT

In the present study, primarily, gas diffusion layer samples containing microporous layers (MPLs), are fabricated using carbon paper substrate, PUREBLACK® carbon powder and polyethylene glycol (PEG) as pore forming agent. The GDLs are studied in single cell fuel cell, to evaluate the effect of porosity of the micro-porous layer on the performance at different operating relative humidity conditions and compared with commercial GDLs. Scanning electron microscopy (SEM) and contact angle measurements indicate crack-free surface morphology and hydrophobic characteristics of the PUREBLACK® based GDLs, respectively. By varying the wt. % of PEG, fuel cell performance is evaluated under relative humidity conditions of 60 and 100 % using H_2/O_2 and H_2/Air at 70 ^oC and the durability is also evaluated for the samples without, with 30% PEG and commercial. The fuel cell performance of the GDL with 30 % PEG (with pore volume 1.72 $cc.g^{-1}$) exhibited higher performance (444 and 432 $mW.cm^{-2}$ at 60 and 100 % RH conditions, respectively using H_2 and air) compared to that without pore forming agent (436 and 397 $mW.cm^{-2}$).

Subsequently, the best performing configuration underwent two different *ex-situ* methods of accelerated stress testing (AST), in water and hydrogen peroxide (30%), for 1000 and 24 h, respectively. The samples were evaluated via contact angle, SEM, and fuel cell performance, before and after the ASTs, and compared to similar configuration, using carbon powder VULCAN® (XC-72R), and aged in the exact same conditions. Contact angle and SEM demonstrated greater degradation of VULCAN® carbon, especially in hydrogen peroxide, where carbon corrosion caused surface cracks and change in hydrophobicity. The fuel cell performance and durability, evaluated at 60 and 100% RH at

70 ^{o}C, using O_2 and air as oxidants, confirmed that VULCAN® carbon is more prone to carbon corrosion, with significant performance loss (12-19%) in contrast to PUREBLACK® that demonstrated higher carbon corrosion resistance due to its graphitized surface.

THIS DISSERTATION IS DEDICATED TO MY LOVING PARENTS, ANNA AND MANOLIS, MY SIBLINGS, DESPINA AND IOANNIS, AND MY GRANDMOTHERS, WHOSE UNLIMITED SUPPORT AND ENCOURAGEMENT ALWAYS MOTIVATED ME TO PURSUE MY DREAMS.

ACKNOWLEDGEMENTS

First and foremost, I would like to thank my advisor, Dr. A. M. Kannan for giving me the chance to work with him, as well as his continuous support and guidance. I would, also, like to express my gratitude to Dr. Ladani, head of the Systems Engineering program in 2018. Her encouragement and guidance helped me overcome some personal struggles I was going through at the time. Furthermore, I want to thank my Graduate Advising Committee, Dr. Nam and Dr. Peng, for the dedicated time and helpful advice towards the completion of this degree. Also, a big thanks to the academic advisor, Amy Riggs, for providing necessary information and useful advice and made the completion of this degree an easy task.

Secondly, I would like to thank my coworkers: Dr. Jyoti Prakash for his unlimited advice and guidance in the experimental procedures, Dr. Xuan Shi for patiently training me on the Fuel Cell equipment and methodologies, and Umesh and Pavan for their assistance with experimental processes. Also, I would like to thank Dr. Ahmad Riaz and Anton Paar Laboratories, Florida, for the assistance with Porosity and Pore Size Distribution measurements.

Last but not least, I would like to thank my collaborators, Q. Wang and N. Chauhan, for their significant contribution in data collection and processing, classmates and friends (Roozbeh, Mohammad, Azadeh, Thien, Jason, Kathy and Alwin) and my boyfriend, Tony Batista, for the support and insightful conversations. I wish you all the best!

TABLE OF CONTENTS

Page

CHAPTER Page

LIST OF TABLES

Table Page

LIST OF FIGURES

Figure Page

Figure Page

1. INTRODUCTION

1.1 Energy consumption

Global energy demand has grown over the years and is projected to grow further till year 2050 [1]. Although, there was a record consumption (3.1 EJ) and a rapid growth (12.2%) of renewable energy in the year 2019, the carbon emissions from energy still grew by 0.5% [2]. This is because electricity demand is mainly supplied by fossil fuels all over the world [3]. Oil, coal, and natural gas are the primary sources for energy production globally, for transportation and electricity generation. Although the production of fossil fuels has been a colossal contributor to economic development for many countries around the world, continued usage, with U.S leading in petroleum consumption, has led to a drastic environmental impact. Besides the environmental degradation caused during production processes, fossil fuels are the major source of greenhouse gas emissions responsible for air and water pollution, health risks and global warming, where CO_2 plays the most significant role [4]. Owing to the high economic growth scenario, EIA also predicted a growth in the carbon emissions until the year 2050. The universal dependence on oil for transportation makes the decreased consumption a difficult task. Internal combustion engines burning fossil fuels are the main contributors of global CO_2 emissions (~ 8.5 GT) [1]. This strongly indicates the need to find more clean energy solutions to tackle the climate change especially in the transportation sector.

Renewable energy sources have a potential to overcome these challenges, as they originate from naturally replenishable resources including biomass, sunlight, water, and wind. Although renewable sources are usually accompanied with various limitations (e.g.,

during sunlight, for solar), when combined with energy storage solutions, they can be a reliable energy source year-round. Biomass, hydropower, wind, and solar energy systems are currently being used mainly for electricity and thermal energy generation. Biomass, originating from agriculture and urban sources, is also widely used for transportation fuels, however its production depends on the available sources of each area.

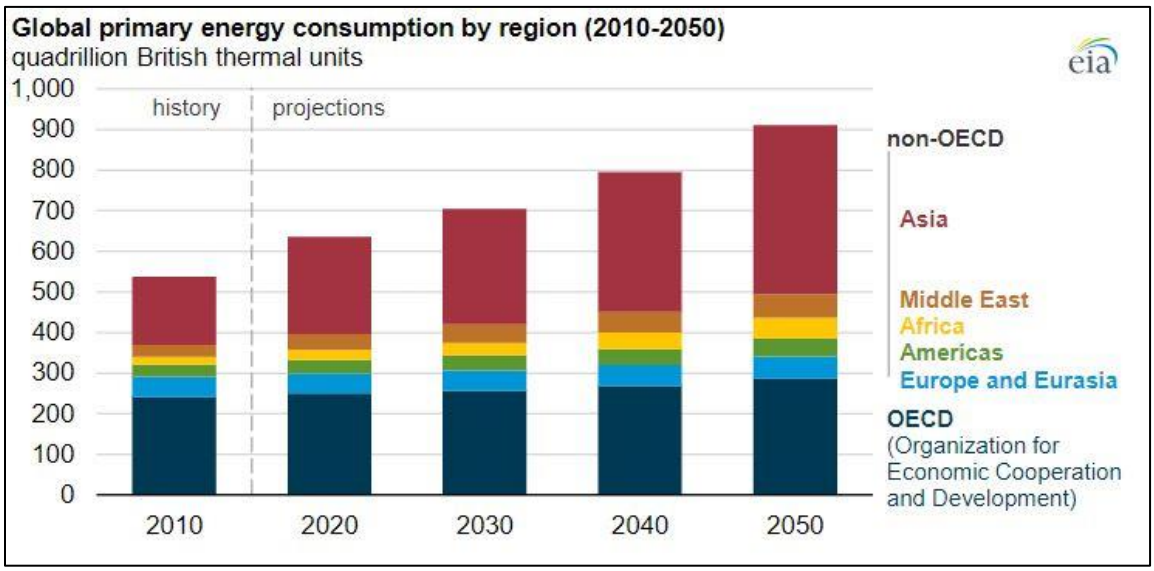

Figure 1. World energy consumption 2010-2050 (IEA) [1].

In this regard, hydrogen energy, which is sustainable and carbon free, is seen as a promising solution [5]. Hydrogen, as an energy carrier, has a potential to eliminate or reduce the environmental pollution, especially the greenhouse gas emissions [6,7]. IRENA predicts that hydrogen will have 6% total final energy consumption by 2050, whereas the hydrogen council suggests that around 18% share can be achieved [8].

1.2 Global initiatives

Recent hydrogen initiatives are forming around the world to promote international collaboration on policies, programs, and projects for quicker commercialized viability of hydrogen and fuel cell technologies in all economic sectors. Several countries are developing hydrogen approaches and goals for hydrogen technologies deployment.

International Partnership for Hydrogen and Fuel Cells in the Economy (IPHE), formed in 2003, is an international governmental partnership, with 21 countries-members and the European Commission. Their goal is to "facilitate and accelerate the transition to clean and efficient energy and mobility systems using hydrogen and fuel cell technologies across applications and sectors". Their priority focuses on accelerating the establishment of hydrogen and FC technologies and infrastructure. The main initiative consists of regulations, codes, standards and safety (RCSS), and education and outreach which cooperates with governments to inform, educate and develop research and development opportunities, to further explore and resolve challenges that accompany the hydrogen technology [9].

In the USA, hydrogen economy initiative H2@Scale is developed by the U.S Department of Energy (DOE). This concept examines the opportunities of large-scale hydrogen production in the US and promotes affordable hydrogen production, transport, storage, and utilization to create funding opportunities in multiple energy sectors. Only in 2020, DOE declared $64 million funding for projects supporting the initiative's vision. Additional, DOE Hydrogen and Fuel Cell Technologies office establishes technical targets

and protocols in an attempt to guide the research and development for hydrogen and FC technologies [10] .

Fuel Cells and Hydrogen Undertaking (FCHJU) is a European organization with a goal to facilitate the market introduction of fuel cell and hydrogen technologies in Europe and comprehend their potential in a carbon-clean energy system. The initiative includes implementation of an optimal research and innovation (R&I) program, by developing a portfolio of clean energy solutions that profit from the properties of hydrogen as an energy carrier and fuel cells as energy converters. Moreover, HyDeal Ambition is comprised by 30 pioneering energy leaders, aiming to deliver 100% green hydrogen across Europe at €1.5/kg before 2030. The production of green hydrogen by electrolysis via solar energy is scheduled to start in 2022 [11,12].

Canada, Japan, the Netherlands, the United States, and the European Commission constitute the Hydrogen Initiative which began at the 10th Clean Energy Ministerial (CEM10) in Canada. This initiative, coordinated by The International Energy Association, targets in promoting international collaboration and establishment of policies, programs and projects that will expedite the hydrogen and fuel cell technology commercialization [13].

The Global Action Agenda, signed by 35 countries, supports principle to guide expanded RD&D on hydrogen, aiming 10 million hydrogen vehicles and 10,000 HRSs in 10 years to promote the use of hydrogen and fuel cells in transportation. Also, in January 2019 Korea announced its Hydrogen Economy Roadmap**,** aiming the production of 6.2 million Fuel Cell Electric Vehicle (FCEV) passenger cars, 40,000 FC buses, 30,000 FC

trucks and 1,200 HRSs by 2040. Additionally, the Strategic Road Map for Hydrogen and Fuel Cells (initially published in 2017) was updated by Japan in 2019, certifying previous targets for transportation, supply, and domestic use of hydrogen.

The Australian government published Australia's National Hydrogen Strategy, which consists of 57 regulatory, infrastructure, transportation, and development actions with a goal of leading the world in hydrogen production and exports [14].

1.3 Hydrogen energy

Hydrogen is a colorless, odorless gas which occurs in opulence in the universe. Nonetheless, on earth it exists in very small amounts in the atmosphere as gas, while it is greatly presented naturally combined with other elements, such as in water. Aside from its abundance, hydrogen offers a plethora of advantages including high energy conversion efficiencies, zero-emissions production from water, ability to be stored in different forms which facilitates long distance transportation, conversion capability to other forms of energy, larger higher and lower heating values (HHV and LHV) than most conventional fossil fuels [15]. Hydrogen has been produced for a variety of applications, but in the last decade, it drew a lot of attention for its energy carrier property, incorporated to stationary and transportation applications, accompanied with the fuel cell technology [16].Since it is not readily available, hydrogen requires additional processes to reach its pure form, Fortunately, a variety of sources, including fossil fuels, nuclear power, biomass, and renewable energy, are applicable for hydrogen production for further applications in fuel and electricity generation [17].

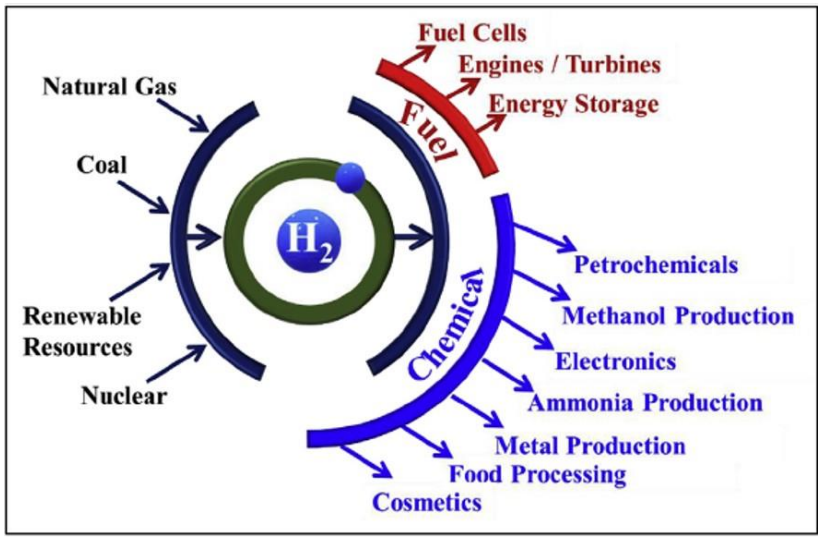

Figure 2. Hydrogen as an energy carrier.

Currently, fossil fuel reformation accounts for about 99% of hydrogen production, through hydrocarbon reforming and pyrolysis techniques. Hydrocarbon reforming incorporates fuel conversion into hydrogen using steam (steam reforming), oxygen (partial oxidation) or a combination of the two (auto-thermal reaction, ATR) [18]. In particular, steam methane reformation (SMR) consists of three major steps: methane (CH_4) contained in natural gas is reacting with high temperature (700 – 1000°C) pressurized steam in an endothermic reaction catalyzed by a nickel-based catalyst, to yield hydrogen, carbon monoxide (CO) and a small amount of carbon dioxide (CO_2), known as syngas. Since this reaction is endothermic, heat is supplied in the reformer by additional methane combustion. Subsequently, the carbon monoxide and steam react in an exothermic reaction, again in the presence of a catalyst, to produce carbon dioxide and hydrogen. Finally, impurities and carbon dioxide are separated from the gas stream, resulting to pure hydrogen as the sole product [19,20]. The chemical reactions of steam methane reformation are represented by

the equations (1) and (2) and as can be seen, the net reaction is endothermic, which indicates the high energy demand of this process.

$$CH_4 + H_2O + \text{heat} \rightarrow CO + 3H_2 \qquad \Delta H = +251 \ \text{MJ/kmol}_{CH4} \tag{1}$$

$$CO + H_2O \rightarrow CO_2 + H_2 \qquad \Delta H = -41.2 \ \text{MJ/kmol}_{CO} \tag{2}$$

This process results in high purity hydrogen gas and 90% of hydrogen recovery. The estimated cost for a facility producing 380,000 kg/day is $2.08 - 2.27/kg depending on carbon capture and sequestration, though to achieve zero carbon footprint these techniques must be integrated [21].

A more energy-efficient process than SMR to produce syngas is the exothermic partial oxidation of hydrocarbons (POX), also known as coal gasification, when coal is used as feedstock, although this process results in increased costs because of larger amounts of solid feedstock and ash byproducts. This process also comprises of three main steps (syngas formation, water-gas shift reaction and gas purification) and can be either catalytic or non-catalytic, depending on the feedstock. In general, two mechanisms have been proposed, the direct mechanism in which hydrocarbons react with oxygen in presence of a catalyst to produce carbon monoxide and hydrogen, and the combustion-reforming mechanism in which hydrocarbons are combusted by oxygen to produce carbon dioxide and water and the unreacted hydrocarbons are converted to water, CO_2, CO and hydrogen by reformation [22,23]. The reaction takes place at ~590°C with feedstock including methane to naphtha, if catalyst is used, or ~ 1300°C with methane, heavy oil and coal, if it is uncatalyzed [24]. The product sulfur is removed by conversion into H_2S, and

subsequently the gas purification step is similar to the one in SMR. Typically, hydrogen cost is calculated between $ 1.34-1.63/kg [25].

Autothermal reforming (ATR) is a combination of SMR and POX, in which natural gas and steam undergo partial oxidation with oxygen in an exothermic reaction (eq. 3), which generates adequate heat to complete the endothermic reaction of carbon dioxide with natural gas producing hydrogen (eq. 4):

$$CH_4 + 3/2\ O_2 \rightarrow CO + 2H_2O \quad (3)$$

$$CH_4 + CO_2 \rightarrow 2CO + 2H_2 \quad (4)$$

The partially oxidized mixture then undergoes further reformation in presence of a catalyst, and end temperatures around 980 to 1200°C. The hydrogen cost of this process is estimated at $1.48/kg.

Methane pyrolysis consists of thermal decomposition of methane in absence of oxygen and yields elemental carbon and hydrogen gas:

$$CH_4 \rightarrow C + 2H_2 \quad (5)$$

The reaction of pyrolysis is endothermic, requiring the input of heat, with temperatures 300 – 1000°C [26]. Although this process does not require any carbon capture or sequestration of waste gas, no carbon dioxide is produced, which lowers the cost (~$1/kg), the main disadvantage is the separation of hydrogen gas due to its low partial pressure [27].

Besides fossil fuels, renewable sources can also be utilized for production of hydrogen gas. Biomass, usually produced from plant and animal waste, can be used for hydrogen production via thermochemical and biological processes. In the first one,

hydrogen and hydrogen rich gases are being produced by pyrolysis or gasification techniques, where methane and carbon monoxide can be further processed via SMR to hydrogen production. The efficiency of this process is highly dependent on the type and size of feedstock and the hydrogen cost ranges from $1.77 – 2.05/kg of H_2. Biologically, the main processes include direct and indirect bio-photolysis and photo and dark fermentation, which involve bacteria/algae organisms, containing hydrogen producing enzymes and can produce hydrogen in certain conditions. The average hydrogen cost of such process is calculated at $2.13/kg. However, this process is governed by limitations such as low hydrogen production and high surface area requirements for adequate light collection.

Solar and wind can be used as a primary energy source to produce electricity, which then is used in water splitting processes such as electrolysis and thermolysis to split water into hydrogen and oxygen [28,29].Electrolysis takes place a unit called electrolyzer, which consist of an anode and a cathode separated by an electrolyte and is categorized by the type of electrolyte. The most matured electrolysis techniques are alkaline, proton exchange membrane (PEM) and solid oxide electrolysis cells (SOEC). In this processes, clean H_2 is produced at the cathode when the electric potential is high. Due to increased energy requirements, electrolysis is not yet competitive to other techniques, and although electrolyzers are capable of converting electricity to hydrogen in a storable and portable form, their application is feasible in a small scale production [30].

Thermolysis focuses on water splitting at high temperatures of ~2500°C, which renders this process less sustainable. The chemicals are cycled in a closed loop which

consumes water and yields hydrogen and oxygen. The high temperatures required for this process are generated by concentrating sunlight onto a reactor tower using mirror heliostats or wasted heat from nuclear reactors. Several thermochemical water-splitting cycles incorporating Cu-Cl or SnO_2 catalysts have been proposed in the literature, with a focus on solar collectors [31]. Photoelectrolysis for hydrogen production occurs in an electrolytic cell, characterized by its photocatalyst, which is usually a semi-conductor deposited on the cathode surface, along with a stabilizer [32]. This process is mainly governed by constrains due to charge transport and efficiency of visible light absorption of the semiconductor electrode.

Hydrogen storage is another problem that accompanies hydrogen production methods, for hydrogen economy to become viable. Many researchers have proposed various methods for hydrogen storage, with integration to the renewable energy system being one of the most promising [33,34]. Hydrogen storage methods are classified into physical and material storage, with the latter being broader. The simplest and most commonly used method of hydrogen is under compression. This method has been utilized for years in a variety of gases and is found to be convenient for numerous of applications, including stationary and mobile. The main advantage of compressed gases is the fast rate of filling and release, along with the reduced volume. However, specifically for reactive gases like H_2, compression poses an additional safety concern. Nonetheless, when lightweight capacity is required, carbon fiber composite vessels are used, opposed to metal used for high-capacity requirements [35].

Another physical storage method involves storing liquified hydrogen, with higher energy density per unit volume, however the liquefaction method requires greater energy consumption, and there is an increased loss due to the boil-off phenomenon, which can be addressed by insulating the vessel [36]. For industrial and medical applications, liquid hydrogen storage is achieved in cryogenic containers by vacuum insulated vessels, which allow the storage of the same quantity of hydrogen to either smaller volumes at similar pressures or in similar volumes at lower pressures, providing higher hydrogen densities.

Material based storage can be achieved through chemical systems, to meet the transportation applications needs. However, the property requirements of such a chemical compound, have not been met yet, as the system must demonstrate features including high capacity and cyclic stability, which can be achieved by innovative solutions [35].

The average annual hydrogen consumption is estimated at ~70 million tons in pure form and 45 million tons syngas [37]. Its main usage concerns industrial applications, such as ammonia production for fertilizers, methanol, oil refining among others.

Atmospheric nitrogen reacts with hydrogen in a process called Haber-Bosch to produce ammonia (NH_3), containing 17.8% hydrogen by weight. The reaction is carried out by iron catalysts at temperatures between 400-600°C and pressures from 200 to 400 atm and is described equation (6):

$$N_2 + 3H_2 \Leftrightarrow 2NH_3 \quad (6)$$

Almost 90% of ammonia is used as a precursor for nitrogen-based fertilizers. Both hydrogen and nitrogen are produced on-site at ammonia plants by SMR from a fossil fuel feedstock and low temperature separation of air, respectively [38].

The largest consumption of H_2 occur during oil refining processes, in which hydrogen is produced on-site from natural gas reforming, accounting for 33% of the global hydrogen production . Atmospheric distillation is used to separate the molecules according to their molecular weight. During the separation step, the bottom of the distillation column is heated at temperatures between 350 and 400°C, resulting in oil evaporation. The vapors travel through the column to the top, where the temperature reaches 150°C, leading to condensation at different temperatures along the column, while the heaviest molecules, remain at the bottom. The liquids are collected on trays, depending on the column height they reached, which defines their petroleum cut, while solids, like asphalt and residues, remain in the bottom, and undergo a second separation process. After the separation process, heavy molecules are "cracked" into lighter ones. This conversion process, or catalytic cracking, occurs at 500°C, and converts a percentage of the heavy products into gas, gasoline and diesel [39]. Hydrogen can also be used in this step, to increase product yield by hydrocracking, catalyzed usually by nickel, palladium, or platinum catalysts. Corrosive or air pollutants, like sulfur, are being removed by hydro-desulfurization which uses hydrogen to combine sulfur, producing hydrogen sulfide (H_2S) [40].

Methanol production, through catalytic hydrogenation of carbon monoxide

$$CO + 2H_2 \rightarrow CH_3OH \quad \Delta H = -90.7 \text{ kJ/mol} \tag{7}$$

contributes to 10% of the global H_2 consumption. The process takes place at pressures and temperatures of 50-100 bar and 250°C, respectively. Methanol is a liquid fuel, widely used in transportation, that also has the potential to be produced in zero-carbon processes, along

with H_2 [41]. Besides its wide use as a raw material for forming industrial chemical compounds, such as acetic acid, formaldehyde etc., methanol has been used directly as a fuel in direct methanol fuel cells (DMFC). One of the most exciting applications of hydrogen production is its incorporation in the Fuel Cell technologies, enabling secure energy transition and environmental compatibility.

1.4 Fuel cells

Fuel cells are electrochemical devices that convert chemical energy directly into electricity and heat with high efficiency [32]. Like the electrolyzers, they consist of an anode and a cathode separated by an electrolyte and can be classified according to the electrolyte type [42]. So far, five types of fuel cells have been commercially available, with numerous applications, stationary as well as mobile:

Alkaline fuel cells (AFCs): Being one of the first fuel cells systems developed in 1960, it was widely used in the U.S. space program to produce electrical energy and water on-board spacecraft. They use concentrated aqueous solution of potassium hydroxide (KOH) as electrolyte (35-50% wt. in operating low temperature, <120°C, and 85% wt. in high temperature, ~260°C), due to its high conductivity and boiling point. The electrolyte is sustained in an asbestos matrix, and a variety of non-precious metals as a catalyst can be used such as Ni, Ag, metal oxide, and noble metals, at the anode and cathode to accelerate the reaction. They have demonstrated efficiencies above 60% in space applications, because of the high operating temperatures and pressures which accelerate the kinetics. However, they require high purity gases to operate because any amount of CO_2 from air or

reformed fuel reacts with KOH electrolyte yielding a solid carbonate and destroying the electrolyte's ion mobility.

$$CO_2 + OH^- \rightarrow CO_3^{2-} + H_2O \quad (8)$$

Scrubbing to remove CO_2, along with high hydrogen purity requirements, have been demonstrated to increase the cost, hence their operation is restricted for space applications.

Solid oxide fuel cells (SOFCs): They use a hard, non-porous ceramic compound as electrolytes, usually yttria-stabilized zirconia (Y_2O_3-stabilized ZrO_2). They operate at very high temperatures (600 – 1,000°C), which removes the need for precious-metal catalyst, and reduces cost, however the operating temperatures limits its material selection. SOFCs allow conversion of different fuels, among which hydrocarbon fuels. The high temperature contributes to conversion to power with high efficiency and internal reforming, minimizing emissions of air pollutants and greenhouse gases. Their efficiency is around 60%,which made SOFC an interesting solution for stationary power generation between 2 kW to 100s MW capacity range. However, they are sensitive to sulfur and other contaminants, causing poisoning on the anode, hence the fuels require desulfurization. Furthermore, the high-temperature operation results in a slow startup and requires significant thermal shielding to retain heat and protect personnel, rendering them unsuitable for transportation.

Molten carbonate fuel cells (MCFCs) are also high-temperature fuel cells, operating at 650 °C, thus non-precious metals can be used as catalysts, which reduces the cost. The electrolyte is composed of a molten lithium, sodium and potassium carbonates soaked in a porous matrix. The high temperature operation also offers the advantage of higher system efficiencies and increased flexibility in the use of fuels. However, along with

the use of corrosive electrolyte, which accelerates component breakdown and corrosion, cell life and durability are severely decreased. Molten carbonate fuel cells are being used on natural gas and coal power plants for industrial, electrical, and military applications.

Phosphoric acid fuel cells (PAFCs) were the first fuel cell system to be commercialized. Typically, they are used for stationary power generation, but some PAFCs have been used to power large vehicles, such as city buses. These fuel cells use liquid phosphoric acid (H_3PO_4) as an electrolyte and porous carbon electrodes containing a platinum catalyst, which adds to the cost. During the years, the cell performance has increased due to the use of higher operating temperatures and acid concentrations (200 °C and 100% acid concentrations). Their efficiency is around 40% at generating electricity, and compared to other types of fuel cells, they are less powerful, in regard to weight and volume. As a result, these fuel cells are typically large, heavy, and expensive, as they require much higher loadings of platinum catalyst.

Polymer electrolyte (PEFCs) are divided into 3 subcategories: i) proton exchange membrane fuel cells (PEMFCs), ii) anion exchange membrane fuel cells (AEMFCs) and iii) direct methanol fuel cells (DMFCs). Typically, they need only hydrogen, oxygen from the air, and water to operate. The use of solid polymer electrolytes and non-corrosive components, along with their ability to stop and start quickly, without requiring high temperatures (operate at around 30 – 100°C) results in less wear on system components, higher efficiency, and better durability. The ability to efficiently generate high power densities, makes them attractive for transportation and portable applications. Primary contaminants affecting PEFCs are carbon monoxide and sulfur, while carbon dioxide act

as diluent. Small amounts of CO in the reformed gas, will adsorb on the platinum catalyst, causing catalyst poisoning and block hydrogen from the catalyst sites. Other contaminants such as ammonia, alkali metals, and heavy hydrocarbons not only cause catalyst poisoning, but also accelerate the membrane deterioration. Hence, gas purification, along with the expensive Pt catalyst, increase the cost.

Fuel Cell Type	Operating Temperature (°C)	Electrolyte	Efficiency %	Applications
Alkaline	~ 100	Aqueous solution potassium hydroxide	60	Space, military
Solid Oxide	800 - 1000	Yttria stabilized zirconia	60	Auxiliary power and electric utility
Molten Carbonate	600 - 700	Molten lithium, sodium, and potassium carbonates	45 - 50	Electric utility, industrial and military
Phosphoric Acid	150 - 220	Liquid phosphoric acid	40	Electric utility and transportation
Proton Exchange Membrane	30 - 100	Solid polyperfluorosulfonic acid (Nafion)	35 - 60	Vehicle, portable power, electric utility

Figure 3. Most common types of fuel cell technologies.

1.5 Proton Exchange Membrane Fuel Cells (PEMFCs)

1.5.1 PEMFC Theory

In PEMFCs, hydrogen and hydrogen-rich fuels such as natural gas and biogas can be used to cleanly and effectively provide power in a wide variety of transportation, stationary and portable power applications [43]. PEMFC's high power densities, along with the advantages of low weight and volume, renders them a leading candidate to substitute traditional fossil fuels in transportation applications [6].

The basic single cell configuration of PEMFCs contains an MEA (membrane, catalyst layers and gas diffusion layers) sandwiched between the monopolar plates. Hydrogen gas flows through the flow field channels in the anode side, through the GDL to the catalyst layer. In the catalyst layer, electrons are removed from the hydrogen and through an external circuit are transferred in the cathode catalyst layer. At the same time, hydrogen ions pass through the proton exchange membrane to the catalyst layer on the cathode side. On the cathode side, the hydrogen protons react with the oxygen supplied from the cathode, and the electrons transferred through the circuit to produce heat and water, in an electrochemical reaction shown below [42]:

$$\text{Anode: } H_{2(g)} \rightarrow 2H^{+}_{(aq)} + 2e^{-} \quad (9)$$

$$\text{Cathode: } \tfrac{1}{2}\, O_{2\,(g)} + 2H^{+}_{(aq)} + 2e^{-} \rightarrow H_2O_{(l)} \quad (10)$$

$$\text{Overall: } H_2 + \tfrac{1}{2}O_2 \rightarrow H_2O + \text{heat} \quad (11)$$

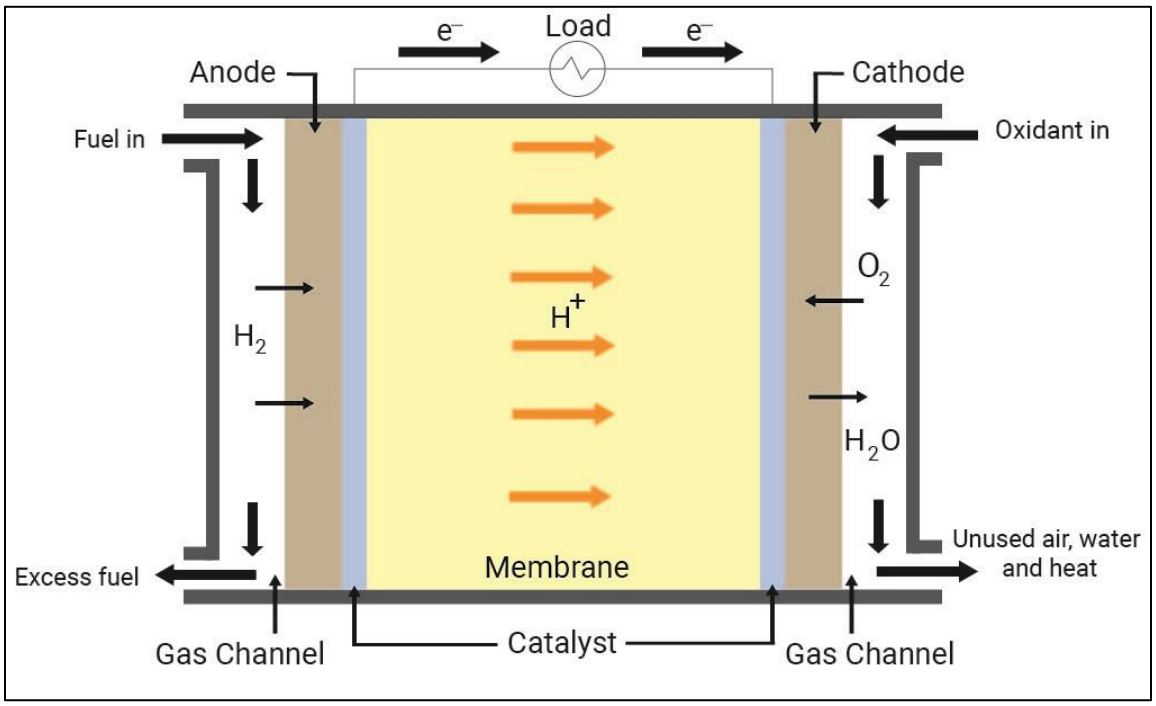

Figure 4. PEMFC single cell configuration and operation.

From a theoretical point of view, the maximum efficiency of a fuel cell is 83%, however practically, the efficiency is around 40% [44]. This is mainly due to a variety of losses (activation, ohmic and mass transport) that occur during fuel cell operation, resulting in lower cell voltage than the equilibrium potential of the cell (1.23 V). Activation losses come from the oxygen reduction reaction (ORR) taking place in the cathode and have the largest impact on fuel cell performance. Although hydrogen oxidation is relatively quick, ORR is governed by slow kinetics, affiliated with a 4-electron transfer to the oxygen molecule and the breaking of an oxygen-oxygen double bond [45]. Ohmic losses result from proton transfer in the membrane and can be minimized by reducing the membrane thickness. Mass transport losses can be diminished by efficient reactant and product

transport to and from the catalyst layers, and is controlled by various parameters in the fuel cell system, such as the GDL and catalyst materials, pore structures and thickness, among others [46].

1.5.2 PEMFC components

PEMFC main components include bipolar plates (monopolar in single cell), seals and membrane electrode assembly (MEA). The monopolar plates have multiple functions in the PEMFCs, as they distribute fuel gas and air uniformly, conduct electrical current from cell to cell in stacks, remove heat from the active area, and provide physical strength and support to the stack. Flow fields channels are machined or stamped into the plate surface to allow gas flow over the MEA. For better sealing, Teflon gaskets must be added around the edges of the MEA to provide a gas-tight seal [47].

The practical employment of fuel cells depends upon achieving strict performance requirements. Many material options have been proposed including non-porous graphite, coated polymer composites and metallic sheets. Graphite plates have demonstrated high corrosion resistance and electrical conductivity; however, their frailty limits their mass production and causes an additional handling difficulty. Polymer composite bipolar plates are made of conductive carbon fillers, for electron and heat transportation, and polymer binder, providing mechanical support and eliminates gas permeability. Composite conductivity of the plates greatly depends on the composition and content of carbon filler and binder. Typically, combination of multiple types of carbon and increased the filler content results in increased composite conductivity [13], as a result of improved carbon cluster connection, however, increased amount of fillers lowers the mechanical strength

by crack formation and eventually material failure. A more rigid structure has been explored by using metal plates. Metals provide high electric and thermal conductivity, low gas permeability and enhanced mechanical support, but their main disadvantage is metal corrosion by the acidic environment, leading to undesired oxidant formation. This issue is being addressed by implementation of coating to protect the metal from corrosion. Coatings usually consist of noble metals, carbon based materials such as graphite or diamond-like, and composites with incorporate carbon mixed with a polymer matrices [13].

The core of a PEM fuel cell is the Membrane Electrode Assembly (MEA), which includes the solid electrolyte membrane, the Catalyst Layers (CLs) and the Gas Diffusion Layers (GDLs). The MEA is sandwiched between the bipolar plates and its structure and material selection is a crucial factor on fuel cell performance. Membrane materials should possess chemical and thermal stability and characteristics that enhance ionic conductivity but eliminate electron transport and reactant gases cross-over. The most widely used membrane material for PEMFCs is perfluorosulfonic acid (Nafion, Du Pont). Its hydrophobic perfluorinated backbone contributes to the mechanical support and chemical stability, and the hydrophilic sulfonated side chains enables water absorption by forming hydrated clusters.

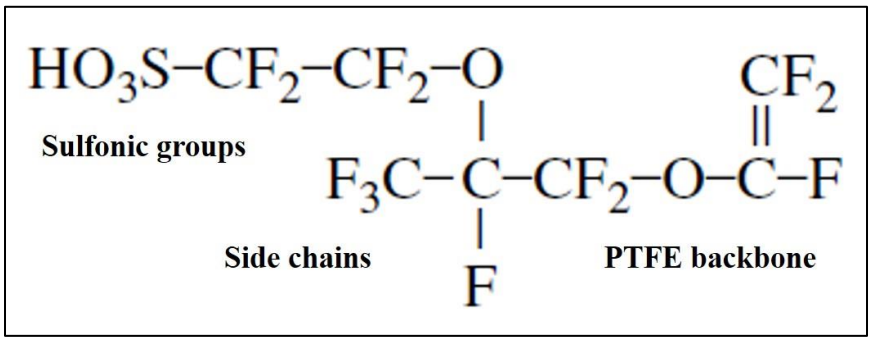

Figure 5. Nafion membrane structure.

Nafion is a copolymer of polytetrafluoroethylene (PTFE) with high protonic conductivity, as well as strength and stability in both oxidative and reductive environments at temperatures below 125^{o} C. However, the main disadvantages are associated with material cost, supporting structure requirements and temperature, which set the limit to PEM fuel cells operational conditions [48]. Also, to maintain the ionic conductivity, the membrane must be hydrated, limiting the PEMFCs temperatures below the boiling point of water.

Conventional catalyst layers include platinum nanoparticles dispersed on a high-surface-area carbon support, mixed with an ion-conducting polymer (ionomer, Nafion), deposited on both the anode and cathode side of the membrane [49]. The contact point of the reactants, catalyst, and electrolyte is traditionally referred to as the three-phase interface [50]. The three-phase boundary (ionomer, catalyst particles, and gas phase) is characterized by high tortuosity in order to enhance the catalytic surface area, to achieve adequate rate for the HOR and ORR. In order to catalyze reactions, the catalyst electrode must provide channels for reactant and products transport, an electrically conductive path for electrons transport and an ion conductive path for proton transport from the electrode to the

membrane, and a balance must be achieved to avoid performance losses and maximize the utilization of the Pt-based catalyst. The ionomer binder facilitates proton transport and dissolves oxygen for reaction on the catalyst surface. Its content is considered crucial as excess ionomer will reduce the gas diffusion pathways and obstruct dissolved oxygen access to catalyst, whereas at low Nafion content, not all the catalyst particles are connected to the membrane for ionic conduction [51]. The optimum Nafion loading reported is around 30 wt.% [13]. Frequently used catalyst and carbon support materials are Pt and carbon black, respectively. Pt possess high catalytic activity, however its scarcity, sensitivity to CO poisoning and high cost, initiated an intensive research activity, focused on ways of reducing the Pt loading and exploring alternative catalyst materials [150]. A considerable amount of publications exists on Pt alloys (Pt-Co, Pt-Ni, Pt-Fe, Pt-V, Pt-Mn, and Pt-Cr) indicating good catalyst kinetics, however it is concluded that Pt mass activity is constricted by increased particle size and structure of Pt alloys [13].

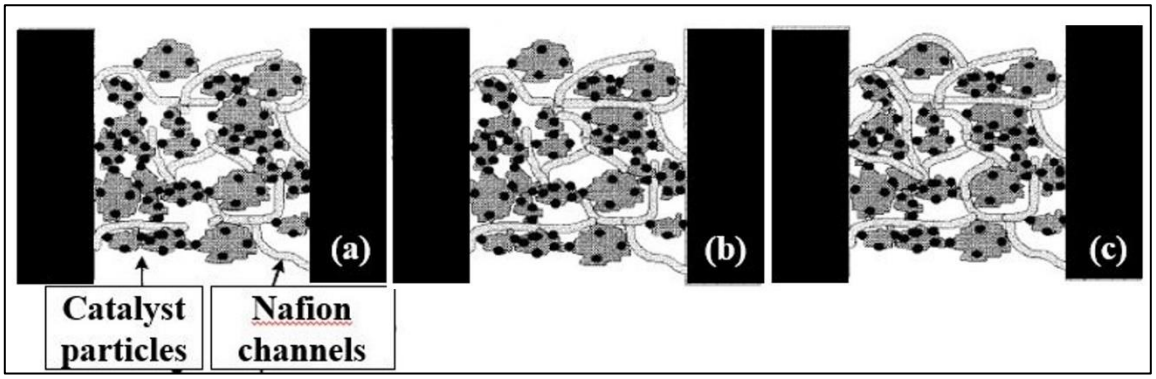

Figure 6. Nafion ionomer content (a) low, (b) desired and (c) high amount.

Gas Diffusion Layers (GDLs) are one of the key components of PEMFCs with several functions. They provide electrical contact between the electrodes and the bipolar

plates and distribute reactants to the electrodes. Furthermore, they allow product water to exit the electrode surface and permit the passage of water between the electrodes and the flow channels [52,53]. Typically, they are made of electrically conductive, porous materials such as carbon paper sheets, coated with PTFE. In many cases, the inner surface of the carbon paper is coated with a high surface carbon and PTFE mixture, known as the microporous layer (MPL), to further assist the GDL functions of water management and gas transport [54]. GDL materials and properties are extensively discussed in Chapter 2.

1.5.3 PEMFC challenges

Explicating PEMFC fundamentals is of critical importance to the upgrading of the technology, through restriction breakthroughs and optimal design configuration. As previously discussed, current PEMFC research focuses on all the system components, with significant progress in design and material fabrication, in the last decade. However, PEMFCs are still governed by several limitations that prohibits them from becoming commercially viable, including cost reduction and performance, reliability, and durability enhancement.

The U.S. Department of Energy (DOE) in a motion to promote the development of a fuel cell power system for automotive applications, among others, generates goals and performance targets for fuel cells. Although the cost of automotive fuel cell system target is significantly reduced from $51/kW in 2012 to $40/kW by 2020, one of the most significant cost components of a fuel cell system remains the platinum catalyst. Currently, researchers focus on approaches that increase platinum utilization and activity in the fuel cell system.

Performance in the terms of power density and specific power are important attributes for light-duty vehicles; however, they are highly dependent on the system design and layout of components rather than the technology itself. The current status for recent fuel cell stacks already exceeds the 2015 targets indicating a power density of 640 W/L and specific power of 659 W/kg. The 2020 targets specify power density and specific power of 650 W/L and 650 W/kg, respectively, with 65% peak energy efficiency.

A key performance factor that will render fuel cell systems competitive with internal combustion engines is durability. To be competitive, fuel cells must demonstrate similar durability and reliability to current internal combustion systems. According to DOE, the latest results manifest durability of 2,500 hours with 10% stack voltage degradation. These results abstain significantly from the 2020 durability target, which identifies durability of 5,000 hours (150,000 miles of driving) with less than 10% performance loss. Another challenge comes along with the operating conditions, as fuel cell systems must be operable under temperatures from below freezing to over boiling point of water and relative humidity conditions from dry to wet [55].

To meet the cost and durability targets of DOE, significant further research is needed. MEAs require substitution of costly materials currently in use, along with improved degradation resistance and low Pt loadings. GDLs greatly effects the performance of a fuel cell in all the polarization regions, however, their mass transport characteristics mainly affect the fuel cell performance and durability. Substantial understanding of liquid water transport in the microstructure and mixed wettability GDL designs is crucial to overcome these challenges [56].

1.6 Scope of study

It has been established that GDLs play a vital role in the fuel cell performance and durability, as they provide channels for gas and water transportation to and from the catalyst layer, respectively, and adequate mechanical support to the catalyst layers by limiting the membrane swelling caused by water absorption. Due to the complicated fuel cell system governed by many interdependent parameters affecting the performance and durability, and with the majority of research focusing on ways to increase the catalysts' utilization and activity, many GDL properties have been understudied and there is a great need for further investigation and understanding on this matter.

The purpose of this study is to examine the effect of various GDL configurations in order to achieve optimized characteristics and parameters, leading to improved fuel cell performance. This goal is achieved by designing and developing GDL configurations, including single and multilayer MPLs, using different contents of a pore forming agent, to facilitate gas transport and water management in the system. Subsequently, the GDL samples are *ex-situ* characterized and the fuel cell performance is evaluated to determine the optimum configuration and material combination, under high and low relative humidity conditions. The fabricated GDLs were compared to a commercial GDL sample, with MPL, to further assist in in-depth comprehension of the parameters.

Besides fuel cell performance, durability of the GDLs is also an area that requires further investigation and understanding of the correlation to the material properties. The microporous layer is not usually thought as another carbon source undergoing carbon corrosion. Hence, while carbon corrosion impact on different catalyst kinetics and behavior

has been very well defined, the contribution of carbon corrosion of the GDL carbon remains unclear.

In this regard, two methods of *ex-situ* accelerated stress tests were implemented on the best performing configuration of the PUREBLACK® GDLs, and a similar configuration, using VULCAN® carbon. Although *ex-situ* ASTs hardly represent the conditions of the GDL in the fuel cell due to the lack of electrolyte and compression, they were selected because they allow characterization without requiring separation from the MEA, and since the catalyst layer also contains carbon materials, distinction between GDL and catalyst layer corrosion is difficult. The main difference between PUREBLACK® and VULCAN® carbons is the partially graphitized structure of PUREBLACK®, which is reported as corrosion resistant, compared to the non-graphitized carbon VULCAN®. *Ex-situ* characterization and performance evaluation of pristine and aged GDL samples occur at the same operational conditions, and the effect of MPL corrosion is estimated by comparing the performance loss at high and low RH conditions, and under H_2/O_2 and H_2/air. In addition, the corrosion effect, due to the electrochemical degradation, is being studied by durability test performed on the pristine GDLs, using H_2/air, of 100 h continuous operation (50 h at 100 and 50 h at 60% RH) under constant current density.

Ultimately, this study represents GDL fabrication methods and materials, for fuel cell performance and durability optimization, examines different MPL configurations of graphitized carbon, isolates the best performing one and compares it to a similar configuration with amorphous carbon. Material properties and characteristics showing increased carbon oxidation resistance and durability of the MPL are, also, proposed.

2. LITERATURE REVIEW

2.1 GDL materials

The GDLs initially consisted of a macroporous layer or substrate, which is usually a sheet of carbon paper or (woven or non-woven) cloth, with pore size between 10-30 μm [57,58]. Originally, they were thought to have a small impact on fuel cell performance [59], however, it was proven later that their effect can be significant, if they possessed the desired characteristics [60]. Newer developments in the GDL fabrication introduced a Microporous Layer (MPL) applied on the inner side of carbon substrates, facing the catalyst layer (Figure 7). This layer is usually a mixture of high surface area carbon, for good electrical conductivity and a hydrophobic agent such as PTFE and has pore size 100-500 nm [61,62].

To enhance mechanical strength, metal based GDLs were originally investigated due to thinner diffusion layer and the ability to produce uniform porous structure [63]. They are structured in the form of a metal mesh, foam or micro-machined metal substrate, and are usually used in Direct Methanol Fuel cells (DMFCs) because of their relatively large pores, enhancing the transport properties of the liquid fuel and the water product [64,65]. A variety of metals were examined [66–70], however the main disadvantage of these substrates is metal corrosion, which was found to accelerate polymer membrane degradation rate [71,72].

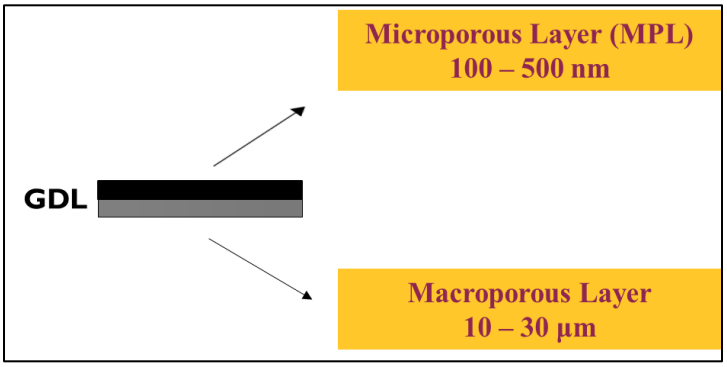

Figure 7. GDL structure.

2.2 GDL fabrication

A variety of carbon substrates, both paper and cloth, is available in the market, and each type exhibits different mass transport, porosity, hydrophobicity and conductivity. Several studies compare the material and structural properties between carbon paper and cloth [73–76]. Carbon paper demonstrated better performance at dry conditions, retaining water in the MEA due to their pore structure, enhancing the membrane conductivity. Carbon cloth substrates, on the other hand, produce higher performance at high humidity conditions, among other property differences [77,78]. Since GDL substrates are not hydrophobic as received, later developments introduced carbon substrates partially coated with a hydrophobic agent, usually PTFE, and sintered at temperatures above 350 ^{o}C, for even PTFE distribution. The PTFE coating proved to provide an open path to the reactant gases, by rejecting the excess water produced from the fuel cell reaction, because of its hydrophobic character [79]. The relationship between hydrophobicity and water transport was first introduced by Staiti et al. [80]. Since then, teflonization is widely used in the GDL manufacturing process and many researchers have studied the effects of PTFE contents, coating techniques and sintering temperatures on various parameters that govern the fuel

cell system [54,81–84]. It is worth noting that the optimized PTFE content improved water management and oxygen gas diffusion in the MEA [85].

GDLs with MPLs have gained a lot of research attention, as their presence and structure influence many parameters, including fuel cell performance. The microporous layer, which mainly consisted of carbon powder and a hydrophobic agent (PTFE), was claimed to have beneficial impact on the fuel cell performance, due to the good electrical properties of carbon powder, and enhance gas transport to the catalyst layer while the hydrophobic agent expels the excess water from the system [86]. The reason for this improvement is claimed to be the fact that when their parameters are carefully balanced, they enhance the water management of the fuel cell system, avoiding catalyst flooding when operate in high relative humidity conditions and drying when relative humidity is low [87,88]. To achieve optimum functional GDLs, a series of properties, such as hydrophobicity (water expelling) and hydrophilicity (water retaining) must be combined, along with, porosity, surface contact angle, bending stiffness, air permeability, water vapor diffusion, electrical/electronic conductivity, crack free surface morphology, high mechanical integrity and increased oxidative stability, and durability at various operating conditions, many of which depend on the fabrication process, materials, and loadings [89–93] .

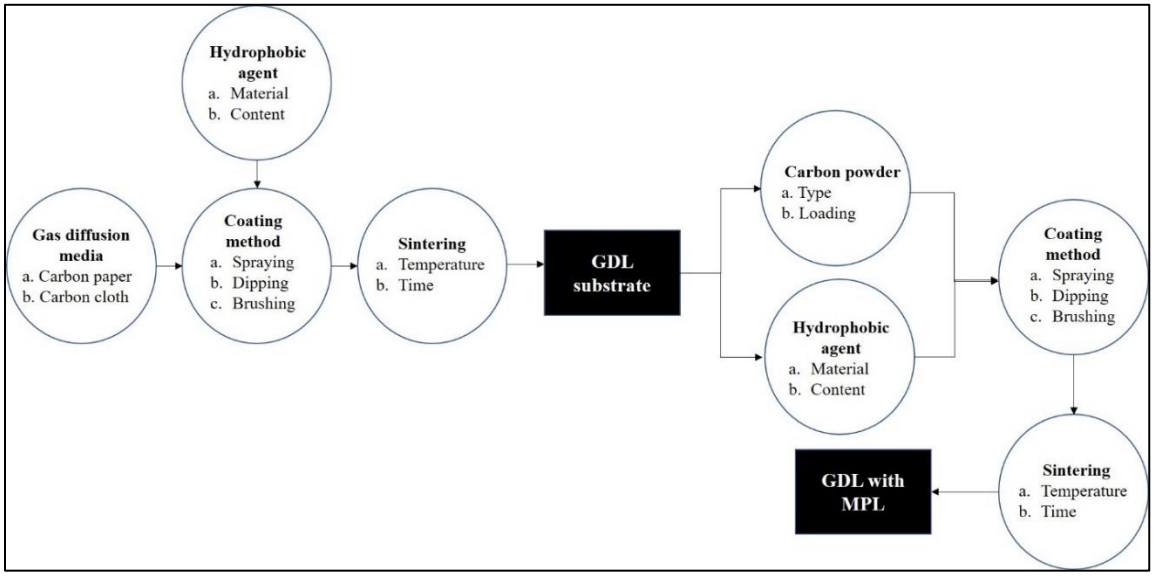

Figure 8. GDL fabrication process

2.3 GDL characteristics

Gas Diffusion Layers (GDLs) are crucial sub-components in Membrane Electrode Assemblies (MEA) of a PEMFC. As they perform a variety of tasks on the fuel cell system due to their functional and support structure, their design and materials must be carefully examined and balanced. Functionally, they provide gas channels that allow the ambient reactant gases to flow through and reach the catalyst layers, and remove the excess water produced at the CLs, and heat. Mechanically they perform high resistance to outside compression and forces to ensure mechanical integrity for the fuel cell system, providing adequate mechanical strength to hold membrane electrode assembly from extension caused by water absorbance of the membrane [94,95]. Therefore, the GDL ideal characteristics include:

- Effective gas transport
- Balanced hydrophobicity
- Electrical/ Electronic conductivity
- Crack-free surface morphology
- High mechanical integrity

Many studies were conducted to understand the effect of different parameters on the fuel cell performance and achieve the optimum material combination. Unfortunately, as the fuel cell system is a system with numerous interdependent parameters, it is difficult to define the optimum GDL configuration and material combination. Numerous studies have demonstrated the MPL significance in the GDL roles; however, further research is needed to address this complex issue.

2.3.1 Transport properties

A typical GDL shows micro, meso and macropores, since carbon substrates have relatively larger pore sizes than the MPLs [95–97]. Porosity and pore size distribution have been closely associated with mass transport [98]. Many studies have concluded that high GDL porosity improves mass transport, which leads to increased fuel cell performance [77,81,97,99]. At high relative humidity conditions, larger pore diameter volume confirmed to decrease flooding at the cathode, so that the reactant gas has an open path to active sites through the smaller, hydrophobic pores [100–102]. Nam indicated larger porosity is better for both the reduction of water saturation and increase in limiting current

density [103]. However, high porosity can decrease the through-plane electronic conductivity and mechanically weaken the structure. The influence of pore-size distribution of GDL on mass transport was found to be stronger than the influence of the total porosity [97].

During the fuel cell operation, liquid water is produced on the interface between the cathode catalyst layer and the MPL. The liquid water can easily move (or transport) mainly through the larger pores of the MPL and the carbon substrate, to the flow field channels [104,105]. The smaller pores of the MPL inhibit liquid water due to their hydrophobic characteristics, serving as paths for transporting the reactant gases to the reaction zone [106]. Due to the inadequate capillary pressure required for the water to enter the smaller pores, the remaining water is driven to the anode side through the membrane, leading to reduced flooding of the GDL and the catalyst layer and improved membrane hydration [107]. Hiramitsu et al. showed that flooding originates at the interface between the GDL and the CL and can be reduced by controlling the GDL pore size in that area [108]. Passalacqua et al. tested four different carbon powders and observed that performance improvement was affected by higher pore volume and low microporosity [109]. Hence, the role of GDL porosity in determining two-phase transport in the GDL is crucial. Due to the random water content within the structure, GDLs with non-uniform porosity have been examined. Graded porosity GDLs have been reported to demonstrate improved performance by promoting water removal and gas transport [110–112].

Porosity, pore size distribution and permeability of the GDL are closely related [113]. In-plane and through-plane permeability depend on parameters, such as thickness, density, hydrophobic agent content, structure, and type of MPL [74,114].

2.3.2 Hydrophobicity/ Hydrophilicity

Hydrophobicity is directly related to water management in the fuel cell and is an important property of both the surface and pores of the GDL. Hydrophilic pores tend to retain water while hydrophobic pores repel the water out. GDL hydrophobicity has been manipulated by varying the PTFE contents. Many studies have been focused on determining the effect of PTFE content on the fuel cell performance [85,115,116]. More precisely, Park and Popov investigated the effect of hydrophobic agent on water and oxygen gas transport. They concluded that the ideal PTFE content in the GDL reduced mass transport limitations and improved oxygen diffusion kinetics. However, they observed that higher or lower PTFE content results in poor fuel cell performance due to decrease in permeability and water flooding, respectively [117]. Consequently, the most commonly reported PTFE content is 33% by weight. However, it was found that the optimum PTFE content depends on parameters such as the carbon type and loading [118,119], and that there is an optimum value for PTFE content at which mass transport limitation are decreased, and above or below which the performance decreases as a result of decreased in porosity and permeability [83,84,120].

2.3.3 Electrical properties

Electron transport through the GDL is affected by the GDL thickness, material and electronic conductivity [121]. Generally, thinner GDLs perform better, as they are characterized by less mass resistance and high electrical conductivity, but thickness needs to be optimized to meet the researcher's needs, as it is material dependent [122,123]. Prasanna et al. concluded that there should be an optimal substrate thickness, at which mass transfer loss, contact resistance and activation potential would be minimum [82]. Zhou et al. concluded that through and in-plane electronic resistances of the GDL are negligible since they demonstrate minimum effect on the fuel cell performance. They also indicated that electrical resistance is material dependent [124]. However, the interface contact resistance between PEMFC components has significant effect, since it depends on material properties, compression, and surface geometry [125].

2.3.4 Surface morphology

The structure of the substrate has a direct effect on the mechanical properties of the GDL. Carbon cloth GDLs are more compressible and flexible while carbon paper is more brittle, providing better mechanical support. The fiber structure plays an important role as it determines properties, such as porosity, permeability, and electrical conductivity [126].

Wang et al. studied the difference between carbon paper and carbon cloth and found that carbon cloth performs better in wet conditions due to the smaller tortuosity and rougher surface which facilitates the detachment of the water droplets. However, the higher tortuosity and smoother surface of carbon paper results in torpidity of water droplets and

operate better in dry conditions [78]. MPL application usually results in smoother surface in contact with the CL which can also be a contributor of the undoubtedly enhanced performance on its presence. Finer carbon particles result in smoother surfaces and smaller pores, hence MPL morphology depends on the type and loading of the carbon powder, as well as the coating method [78].

Several research papers correlate the improved efficiency of GDL with the carbon type and loading. Antolini et al. studied the effect of carbon powder characteristics on the PEMFC performance, using two different types of carbon powder; acetylene black and VULCAN® (XC-72R), and reported that acetylene black performed better [119]. Stuckey et al. introduced the growth of carbon nanotubes nanoforest (CNN) on carbon paper substrates and observed excellent performance on various RH conditions [127]. Park et al. investigated the effect of carbon loading in the MPL by preparing MPLs of different carbon loading on a carbon fiber paper and concluded that the improvement on fuel cell performance highly depends on the carbon loading of the GDL [91]. Wilson et al. reported that for a given carbon loading the electrode performance is a function its structure (porosity and surface area) and composition[128] .

Cracks usually appear on the MPL surface during temperature changes. Although it has been reported that cracks can act like larger pores and assist the transport of water through the GDL, their presence on the MPL surface is not desired because they lead into poor electrical conductivity. Moreover, the Pt catalyst particles dissociation and fall into the cracks and pores which results in reduced support for the catalyst and rapid MPL degradation by accumulating water and forming defects around the cracks [117,129,130].

On the other hand, the smooth, crack-free surface and homogenous nature of MPL could lead to uniform reactant gas transport to the reaction zone and effective water removal, avoiding flooding [121].

2.3.5 Mechanical properties

The GDL provides mechanical strength to support the membrane and catalyst layer. The structure of the substrate has a direct effect on the mechanical properties. The materials mostly used are carbon cloth or carbon paper. Carbon cloth has a rougher surface, which is beneficial in wet conditions, because water droplets detach easily. However, since it is compressible, it intrudes into the flow field channels, causing non uniform gas flow, which subsequently affects the fuel cell performance [126]. Carbon paper, on the other hand, has a smoother surface, and is shown to perform better under dry conditions, where the water production in the fuel cell is suppressed. Furthermore, it is brittle, which means that it is characterized by higher compressive strength and provides better mechanical support and uniform gas flow throughout the system. Kandlikar et al. mentioned that because of the heterogeneous structure of non-woven GDLs, the substrate intrusion into the channels is non-uniform and thus it affects reactants flow distribution, causing pressure drop, decreased fuel cell performance and durability [131]. Applied compression on the GDL results in structure deformation, affecting the surface morphology by smoothening of the rough GDL surface at low compression, or collapsing GDL pores at higher compression [132].

2.4 GDL degradation

Degradation studies have been focused mainly on the degradation of the catalyst layers [133,134], but the fuel cell performance is also affected by the degradation of the GDLs [135]. The GDL's two primary roles are to facilitate water transport and provide oxygen pathways to enter reactant sites with reduced resistance to mass transport [95,99,136,137]. Polytetrafluoroethylene (PTFE) treatment alongside the addition of a carbon-based microporous layer can be done to improve the functions of the GDL [138]. It was found that the main effects of GDL degradation were, increase in mass transport resistance and decrease in hydrophobicity [99,133–135,137,139]. One of the longest recorded studies was done by Bosomoiu et al. [135], which reported the degradation of the GDL hydrophobicity after 1000 hours of operation under in situ conditions. This illustrates the need for accelerated degradation methods to reduce the use of time and other resources [140].

Several protocols have been developed for in situ accelerated degradation of the GDLs, like freeze/thaw cycling which focuses on the effects of mechanical degradation on the performance of the cell [141,142]. Although, there was a significant damage to the membrane and catalyst layer in the in situ freeze/thaw cycling performed by Kim et al. [143], the effect on the GDL structure was insignificant. GDL mass transport losses were attributed to the PTFE degradation during the in situ ageing performed by Wu et al. [144]. To overcome these challenges and to isolate the degradation of the GDL, ex situ methods have been developed and performed where loss in hydrophobicity was observed [99,145,146]. Park et al. provides a comprehensive study which reviews the durability and

degradation of the GDL in the PEMFC [147]. GDL degradation can be characterized in two main categories, mechanical and chemical degradation. Any physical breakdown of the GDL can be classified as the mechanical degradation whereas dissolution by water, erosion by gas flow, and corrosion of electric potential are the main factors for chemical degradation, due to the structural breakdown during conditions like local fuel starvation, start-up and shut-down, where the water washes away the carbon [147,148].

To isolate the effect of oxidizing conditions on the MPL from effects on other components of the fuel cell, two ex-situ ageing methods were implemented in this study. First method implements GDL ageing in 30% hydrogen peroxide (H_2O_2) solution at 90°C for 24 hours. Carbon corrosion is mainly facilitated by the production on hydrogen peroxide in the fuel cell [149,150], which takes place when the two electron reduction of the oxygen on the platinum catalyst occurs [151,152].

$$O_2 + 2e^- + 2H^+ \rightarrow H_2O_2 \quad (E_0 = 0.695\ V_{RHE}) \tag{12}$$

The second method incorporates GDL ageing by immersion in water at 80°C up to 1000 hours. Complete oxidation of elemental carbon by water produces carbon dioxide when the anodic potential is adequate [153,154] :

$$C + 2H_2O \Leftrightarrow CO_2 + 4H^+ + 4e^- \ (E_0 = 0.207\ V_{RHE}) \tag{13}$$

In conclusion, in porous electrode reactions such as GDLs, isolated parameters are very difficult and time consuming to evaluate, since many parameters are interdependent and complicated factors are involved, thus mathematical models and simulations can be very useful tools [155,156].

3. MATERIALS AND METHODS

3.1 Materials

The materials used for the MEA synthesis and GDL fabrication and degradation are presented in Table 1.

Table 1. List of materials and chemicals

No	Material	Supplier
1	Carbon paper	Hollingsworth & Vose Company
2	AvCarb GDS 2120	The fuel cell store
3	PUREBLACK® carbon	Superior Graphite Co.
4	VULCAN® carbon	Cabot Co.
5	Isopropyl alcohol	Sigma Aldrich
6	Polyethylene glycol	Sigma Aldrich
7	Sodium dodecyl sulfate	Acros Organics
8	Hydrogen peroxide	Carolina
9	Potassium permanganate	Carolina
10	Sodium oxalate	Carolina
11	Polytetrafluoroethylene (PTFE)	Dupont
12	Nafion membrane	Ion Power Inc
13	Electrocatalyst	Tanaka
14	Nafion solution	Ion Power Inc

15	Deionized water	In-house

3.2 Characterization Methods

Two characterization methods of GDLs influence the fuel cell performance: ex-situ (GDLs alone) and in-situ (within the fuel cells) methods. Various GDL properties, such as porosity hydrophobicity, and morphology, can be examined by ex-situ methods [157]. The ex-situ method can be very useful as a process control tool; however, in-situ methods are of equal importance as they are critical for understanding the GDLs under actual fuel cell operating conditions. The in-situ characterization of the GDLs can be conducted by assembling and testing PEMFC single cells. Galvanostatic polarization curves can be used to characterize GDLs at various RH conditions and temperatures using H_2/O_2 or H_2/air in PEMFC [158].

3.2.1 Scanning Electron Microscopy (SEM)

The scanning electron microscope (SEM) is one of the most adaptable instruments available for microstructure morphology examination and analysis. The electron gun, located on the top of the column, produces the electrons and accelerates them to an energy level of 0.1–30 keV. The electron beam diameter is too large to form a high-resolution image, so electromagnetic lenses and apertures are used to focus and define the electron beam and form a small, focused electron spot on the specimen. Images are formed by moving the electron beam across the specimen using deflection coils inside the objective lens. At the lower part of the column the specimen stage and controls are located. The

secondary electrons from the specimen are attracted to the detector by a positive charge. In scanning electron microscopy visual inspection of the surface of a material utilizes two types of signals, secondary and backscattered electrons. They are constantly being produced from the surface of the specimen while under the electron beam. High-vacuum environment is required, to avoid electron scattering by the air [159]. In the current study, SEM XL-30 was used (Arizona State University, Tempe Campus).

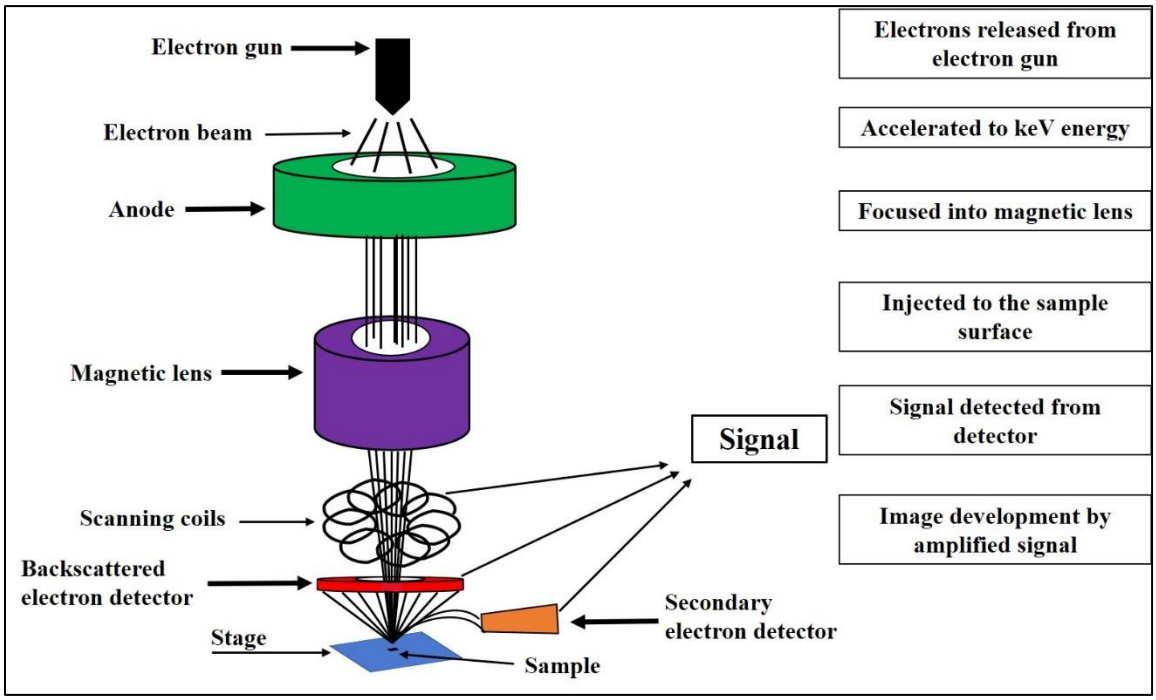

Figure 9. SEM schematic design and description

3.2.2 Contact Angle

The contact angle is a method used to determine how likely a surface is to be wetted by water. The measured angle is the angle at the interface where water, air, and solid meet. Low contact-angle values demonstrate a tendency of the water to spread and adhere to the surface (hydrophilicity), whereas high contact-angle values show the surface's tendency to

repel water (hydrophobicity). The simplest and most used method for surface-wetting characterization is sessile-drop goniometry. This method determines the contact angle from the shape of the droplet and can be applied to a wide variety of materials [160].

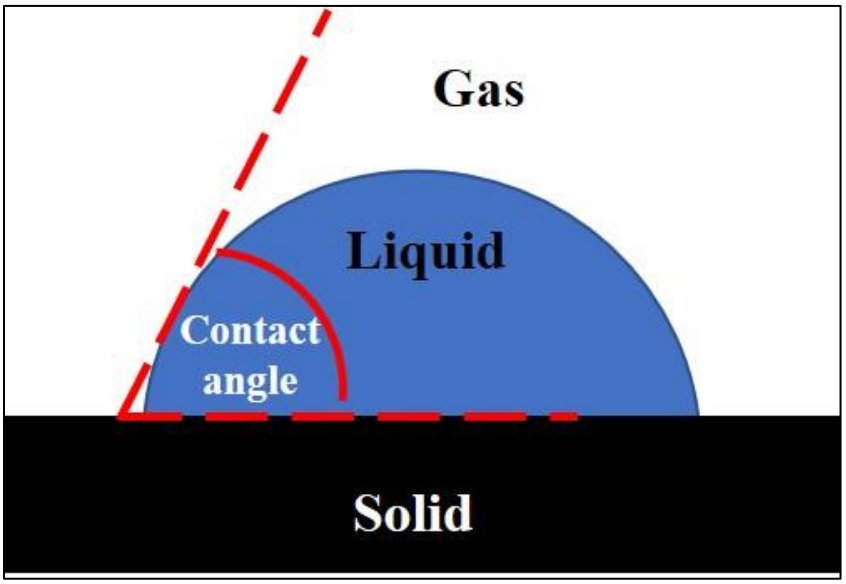

Figure 10. Contact angle measurement.

3.2.3 Mercury Intrusion Porosimetry

Mercury intrusion porosimetry (MIP) is a technique utilized for the evaluation of porosity, pore size distribution, and pore volume to characterize a wide variety of solid and powder materials. The instrument, known as a porosimeter, employs a pressurized chamber to force mercury to intrude into the voids in a porous substrate. As pressure is applied, mercury fills the larger pores first. As pressure increases, the filling proceeds to smaller and smaller pores. The volume of liquid metal that penetrates a solid is measured as a function of applied pressure. Both the inter-particle pores (between the individual particles) and the intra-particle pores (within the particle itself) can be characterized using this technique. The Washburn Equation (equation (14)) relates the applied pressure to pore

diameter using physical properties of the non-wetting liquid (mercury). The physical properties include the contact angle between the mercury and the material, as well as surface tension [161].

$$P = \frac{-2\gamma cos\theta}{r} \quad (14)$$

Where P: the imposed pressure, r: the pore radius, γ: the surface tension of mercury, θ is contact angle of mercury with the material. The values of γ and θ are 480 erg/cm^2 and 140° respectively. The Washburn equation is generally accepted as a practical method of analyzing very complex pore systems, since pores are rarely cylindrical.

3.2.4 Fuel Cell Testing

A polarization curve is used to assess the performance of a fuel cell. It is a method widely utilized and it provides an easy comparison to other published data. The polarization curve depicts the voltage output for a given current density loading of the fuel cell. Polarization curves are taken with a potentiostat/galvanostat drawing a fixed current from the fuel cell and measuring the fuel cell output voltage. Slowly varying the steps on the load on the potentiostat, the voltage response can be determined [162]. Figure 8 shows the Fuel Cell Testing Equipment.

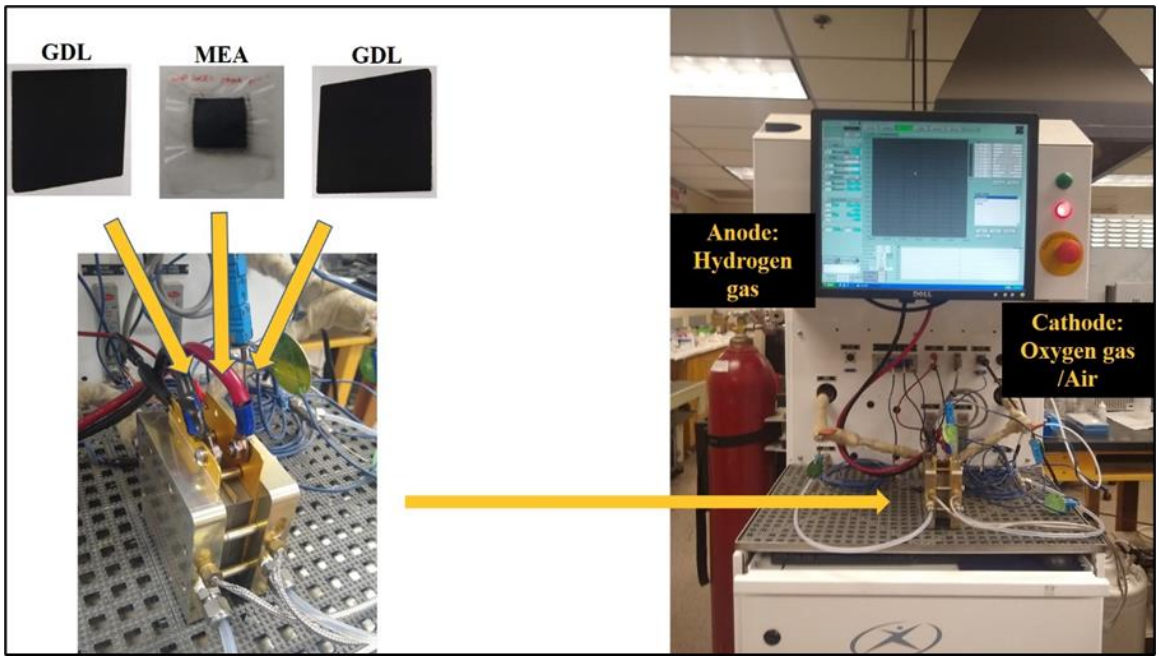

Figure 11. Fuel cell testing equipment

The theoretical Open Circuit Voltage (OCV) for PEMFC with pure H_2 is 1.23V; however, the actual performance is lower due to cell resistance, slow kinetics of the oxygen reaction and gas transport limitations. The polarization curve has three areas of interest when it comes to losses, depicted in Figure 12 [44]:

- At low current densities, the cell potential drops as a result of the activation polarization.
- At intermediate current densities, the cell potential drops linearly with current due to ohmic losses.
- At high current densities, the cell potential drops as a result of concentration polarization.

Activation polarization is the voltage overpotential required to overcome the activation energy of the electrochemical reaction on the catalytic surface. This type of polarization dominates losses at low current density and measures the catalyst effectiveness at a given temperature. This is a complex three-phase interface problem, since gaseous fuel, the solid metal catalyst, and electrolyte must all make contact. The catalyst reduces the height of the activation barrier, but a loss in voltage remains due to the slow oxygen reaction [163]. The total activation polarization overpotential is 0.1 to 0.2 V, which reduces the maximum potential to less than 1.0 V even under open-circuit conditions.

The ohmic polarization is typically dominated by electrolyte conductivity, which is primarily a function temperature. Specifically, in the case of PEM fuel cells, water content can also play a part in ohmic polarization. A reduction in losses can be achieved through advanced conductive materials, thinner electrolytes, or an optimal temperature/water balance. One of the most effective methods of reducing ohmic loss is to use a better ionic conductor for the electrolyte layer, or a thinner electrolyte layer since the electrolyte component of a fuel cell dominates the ohmic losses [164]. Since the fuel cell must continuously be supplied with fuel and oxidant to produce electricity, products must continuously be removed to reach maximum fuel cell efficiency. The reactant and product concentrations within the catalyst layer determine the fuel cell performance.

In PEMFCs, liquid water accumulation and pore blockage in the pores of the electrolyte, can result in significant mass transport limitations. Concentration loss can be minimized by the optimization of the mass transport in the fuel cell electrodes and flow structures [165]. On the fuel cell, when the current is changed, heat and water balance

change, and it may take several minutes to hours for the fuel cell to reach a new equilibrium point. During testing, a designated period of time should be used to allow the fuel cell to reach the new equilibrium. The load can be adjusted in various ways. Typically, the load is set to increase or decrease by a certain step-size. The data can be recorded at multiple current or voltage points.

A difference in polarization curves between a cell operating with air and pure oxygen are often used to characterize flooding or cathode problems. The difference in cell voltage between pure oxygen and air results from the difference in the concentration of oxygen at the catalyst surface and should be nearly constant at any current density. At higher current densities, mass transport problems can be identified by an increase in cell potential difference between oxygen and air [166].

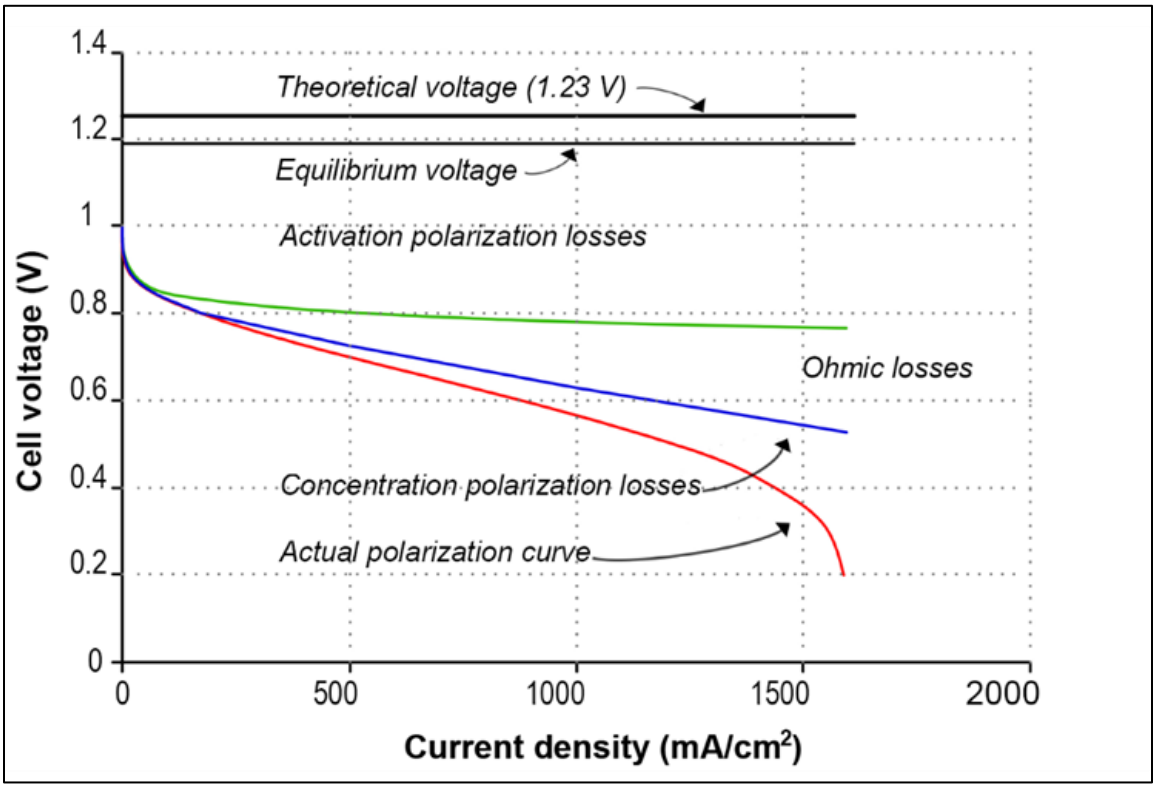

Figure 12. Representation of polarization losses

4. EXPERIMENTAL

4.1 Fabrication of GDLs configurations with PUREBLACK®

Non-woven, teflonized carbon paper (GD07508G) from Hollingsworth & Vose Company, USA was used as substrate. Nano-chain carbon powder PUREBLACK® 205-110, from Superior Graphite Co., Teflon Emulsion (PTFE DISP30) from Dupont, sodium dodecyl sulfate (SDS) from Acros Organics (CAS# 151-21-3) and polyethylene glycol (PEG-1500) from Aldrich Chemistry (CAS# 25322-68-3) were used for preparing slurry for fabricating the MPL. Briefly, 0.5 g of PUREBLACK® carbon was dispersed in 80 mL isopropyl alcohol solution (Sigma-Aldrich, 99.7%, CAS# 67-63-0) containing 120 mg of SDS and various amounts of PEG (see Table 1), by sonication for 30 min, followed by stirring for 60 min. The Teflon emulsion (34 wt. %) was added dropwise into the mixture and stirred for 15 min to obtain homogenous slurry. A 10 x 10 cm^2 carbon paper substrate was coated with the carbon slurry by micro-spray technique. The coated samples were dried at room temperature overnight and sintered in air at 350 °C for 30 min, to achieve uniform distribution of PTFE on the carbon powder and thermal decomposition of PEG [167]. Subsequently, the samples were rinsed thoroughly in DI water to remove the SDS and the residual PEG.

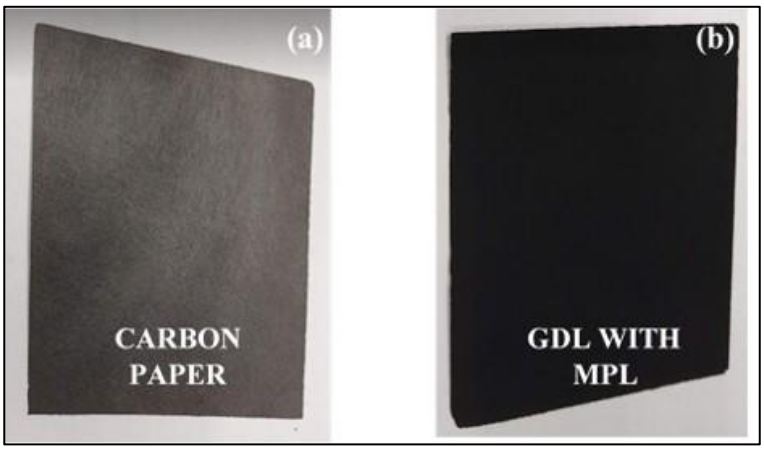

Figure 13. Fabricated gas diffusion layer (a) without and (b) with MPL

As shown in Figure 14, GDLs samples were fabricated with MPLs with and without PEG in single, and four-layer configurations, as described above, for each sublayer. The total carbon loading on the MPL was 3 ± 0.15 mg.cm^{-2} for all samples. Each sublayer was created with the same amount of carbon powder within a GDL sample by only varying the PEG (wt. %) content for the porosity graded GDL fabrication. Figure 11 provides the configuration of the three different GDL samples with the sequence of porosity gradient from the flow field plates to the catalyst layer in the MEA. The surface morphology and cross-section of the GDL samples were examined by XL-30 Environmental FEG (FEI) Scanning Electrode microscope (XL30ESEM-FEG). Surface-wetting characteristics of the GDLs was evaluated by performed sessile-drop goniometry (Krüss Easy Drop), using IPA-water mixture (30:70). The pore size distribution of the GDL samples was analyzed in low and high-pressure modes using PoreMaster-60 Automatic Mercury Intrusion Analyzer (Quantchrome Tech, Florida). The commercial GDL (AvCarb GDS 2120) from Fuel Cell Store was employed for fuel cell performance comparison.

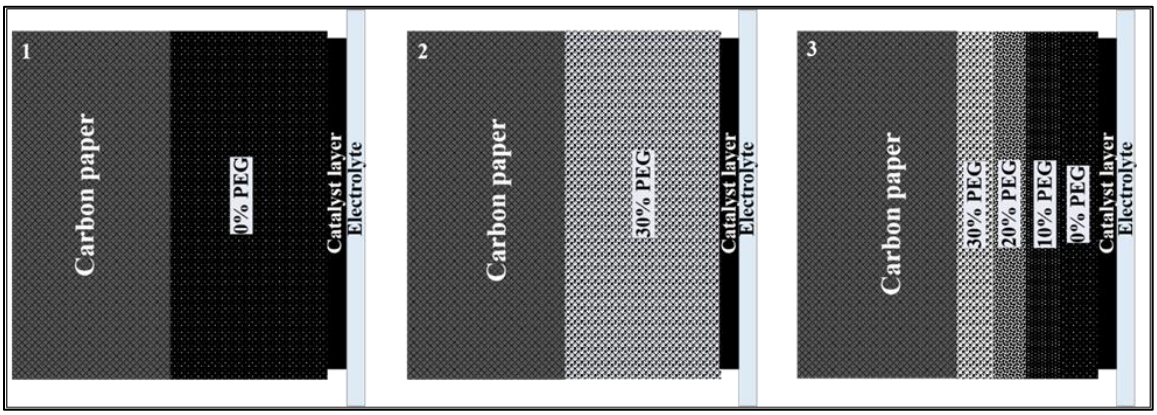

Figure 14. Configuration of gas diffusion layer samples 1 - 3.

4.2 Fabrication of GDLs for Accelerated Stress Testing

Nano-chain carbon powder PUREBLACK® 205-110 from Superior Graphite Co. and VULCAN® (XC 72R GP-3875) from Cabot Co., Teflon Emulsion (PTFE DISP30) from Dupont, sodium dodecyl sulfate (SDS) from Acros Organics (CAS# 151-21-3) and polyethylene glycol (PEG-1500) from Aldrich Chemistry (CAS# 25322-68-3) were used for slurry preparation for the MPL. Briefly, 0.5 g of PUREBLACK® carbon was dispersed in 80 mL isopropyl alcohol solution (Sigma-Aldrich, 99.7%, CAS# 67-63-0) containing 120 mg of SDS and 30%wt. PEG by sonication for 30 min, followed by stirring for 60 min. The Teflon emulsion (34 wt. %) was added dropwise into the mixture and stirred for 15 min to obtain homogenous slurry. A 10 x 10 cm^2 carbon paper (GD07508T, Hollingsworth & Vose Company, USA) was used as a macro-porous layer substrate. was coated with the carbon slurry by micro-spray technique. The coated samples were dried at room temperature overnight and sintered in air at 350 °C for 30 min, to achieve uniform distribution of PTFE on the carbon powder and thermal decomposition of PEG. The total

carbon loading on the MPL was 3 ± 0.15 mg.cm^{-2} for all samples. Subsequently, the samples were rinsed thoroughly in DI water to remove the SDS and the residual PEG.

4.3 Accelerated Stress Tests (AST)

Two methods, in warm water and warm hydrogen peroxide, were employed for accelerated stress testing of GDL samples made with PUREBLACK® and VULCAN®.

4.3.1 AST in water

GDL samples (5 Nos. of 2.5 × 2.5 cm^2), immersed in deionized water, were placed in a constant temperature oven, and maintained for 1000 h at a temperature of 80 °C. Ultimately, the samples were rinsed in deionized water and dried at 80 ºC overnight [145,168]. Although this process does not represent the conditions of the GDL in a PEMFC cathode, it allows characterization of the GDL substrate and MPL without requiring separation from the MEA. Due to the lack of electrolyte, the electrochemical corrosion is impossible, however, despite the slow kinetics of these reactions at 80°C, direct reaction between the carbon surfaces and water is possible. Possible hydrophobicity loss can be caused due to accumulation of oxygen-containing groups on the surface of the GDLs and PTFE fall off [169].

4.3.2 AST in hydrogen peroxide

To facilitate accelerated degradation of the gas diffusion layer through carbon corrosion, the GDLs were submerged in a 30 % solution of hydrogen peroxide at 90°C for 24 hours. During degradation, the H2O2 concentration was determined by manganometric redox titration with KMnO4 every 8 h. Following degradation, the samples were rinsed

and soaked in deionized water for 12 hours and dried in the oven at 80°C overnight [170,171].

Both the PUREBLACK® and VULCAN® GDLs were examined before and after ASTs for surface morphology (XL-30 Environmental FEG (FEI)) Scanning Electrode microscope (XL30ESEM-FEG), surface-wettability (Krüss Easy Drop, using IPA-water mixture (30:70)), and pore size distribution (PoreMaster-60 Automatic Mercury Intrusion Analyzer, Anton Paar QuantaTec Inc, Florida).

4.3.3 Manganometric redox titration

To determine the hydrogen peroxide concentration during the AST process, manganometric redox titration was implemented. Potassium permanganate ($KMNO_4$) was used as titrant due to its strong oxidizing effect and color which makes the use of an indicator, for the visual detection of equilibrium point, unnecessary. In brief, 3.3 g of potassium permanganate, Crystal (Carolina, CAS # 7789-00-6), was transferred in 1L of boiling water, to accelerate the reaction kinetics, and stirred. The solution was strained through a glass wool funnel to remove byproducts and impurities and stored in a dark container, since its decomposition reaction is catalyzed by light. For standardization of the oxidizing solution, 0.2 g of sodium oxalate ($Na_2C_2O_4$, Carolina, CAS # 2-76-0) was dissolved in 250 mL of deionized water. 10 mL concentrated sulfuric acid (Sigma Aldrich, Reagent Grade 96%, S.G: 1.84, CAS# 7664-93-9) were added in the solution to enhance oxidation ability of the $KMnO_4$ during titration. The sodium oxalate solution was heated to 70 ^oC and was titrated with potassium permanganate until equilibrium was achieved

(light pink color). The concentration of potassium permanganate solution was calculated by equation (15) to be 0.1N.

$$N = \frac{m_{oxalate}*1000}{V_{titrant}*67} \quad (15)$$

GDL samples were aged in 30% hydrogen peroxide solution at 90 °C for 24 h. To determine the change in hydrogen peroxide concentration during the aging process, ~10 g of hydrogen peroxide solution was diluted in 250 mL water and an aliquot was transferred to a beaker containing 10 mL sulfuric acid and titrated using potassium permanganate until light pink, according to the chemical reaction described by equation (16):

$$5\ H_2O_2 + 6\ H^+ + 2\ KMnO_4 \Leftrightarrow 5\ O_2 + 2\ Mn^{2+} + 8\ H_2O + 2\ K^+ \quad (16)$$

The concentration of hydrogen peroxide was calculated using equation (17):

$$\%\ H_2O_2 = \frac{V*N*0.01701*DF}{m} \quad (17)$$

Where V: the volume of potassium permanganate used in mL, N: potassium permanganate normality, 0.01701: weight per milliequivalent of H_2O_2, DF: dilution factor, m: mass of weighted sample in grams.

4.4 Membrane electrode assembly fabrication and fuel cell evaluation

Catalyst Coated Membranes (CCMs) were fabricated using Pt catalyst (TEC10E50E, 46 % Pt on carbon, Tanaka) ink in isopropyl alcohol (15 mL for 1g of

catalyst) containing 1.2 mL Nafion dispersion (LIQUION LQ-1105, 5 wt. % Ion Power, Inc.,) [172]. Nafion membrane (Membrane NR-211) from Ion Power, was coated with catalyst (geometrically active area: 5 cm^2) ink using micro-spray technique to obtain Pt loading of ~0.4 mg per cm^2 on both the anode and cathode sides. A single cell fuel cell (Fuel Cell Technologies Inc, USA) was used for evaluating the membrane electrode assemblies with the CCMs and GDL samples. Silicone coated fabric gaskets (Product # CF1007, Saint-Gobain Performance Plastics, USA) were used to achieve gas sealing with uniform torque of 4.5 Nm. The fuel cell performance was evaluated at 70 °C using Greenlight Test Station (G40, Hydrogenics, Canada) using H_2/O_2 and H_2/Air, by galvanostatic polarization method. Various RH conditions (60 and 100 %) of the fuel cell test cell was controlled by varying the humidity bottle temperatures. The anode and cathode gas flow rates were set to 200 and 300 SCCM, respectively throughout the testing. The fuel cell durability was evaluated for the MEA with the PUREBLACK® and VULCAN® based GDLs containing 30% PEG, and the commercial GDL, using H_2/Air at 60 and 100 % RH condition at constant current (600 $mA.cm^{-2}$).

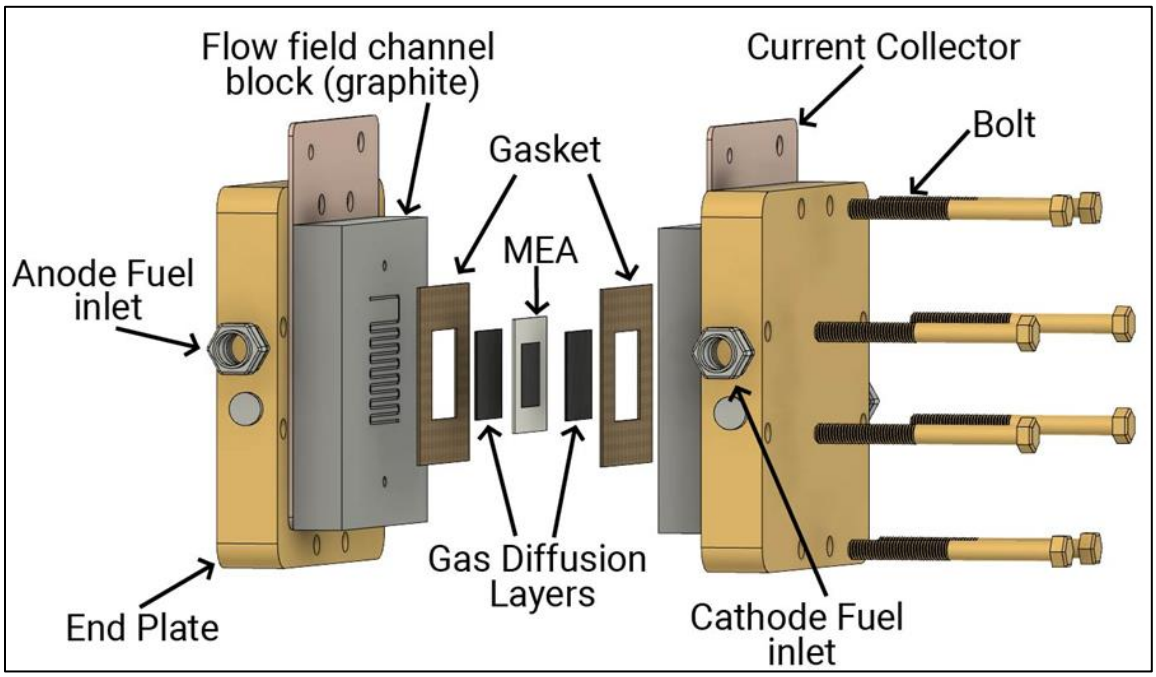

Figure 15. CAD model of single-cell fuel cell.

5. RESULTS AND DISCUSSION

5.1 Design and development of gas diffusion layers using pore forming agent for PEMFCs at various RH conditions.

5.1.1 Surface morphology and cross-section of GDLs

Figure 16 shows the surface morphology of PUREBLACK® based GDLs with and without PEG along with the commercial GDL sample. As seen from Figures 16(a) and 16(c), the sample 1 (single MPL sublayer without PEG) and sample 3 (four MPL sublayers with the top layer without PEG), the surface appeared to have relatively smaller pores compared to the sample 2 (single MPL sublayer with 30 % PEG). However, the commercial GDL exhibited larger mud-cracks in multiple locations on the surface (Figure 16(d)). Although it has been reported that larger pores can reduce electrical conductivity [117], the smooth, crack-free surface and homogenous nature of MPL could lead to uniform reactant gas transport to the reaction zone and effective water removal, avoiding flooding [173]. The cracked surface of the commercial GDL (Figure 16(d)) could cause poor electrical conductivity and rapid MPL degradation by accumulating water and forming defects around the cracks [117,130]. In particular, non-uniform reactant gases distribution and water removal could also lead to hot spots at the reaction zone.

Table 2. Configuration and properties of gas diffusion layer samples.

Sample ID	MPL sublayer	PEG (wt. %)	Contact angle (Degrees)	Pore volume ($cc.g^{-1}$)	Low pressure pore diameter (μm)	High pressure pore diameter (nm)	Porosity %
1	1	0	130 ± 2	1.48	47	90	~50
2	1	30	115 ± 2	1.72	44	90	~55
3	4	0,10,20,30	125 ± 2	1.23	43	90	~40
Commercial	1	-	87 ± 2	1.45	54	~300	~50

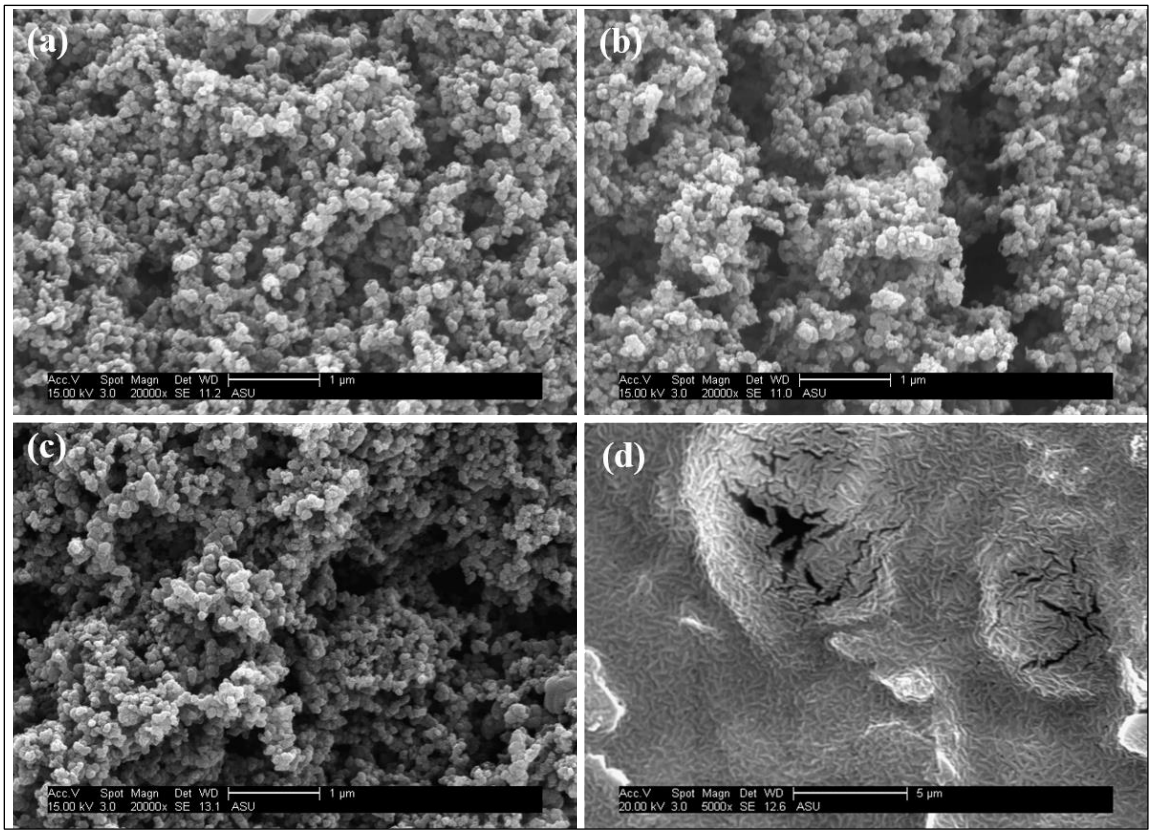

Figure 16. Scanning electron micrographs of (a) to (c) PUREBLACK® based GDLs (samples 1-3), and (d) commercial GDLs (AvCarb GDS 2120).

Cross-sectional images were also recorded for the PUREBLACK® based GDLs with and without PEG along with the commercial GDL sample in order to examine the bulk characteristics. As seen from Figure 17(a)-(c), the MPL thickness of the PUREBLACK® based GDLs range between 60-70 μm. However, accurate measurement was difficult due to carbon bleed through the uncoated side of the macroporous substrate. The commercial GDL (Figure 17(d)) shows a relatively thinner MPL coating of 25-30 μm, making the electrode more sensitive to flooding as the MPL provides higher back-diffusion rate from the cathode to the anode through the membrane, reducing the liquid water saturation level in the catalyst layer [174].

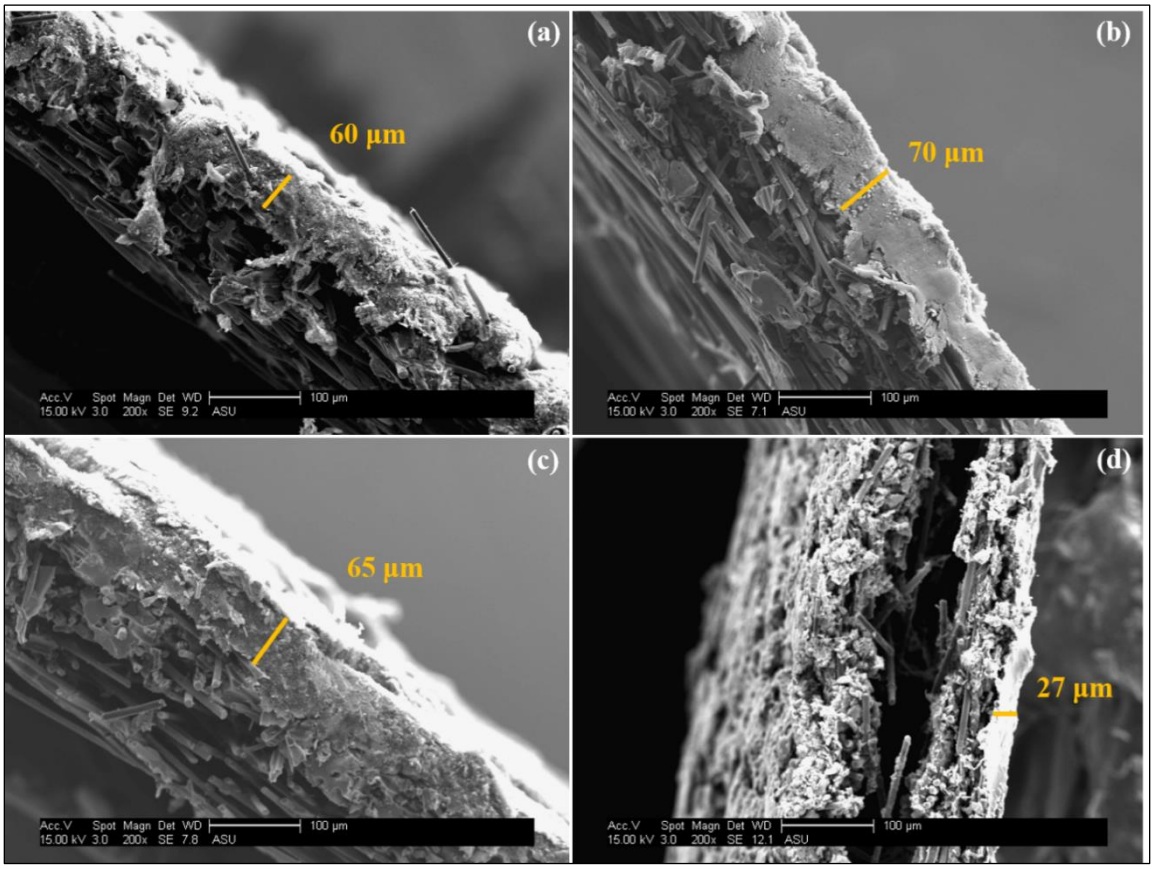

Figure 17. Scanning electron micrographs (cross-section) of (a) to (c) PUREBLACK® based GDLs (samples 1-3), and (d) commercial GDLs (AvCarb GDS 2120).

5.1.2 Contact angle

The surface wettability was assessed for the PUREBLACK® based GDLs with and without PEG along with the commercial GDL sample in order to examine the hydrophobic and hydrophilic characteristics of the MPL surface, using IPA-water mixture (30:70). As all the PUREBLACK® based GDL samples had 34 wt. % PTFE in the MPL, the surface was expected to display hydrophobic characteristics. As shown in Figure 18(a)-(c), the contact angle values are about 130, 115 and 125 degrees and the variation are well within two degrees for five samples in each category (see Table 2). Relatively higher hydrophobic

surface of the MPLs was expected to facilitate the gas flow to the catalyst layers by removing the excess liquid water efficiently [175]. It is worth noting that the lower contact angle for the GDL sample 2 (Figure 18(b)) is an indication of the higher porosity of the MPL. The trend in the contact angle values are in the following order (see Figure 14 (1, 2 and 3)):

GDL #2 (PEG = 30%) < GDL #3 (PEG = 0, 10, 20, 30 %) < GDL #1 (PEG = 0%)

However, the commercial GDL showed hydrophilic characteristics with a contact angle of 87 degrees, which could lead to flooding and lower fuel cell performance at 100 % RH condition [105].

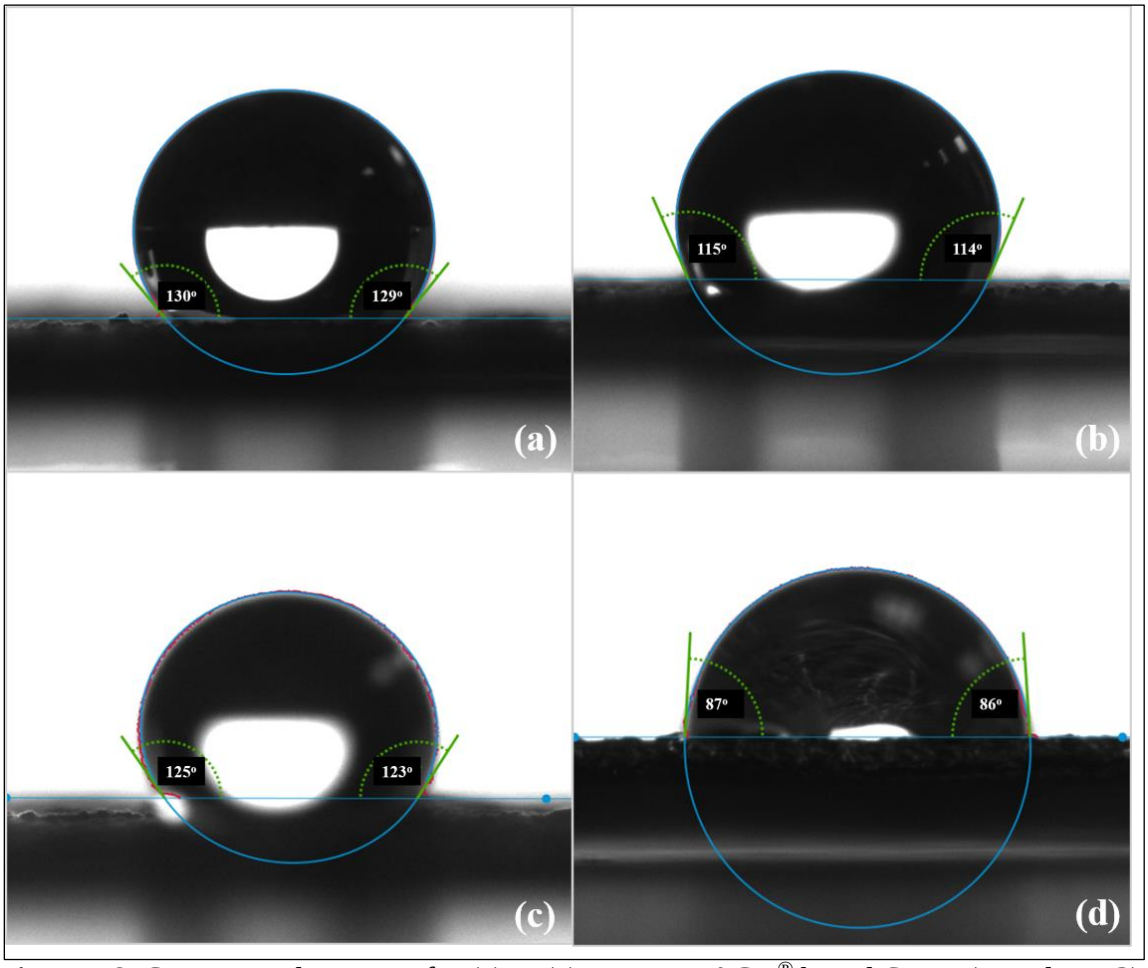

Figure 18. Contact angle images for (a) to (c) PUREBLACK® based GDLs (samples 1-3), and (d) commercial GDLs (AvCarb GDS 2120).

5.1.3 Pore size distribution

In order to study the effect of pore forming agent on the fuel cell performance in various RH conditions, the pore size distribution was measured for the GDL samples by mercury porosimetry at low and high pressures. Figure 19 compares the pore size distribution for the PUREBLACK® based GDLs with and without PEG along with the commercial GDL sample. The high-pressure region below 1μm, represents the meso- and micropores of the MPLs responsible for gas transfer and the low-pressure region above 1μm, where the majority of pores appear, represents the larger macropores responsible for

water expelling [83,176]. As seen from Figure 19, the GDL with 30 % PEG (sample 2) also shows nanopores (shoulders in the range of 20–40 nm), which might keep the product water at the catalyst layer/electrolyte reaction zone for retaining the electrolyte conductivity at lower RH operating conditions. The total pore volume of the GDL with 30 % PEG is also the highest (1.72 $cc.g^{-1}$, Table 2) among all the samples, providing the required amount of reactants for extending the limiting current density, specifically with air as oxidant. In addition, the sample 2 exhibits the highest pore size distribution in the low-pressure region (macroporous carbon substrate), confirming its capability of efficient water removal. The total pore volume and the pore diameter values (high pressure for smaller pores in the MPL and the low pressure for larger pores in the carbon paper substrate) are also consolidated in Table 2.

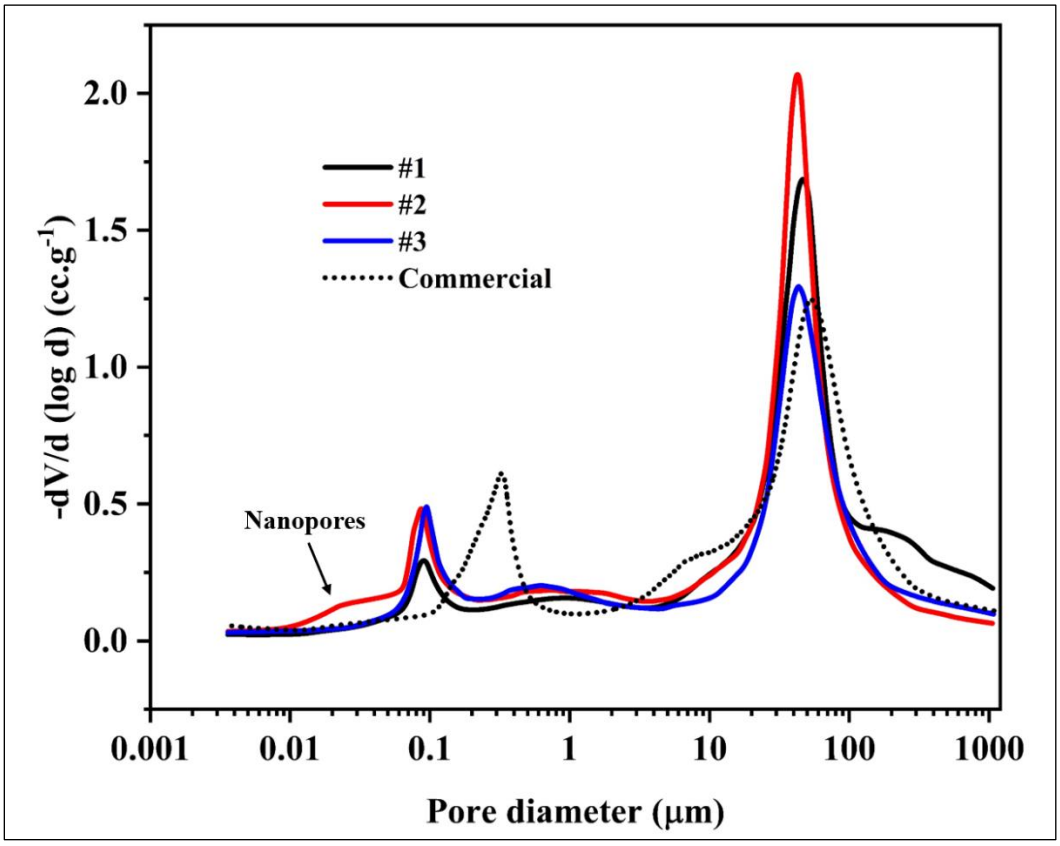

Figure 19. Pore size distribution for PUREBLACK® based GDLs (samples 1-3) along with commercial GDL.

As seen, the creation of pores using PEG (sample 2 and 3) significantly increased the pore size distribution compared to the GDL without PEG (sample 1), leading to better gas transport to the reaction zone. However, the commercial GDL manifests with larger pore sizes in both of the regions, probably due to surface cracks along with relatively larger pores in the MPL, with poor water transport characteristics both at lower and higher RH conditions. Considering the four sub-layer configuration of the GDL sample 3, the decreased pore size distribution observed in the low-pressure area can be attributed to

larger pore blockage of one MPL sublayer when the next sublayer is deposited [177], which might lead to flooding at higher RH conditions.

5.1.4 Fuel cell performance

The fuel cell performance for all the PUREBLACK® based and commercial GDL samples are shown in Figures 20 and 21 using H_2/O_2 and H_2/air, respectively at 60 and 100 % RH conditions at 70 ^oC. In order to minimize membrane dehydration, the MEAs were evaluated at 100 % RH first before lowering the RH condition to 60 % on both the anode and cathode sides. Figures 20(a) and 21(a) depict the fuel cell performance for the PUREBLACK® based GDLs (sample 1) without pore forming agent using O_2 and air as oxidants at 60 and 100 % RH conditions.

At 100 % RH, the peak power density is much lower (1255 $mW.cm^{-2}$) compared to that at 60 % RH (1430 $mW.cm^{-2}$) with O_2 as oxidant (Figure 20(a)). Similar trend is also observed with air as oxidant, with peak power density values of 436 and 397 $mW.cm^{-2}$ at 60 and 100 % RH, respectively (Figure 21(a)). GDL sample 1 without PEG showed lower pore volume (see Figure 19), causing the MEA to flood at 100 % RH condition [178] with reduced performance. Figures 20(b) and 21(b) show the fuel cell performance using PUREBLACK® based GDL with 30 % PEG as forming agent in the MPL using O_2 and air as oxidants, respectively. As seen from Figure 20(b), the peak power density values of 1325 $mW.cm^{-2}$ at 100 % RH and 1355 $mW.cm^{-2}$ at 60 % RH are observed. Similar performance trend is shown with air as oxidant (Figure 21(b)) with peak power density values of 444 and 432 $mW.cm^{-2}$ at 60 and 100 % RH, respectively. Almost similar fuel cell performance at both 60 and 100 % RH (using O_2 or air) can be attributed to higher porosity

(see Figure 19), facilitating better water transport without any flooding, in particular at 100 % RH conditions [179]. Slightly higher peak power density for the MEA with the GDL sample 2 using air as oxidant at 60 % RH could be due to the presence of nanopores (Figure 19) in retaining the product water without drying of the electrolyte [180].

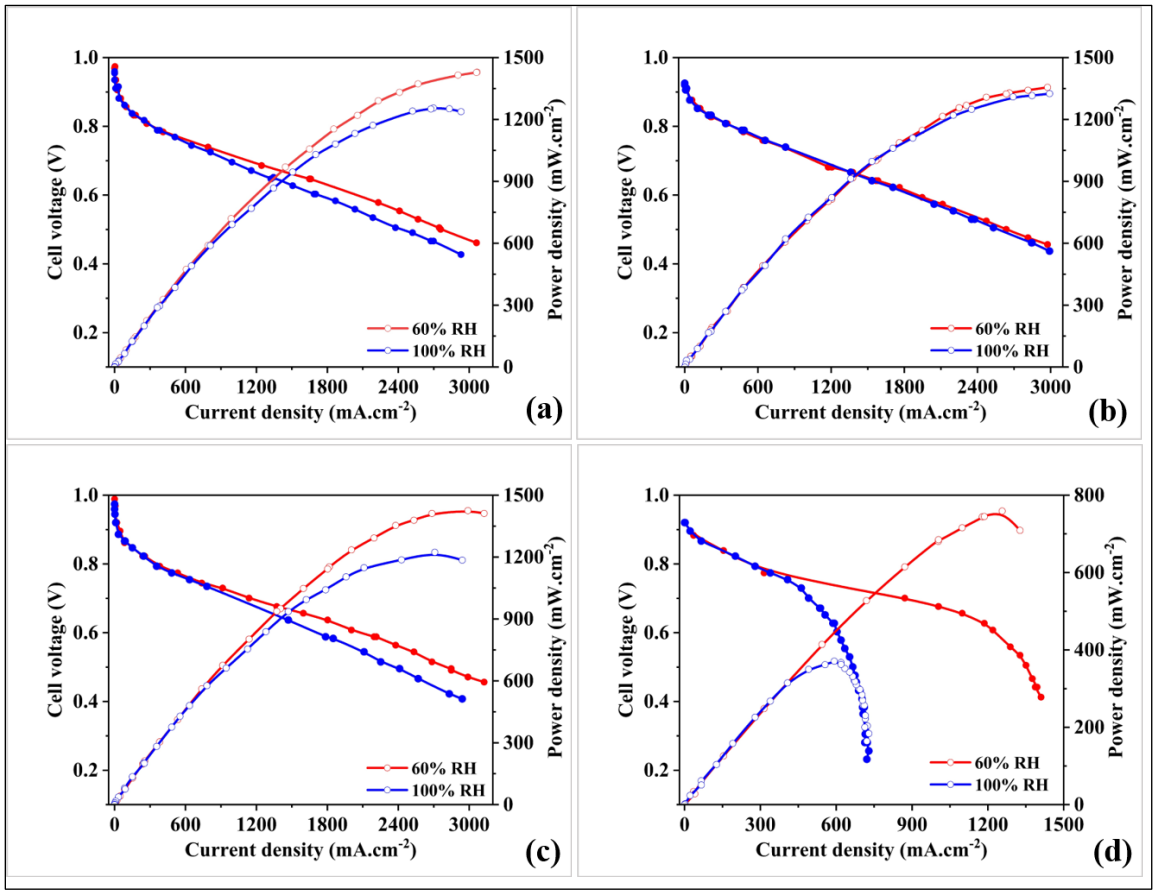

Figure 20. Fuel cell performance at 70 ºC using H_2/O_2 at 60 and 100 % RH for MEAs with (a) to (c) PUREBLACK® based GDLs (samples 1-3), and (d) commercial GDLs (AvCarb GDS 2120).

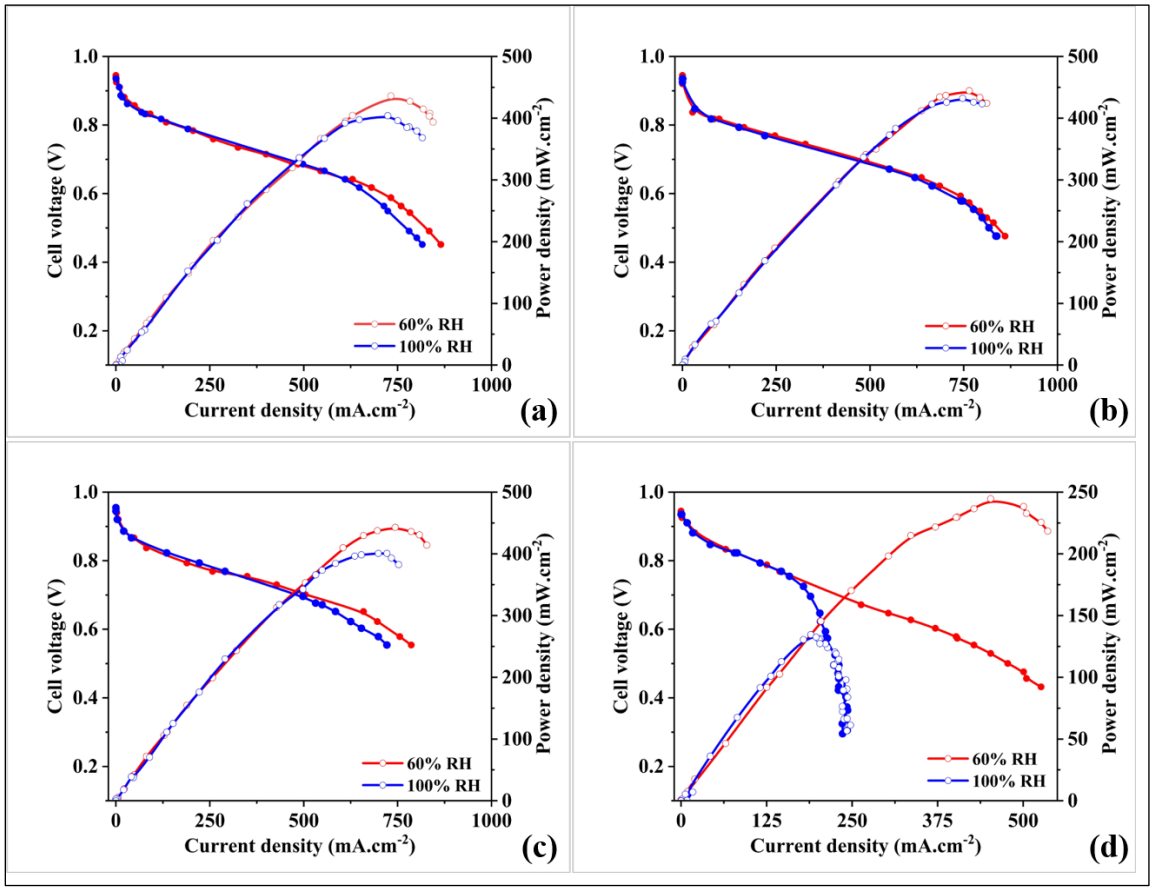

Figure 21. Fuel cell performance at 70 ºC using H_2/air at 60 and 100 % RH for MEAs with (a) to (c) PUREBLACK® based GDLs (samples 1-3), and (d) commercial GDLs (AvCarb GDS 2120).

Figures 20(c) and 21(c) show the fuel cell performance using PUREBLACK® based GDL (sample 3) with graded porosity (0, 10, 20, 30% PEG) using O_2 and air as oxidants at 60 and 100 % RH conditions. Evidently, the graded porosity did not seem to have a significant effect in the fuel cell performance, as the peak power densities for 60 and 100 % RH appears to be 1425 and 1224 mW.cm^{-2} with O_2 gas, and 442 and 400 mW.cm^{-2} with air as oxidant gas, respectively. Since the first MPL sublayer deposited on the carbon substrate has greater amount of PEG and followed by sublayers with gradually

decreased amount of PEG, the MPL carbon can block some of the larger pores created in each previous sublayer. This configuration with reduced amount of macropores (Figure 19) required for water transport is prone to flood at 100 % RH condition, leading to lower fuel cell performance [177].

The fuel cell performance is shown in Figures 20(d) and 21(d) for the MEAs with commercial GDL using O_2 and air as oxidants at 60 and 100 % RH conditions, solely for comparison purposes. The commercial samples exhibit very poor performance of 761 $mW.cm^{-2}$ at 60 % RH and 370 $mW.cm^{-2}$ at 100 % RH in H_2/O_2. Similar trend is also exhibited using H_2/air, with peak power densities of 258 and 134 $mW.cm^{-2}$ at 60 and 100 % RH, respectively. Presumably, the commercial GDL sample with cracked surface morphology [117] (see Figure 16) along with highly the hydrophilic characteristics [105] (see Figure 18) of the microporous layer, and lower pore volume (see Figure 19) of the macroporous layer do not promote efficient water transport mechanism. In addition, the thinner MPL can enhance the liquid water saturation level in the GDL, leading to reduced membrane conductivity, compromising the fuel cell performance [156].

5.1.5 Durability test

GDL samples without and with 30 % PEG on the MPL (samples #1 and 2) were selected for durability test, because of their high and stable performance using H_2/air as oxidant in lower and higher RH conditions. Initially, the system was fully hydrated, and polarization measurements were carried out prior to each RH change [181]. Figure 22(a) shows the fuel cell performance for the MEA with the GDLs without PEG and Figure 19(b) containing 30 % PEG using H_2/air at 60 and 100 % RH, prior to evaluating the performance

stability at each RH condition. Figure 22(d) and (e) show the cell voltage at 600 $mA.cm^{-2}$ for 50 h at 100 % RH first and then for 50 h at 60 % RH conditions for the MEAs containing GDLs without and with 30% PEG, respectively.

As can be seen from Figure 22(b), the fuel cell performance remains identical at 60 % RH after 50 h of continuous cell operation and at 100 % RH, with a peak power density of ~400 $mW.cm^{-2}$ with a negligible degradation. As demonstrated in Figure 22(a), the fuel cell performance is slightly higher at 60% RH and although the voltage is higher, there is a fluctuation between 0.59 to 0.62V after ~35h of continuous operation (Figure 22(d)), possibly due to temporary O_2 starvation caused by flooding [182]. At 100% RH, the voltage slightly decreases to 0.58V, however the difference is insignificant as the fuel cell performance is not governed by mass transport at this region. As reported in the literature [183,184], the PUREBLACK® carbon with well-defined graphitic structure in the GDL is known to resist the corrosion during fuel cell operation. In addition, it is also reported that the fuel cell performance improvement at 60% RH after 10h of accelerated testing confirmed the assumption that in saturated conditions (100% RH), O_2 transport to the reaction zone was reduced due to flooding, especially at high current densities with the dominance of mass transport [185]. Evidently, the cell voltage remained fairly stable around 0.58 V both at 60 and 100 % RH conditions, demonstrating the suitability of the nano-sized core-shell PUREBLACK® carbon based microporous layer with 30 % PEG [186,187]. The commercial GDL sample was also tested for durability (Figures 19(f)) but the fuel cell performance was very poor due severe flooding (Figure 22(c)). The lower FC

performance is also the reason why the durability test for the commercial GDL was conducted at lower current density (at 400 mA.cm-2) compared to GDLs #1 and #2.

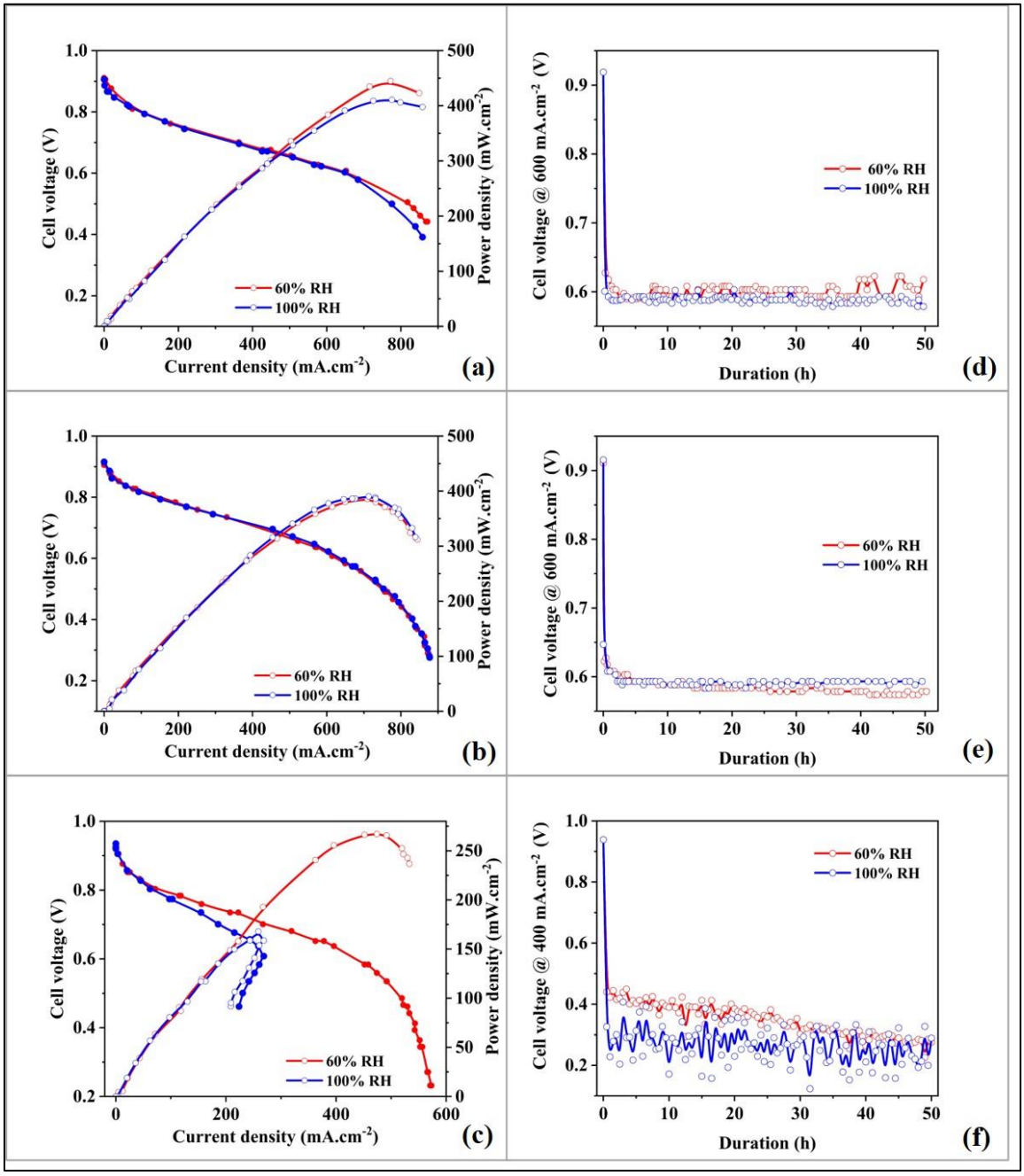

Figure 22. Fuel cell performance at 70 °C using H_2/air at 60 and 100% RH for 1, 2 and commercial sample, respectively (a)-(c) (b), and durability at 600 mA.cm^{-2} for samples 1 and 2 (d)-(e), and at 400 mA.cm^{-2} for the commercial sample (f).

5.2 Accelerated stress tests on gas diffusion layers with different carbon types for PEMFCs at various relative humidity conditions.

5.2.1 Surface morphology

Surface morphology of the samples was examined by Scanning Electron Microscopy and shown in Figure 23. As seen, the surface appears relatively smooth for both pristine samples (Figure 23(a) and (d)). After immersing the PUREBLACK® sample in warm H_2O_2 (30%) for 24 h, the surface manifests black spotting but there are no signs of deep penetration or cracks in the MPL layer (Figure 23(b)). This indicates that if there are wettability changes, they may only be superficial and not affect the pore hydrophobicity [188]. Figure 23(c) shows the surface of the PUREBLACK® GDL after 1000h in warm water.

The surface of the aged GDL appears rough and carbon loss, exposing the carbon fiber of the substrate and larger pores, is apparent compared to its pristine form (a). It has been confirmed that water facilitates chemical carbon corrosion, where carbon is washed away as carbon dioxide [148,189]. On the other hand, the VULCAN® GDL, aged in H_2O_2, in Figure 23(e) demonstrates cracks and cavities/dents, resulting from surface oxidation and can alternate the wettability characteristics, resulting in water management changes, porosity loss and mechanical degradation [130,170,190]. The effect of roughness of the MPL due large cracks has also been confirmed by Wang et al. [93], and is linked to hydrophobicity change [191,192]. Figure 23(f) shows the VULCAN® GDL aged in water for 1000h. Carbon loss and higher surface roughness are apparent due to carbon corrosion

from water, which can lead to modifications in pore surface characteristics and morphology [193,194].

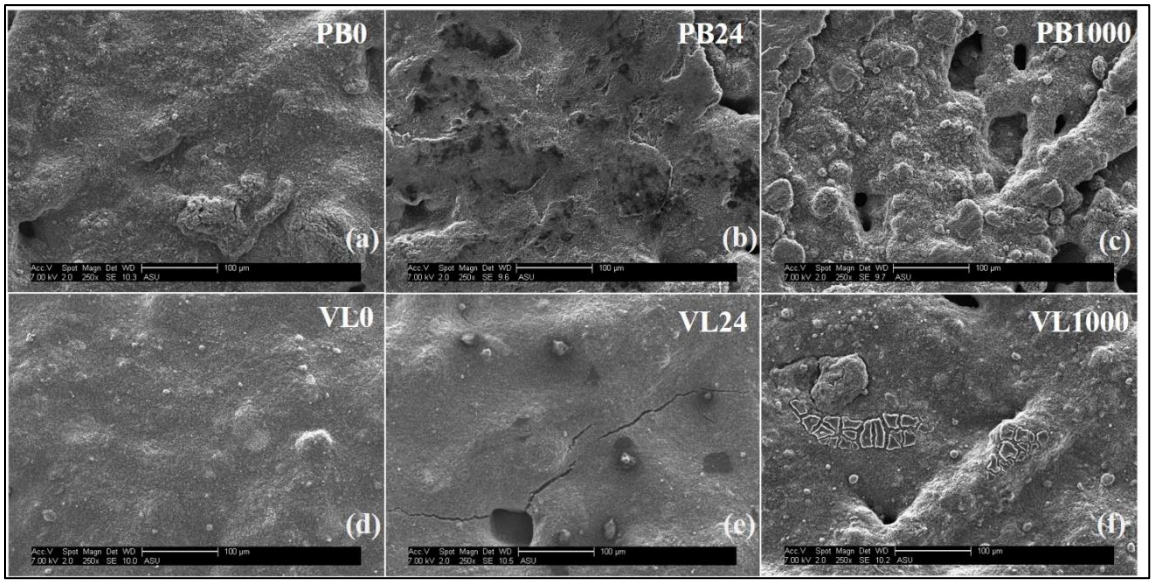

Figure 23. Surface morphology on GDLs with PUREBLACK® (a) pristine, (b) 24 h in hydrogen peroxide, (c) 1000 h in water, and VULCAN® (d) pristine, (e) 24 h in hydrogen peroxide and (f) 1000 h in water.

5.2.2 Contact angle

Surface-wetting characteristics were examined by sessile drop goniometry and are shown in Figure 24. As can be seen, the contact angle for both PUREBLACK® and VULCAN® based GDLs has been decreased, with a greater decrease on VULCAN® GDLs. A drop in contact angle measured on MPLs of about 14 and 95 degrees for PUREBLACK® and VULCAN® carbon, respectively, for AST in hydrogen peroxide and 6 and 69 degrees for PUREBLACK® and VULCAN® respectively, for AST in warm water, revealed a change from a hydrophobic surface (~137°) to a hydrophilic one (~68°) over the course of 24 and 1000 hours for VULCAN®, though, the samples with PUREBLACK® MPL showed

a much slower change over the same period (Table 3). VULCAN® carbon, unlike PUREBLACK®, is not graphitized, and this, along with other structural differences (particle size, pore size and volume) can be the main reason of VULCAN®'s hydrophobicity loss in the presence of corrosive conditions [119,183,195]. The dramatic change in hydrophobicity on the VULCAN® MPL may be affected by parameters such as loss of hydrophobic MPL surface [170], porosity change [194,196], resulting in poor water management [170,188], increased surface roughness due to surface cracks [191,192], or PTFE decomposition, although it is possible that the latter does not occur in a high degree, as PTFE loss is not observed in SEM images (Figure 23), which indicates that PTFE decomposition may not the primary reason of decreased hydrophobicity [137,197]. The effect of PUREBLACK® concerning hydrophobicity loss appears smaller than VULCAN®, as graphitization has been reported to reduce surface heterogeneity and increase corrosion stability [171,198–201].

Table 3. Summarized results before and after ASTs.

Sample ID	**Contact angle (degrees)**	**Total porosity (%)**	**Performance degradation (%)**			
			O_2		**Air**	
			100%	**60%**	**100%**	**60%**
PB0	140	58	-	-	-	-
PB24	126	65	14	6	10	2
PB1000	134	60	14	5	12	2
VL0	136	63	-	-	-	-
VL24	43	69	15	12	19	11
VL1000	68	65	19	12	16	16

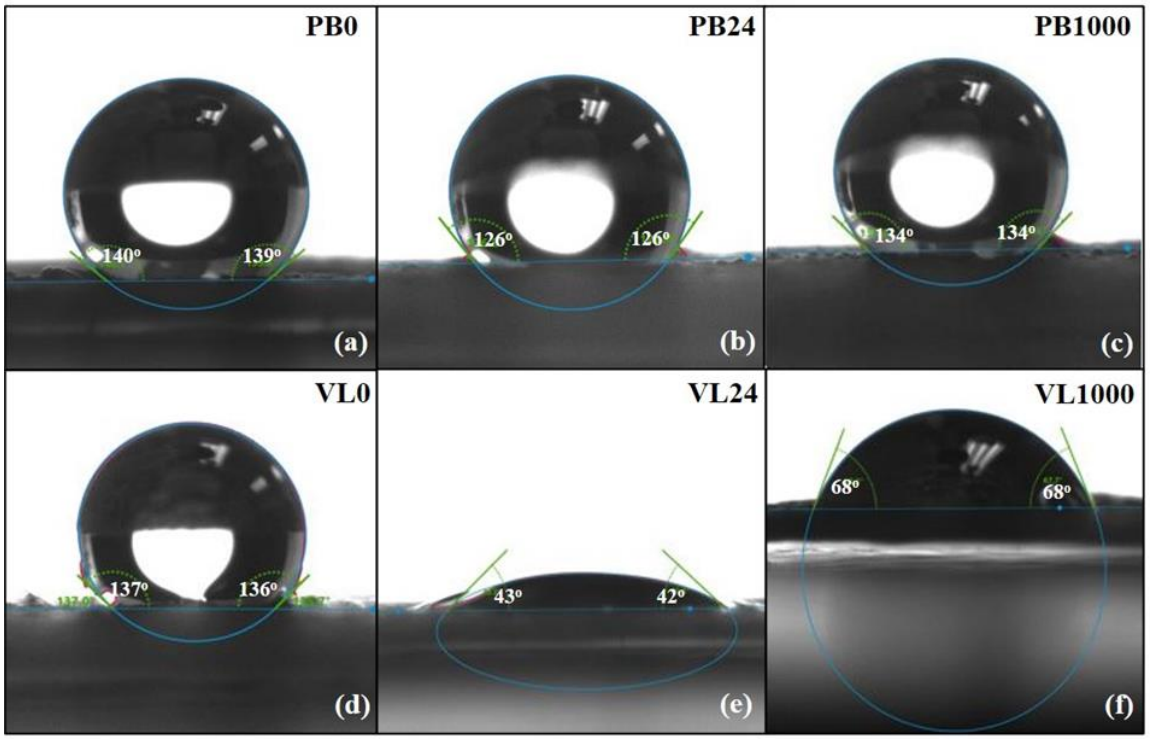

Figure 24. Contact angle on GDLs with PUREBLACK® (a) pristine, (b) 24 h in hydrogen peroxide, (c) 1000 h in water, and VULCAN® (d) pristine, (e) 24 h in hydrogen peroxide and (f) 1000 h in water.

5.2.3 Porosity and pore size distribution

Porosity and pore size distribution measurements were conducted using mercury intrusion porosimetry for PUREBLACK® and VULCAN® GDLs, before and after degradation, to examine the pore characteristics. The porosity values are presented in Table 3 and the pore size distributions are depicted in Figure 25(a) and (b) for PUREBLACK® and VULCAN®, respectively. Total porosity values demonstrate increased porosity for all aged GDL samples compared to the pristine ones, which was apparent from the SEM micrographs (Figure 23), showing clearly material loss and penetrated surface, resulted from carbon corrosion, on the aged samples (Figure 23 (b),(c),(e) and (f)). Although, the

porosity changes, due to aging processes, can be considered insignificant [202], pore size distribution demonstrates significant variations between the aged and pristine samples [97]. To associate the different pore size ranges to the changes in the structure, the GDL pores are categorized according to size into 3 groups, which include the macropores, with median pore diameter above 20 μm, the micropores (median pore diameter below 0.1 μm), and the mesopores (with median pore diameter range between 0.1 and 20 μm). As can be seen from Figure 25, both types of carbon show an increase in the macropore area, which indicates structural change on the GDL after the two accelerated tests. In the micropore region, the aged VULCAN® GDLs demonstrate a significant decrease, which leads to the assumption that carbon corrosion led to destruction of smaller pores, resulting in the creation of larger pores. This is evident by the SEM (Figure 23 (e)) and hydrophobicity loss (Figure 24 (e)), where larger pores on the MPL surface and cracks are visible and surface wetting characteristics have been completely changed. Similar effect seems to occur after aging in water, although in this case the main reason seems to be the PTFE decomposition (Figure 23 (f)), uncovering larger pores and leading to hydrophobicity loss (Figure 24 (f)). It is widely known that larger hydrophilic pores enhance liquid water transport and smaller hydrophobic pores facilitate gas diffusion [147], however, although the increase in larger pores enables water transport, it decreases through-plane electronic conductivity and, the cracks filled with water limit gas permeability, and as a result, fuel cell performance will be reduced [77,176]. PUREBLACK® GDLs exhibit similar trends, however the changes in pore size distribution are not as dramatic. The carbon loss (Figure 23 (c)), when the GDL was aged in water, resulted in creation of larger pores, as shown in Figure 25 (a), however,

the hydrophobic characteristics of the surface persists (Figure 24 (c)). Furthermore, the aged in hydrogen peroxide GDL, despite of a small drop in contact angle (Figure 24 (b)), which can be resulted by increased porosity, does not indicate any significant changes on surface (Figure 23 (b)), hence it can be assumed that PUREBLACK® shows higher corrosion resistance than VULCAN® carbon [203].

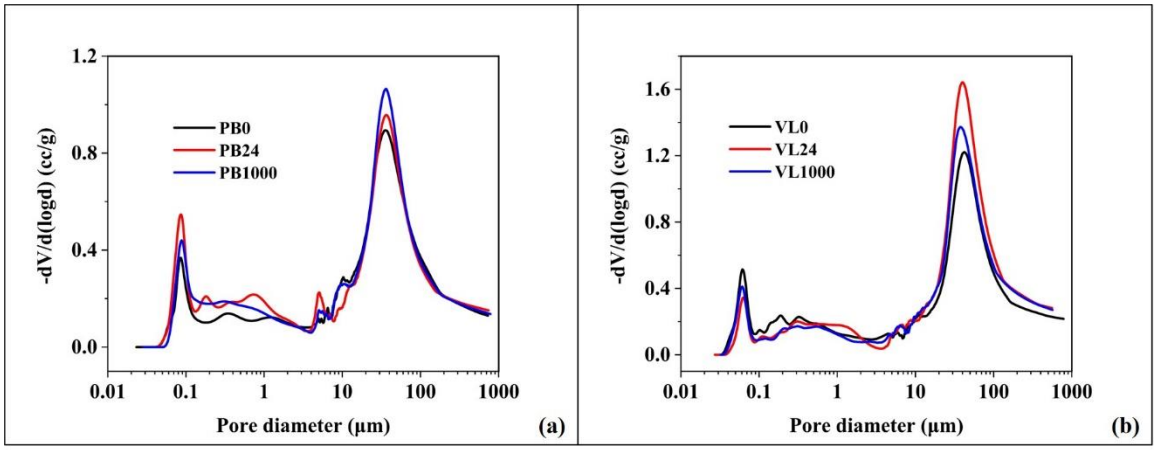

Figure 25. Pore size distribution before and after ASTs for (a) PUREBLACK® and (b) VULCAN® GDLs.

5.2.4 Fuel cell performance

The fuel cell performance for PUREBLACK® and VULCAN® based GDLs was evaluated at 60 and 100% RH in H_2/O_2 and H_2/air at 70 ^oC, before and after both AST methods and the percentage of performance loss is summarized in Table 3. Figure 26 shows the fuel cell performance of PUREBLACK® and VULCAN® carbon GDLs before and after 24 h in hydrogen peroxide. As seen, polarization curves at high RH (Fig 26(a) and (c)) exhibit significant mass transport loss after for both types of carbon. The configuration of the PUREBLACK® GDL with 30% wt. PEG as pore forming agent, was shown to withstand flooding during fuel cell operation, due to its pore size distribution and surface

morphology, hence demonstrated similar fuel cell performance at both 60 and 100% RH, which is demonstrated here as well [129]. However, after aging in hydrogen peroxide for 24 h, at high RH conditions there is a significant performance drop (14 and 10% loss in H_2/O_2 and H_2/air, respectively).

Hydrogen peroxide facilitates chemical corrosion of carbon, which severely affects the fuel cell performance by increased accumulation of liquid water in the aged GDLs [204], hence flooding is the main reason of fuel cell performance loss at high RH conditions (Figure 26(a) and (c)) [205]. The limiting current is determined at the lowest stable operating voltage of the fuel cell [206]. When the fuel cell is flooded, product water covers the GDL pores, prohibiting the reactant gases to reach the catalyst layer, therefore a drop in voltage, associated with mass transport loss, is observed in lower current densities [206,207]. Evidently, for the PUREBLACK® GDL the fuel cell shows mass transport loss when current density is around 1500 mA cm^{-2} in H_2/O_2 and 600 mA.cm^{-2} for H_2/air at high RH conditions. However, for VULCAN® GDL the fuel cell performance degradation is greater (15 and 19% in H_2/O_2 and H_2/air, respectively) and the mass transport loss appears around 1000 mA.cm^{-2} in H_2/O_2 and 400 mA.cm^{-2} in H_2/air.

Under low RH condition (see Figure 26(b) and(d)), the effect of water content in the system is suppressed, thus the mass transport loss is negligible [204]. The performance degradation for PUREBLACK® at 60% RH is less than 10% in all conditions and can be considered negligible. However, even though the performance loss for VULCAN® GDL is lower at 60 than at 100% RH conditions, it is still considered significant (12 and 11% loss

in H_2/O_2 and H_2/air, respectively), which can indicate that VULCAN® carbon is more prone to carbon corrosion, alternating the GDL structure in a higher degree [183,199,208,209].

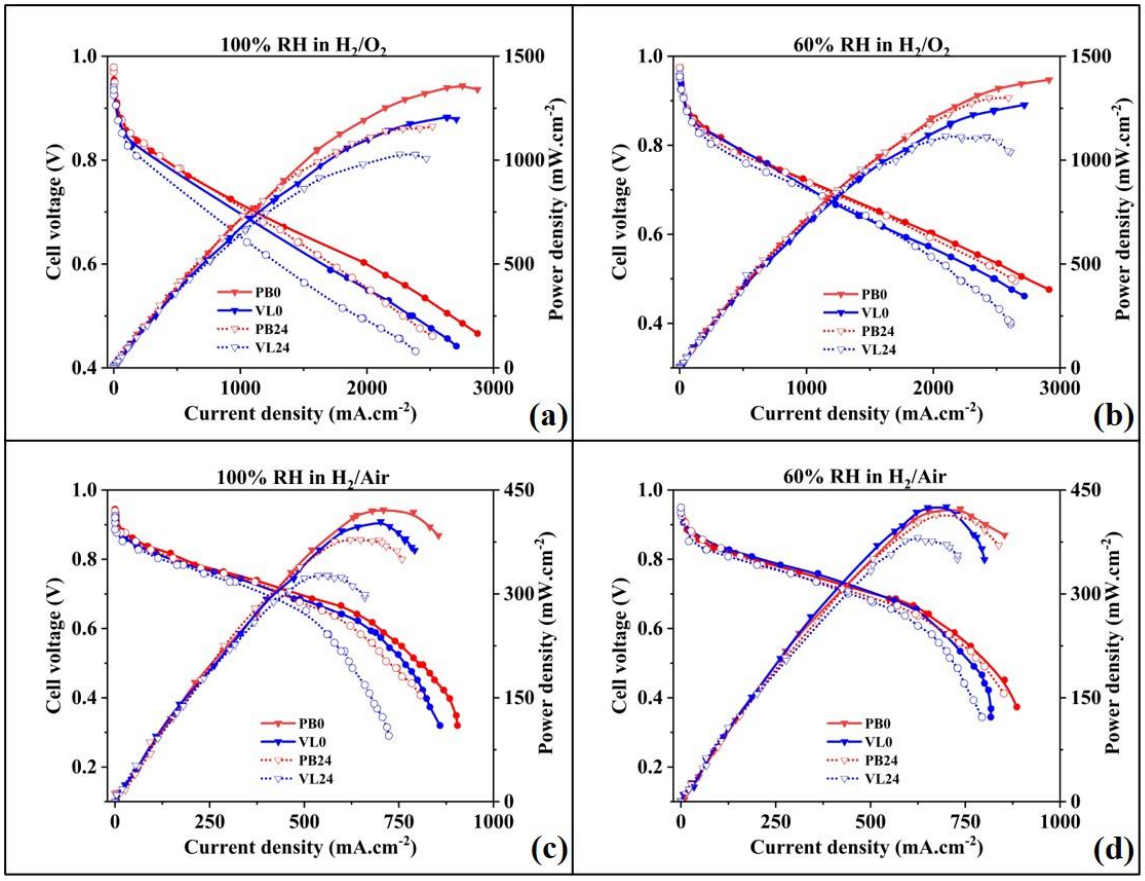

Figure 26. Fuel cell performance of PUREBLACK® and VULCAN® GDLs before and after AST in hydrogen peroxide in H_2/O_2 at (a) 100%, (b) 60% RH and H_2/air at (c) 100% and (d) 60% RH.

The fuel cell performance of both carbons, before and after AST method in water, at 60 and 100% RH in H_2/O_2 and H_2/air, is depicted in Figure 27 and the performance loss percentage is summarized in Table 3. Similar to AST in hydrogen peroxide (Figure 26), greater mass transport loss appears when the RH is high, in both oxygen and air conditions

(Figure 27 (a) and (c)). However, it appears that performance degradation is greater for VULCAN® carbon, leading to the assumption that VULCAN® has lower carbon corrosion resistance compared to PUREBLACK®.

At low RH conditions (Figures 27(b) and (d)), the flooding effect caused by the GDL degradation minimizes, however, it is apparent that VULCAN® carbon exhibits significant performance loss (12 and 16% in O_2 and air, respectively) (Table 3), whereas PUREBLACK® performance degradation can be considered negligible (5 and 2% in O_2 and air, respectively) (Table 3).

The apparent carbon corrosion resistance of PUREBLACK® can be the result of (a) graphitization during fabrication process, and (b) better material properties (smaller particle and pore size, higher pore volume). Graphitized carbons with hydrophobic surface have been proven to prevent carbon corrosion [208,209]. The corrosion effects on VULCAN® GDL appear more severe than PUREBLACK®, leading to the assumption that VULCAN® carbon is more prone to carbon corrosion probably due to its non-graphitized form [171,199].

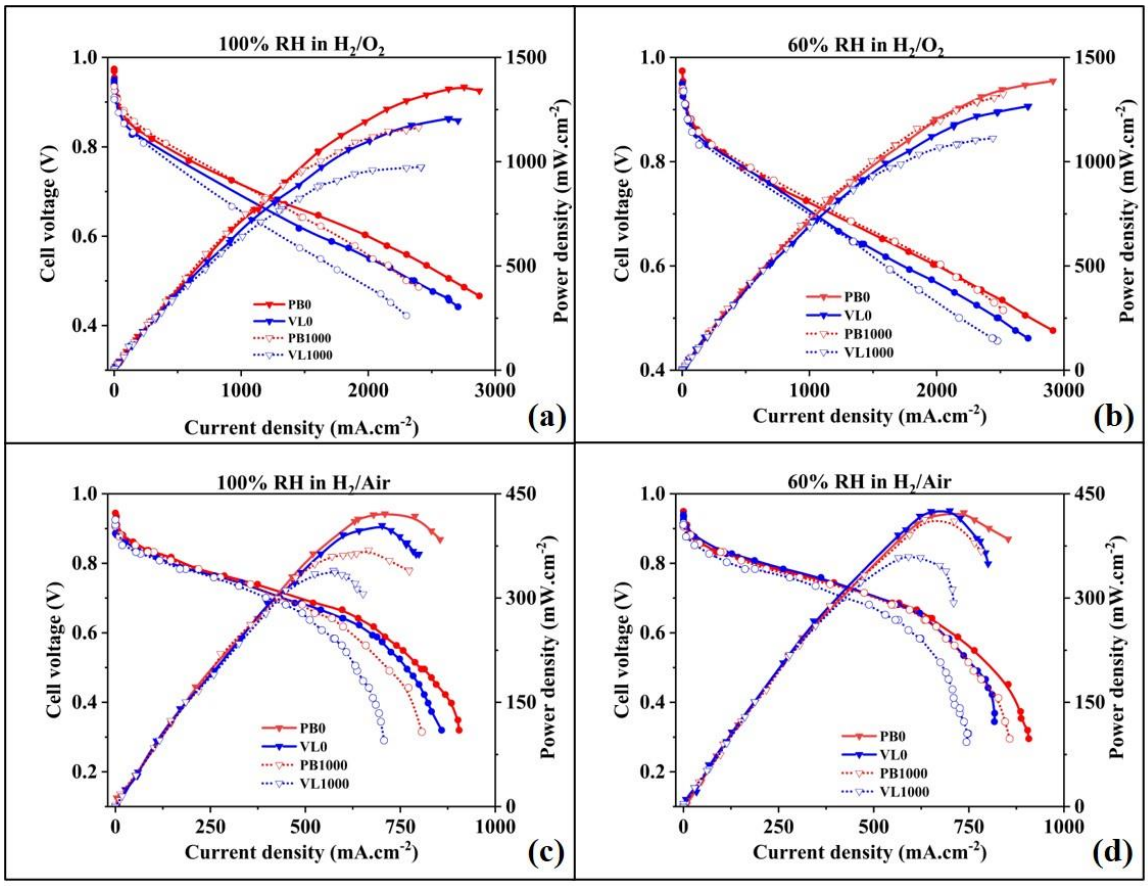

Figure 27. Fuel cell performance of PUREBLACK® and VULCAN® GDLs before and after AST in water in H_2/O_2 at (a) 100%, (b) 60% RH and H_2/air at (c) 100% and (d) 60% RH

5.2.5 Durability

Pristine samples of PUREBLACK® and VULCAN® GDLs with 30 % PEG on the MPL (samples PB0 and VL0) were selected for durability test, to examine the behavior of the two different carbons, using H_2/air as oxidant in lower and higher RH conditions. Initially, the system was fully hydrated, and polarization measurements were carried out prior to each RH change. The MEAs were evaluated at 100 % RH for 50 h, followed by

50h at 60 % RH condition, on both the anode and cathode sides, in order to achieve optimum membrane hydration.

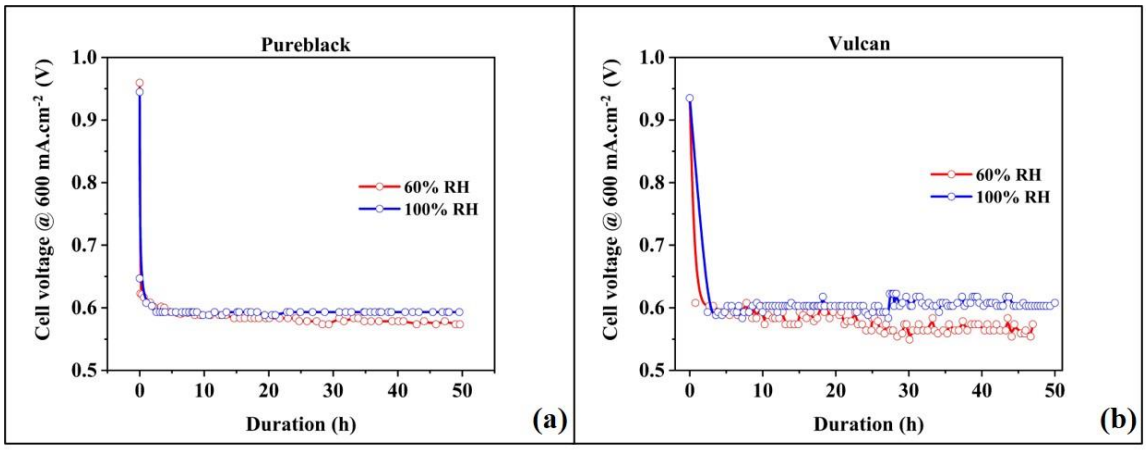

Figure 28. Durability test using H_2/air for 50h at 100% and 50 h at 60% RH at 70 ^oC and constant current density of 600 mA.cm-2 for pristine (a) PUREBLACK® and (b) VULCAN® GDLs.

Figure 28(a) and (b) show the cell voltage at 600 $mA.cm^{-2}$ for 50 h at 100 % RH first and then for 50 h at 60 % RH conditions for the MEAs containing PUREBLACK® and VULCAN® carbon, respectively. As demonstrated in Figure 27(d), the fuel cell performance of VULCAN® GDL is slightly higher at 60% RH and there is a fluctuation between 0.55 to 0.60V after ~30h of continuous operation (Figure 28(b)), possibly due to temporary O_2 starvation caused by flooding [43], and at 100% RH, the voltage increases from 0.60 to 0.62V. The hydrophobicity loss decreases the ability to discharge the water and therefore causes flooding within the GDL. The high stability of the water droplet makes it difficult to detach the droplet from the GDL surface. Therefore, O_2 starvation occurs due to channel clogging, leading to a voltage instability of the fuel cell [137].

PUREBLACK® carbon in the GDL is known to withstand carbon corrosion during fuel cell operation due to its well-defined graphitic structure [183,203]. Clearly, stability of the cell voltage around 0.59 V both at 60 and 100 % RH conditions (Figure 28(a)), demonstrates the suitability of PUREBLACK® carbon based MPL with 30 % PEG for GDL fabrication [129,186].

6. SUMMARY AND CONCLUSIONS

Gas diffusion layers (GDLs) are essential components of proton exchange membrane fuel cells (PEMFCs), as they carry out multiple important functions including transportation of reactants to and from the reaction sites and removal of excess water from the system. The material properties and structural characteristics of both the substrate and the microporous layer demonstrate a strong influence on the fuel cell performance.

The microporous layers of GDLs were fabricated in single and multi-layer configurations with carbon powder PUREBLACK® and different PEG contents, characterized and compared to a commercial GDL with MPL. Evidently, the best performing GDL configuration was the one containing 30% PEG. The surface morphology and contact angle measurements revealed crack-free surface morphology and increased hydrophobicity for PUREBLACK®, in contrast to surface cracks and hydrophilic characteristics for the commercial. Furthermore, as evaluated by mercury porosimetry, the GDL with 30 % PEG showed the highest pore volume (1.72 $cc.g^{-1}$) among all the other samples, along with the presence of nanopores. These GDL modifications resulted in stable peak power density values at 60 and 100 % RH conditions in the case of air and O_2 as oxidants at 70 ^oC, with effective gas distribution and water management, even at 100 % RH condition. It is worth mentioning that the fuel cell performance using H_2/O_2 and H_2/air, at 60 and 100 % RH conditions is significantly higher for the PUREBLACK® based GDLs compared to the commercial GDLs due to the presence of crack-free surface morphology and finer pores, along with the hydrophobic microporous layer. From the durability testing of 100 h at 600 $mA.cm^{-2}$ (50 h at 100 % RH and 50 h at 60 % RH conditions) for the

PUREBLACK® based GDLs with 30 % PEG in the fuel cell, it is confirmed that the optimum pore size distribution and the crack-free hydrophobic surface are very important properties for the stable performance.

Subsequently, the best performing GDL configuration was subjected to two methods of *ex-situ* AST (water and hydrogen peroxide), to evaluate the fuel cell performance and stability, and compared to similar configuration containing VULCAN® carbon. SEM and contact angle measurements showed that the degradation effects on the MPL after accelerated stress testing in water and hydrogen peroxide were more severe on VULCAN® carbon, with a dramatic contact angle drop from 136^{o} to 68^{o} and 42^{o}, respectively, compared to PUREBLACK®. Pore size distribution, also, demonstrates destruction of micropores and creation of macropores, in higher rate for VULCAN® carbon than in PUREBLACK®. Additionally, the fuel cell performance before and after ASTs showed greater performance loss for VULCAN® carbon in all conditions (12-19% loss), whereas for PUREBLACK® the performance degradation was noteworthy at high RH conditions (10-14%), however at low RH conditions it could be considered negligible (2-6%). *In-situ* durability testing also confirmed the importance of graphitized carbons, such as PUREBLACK®, on demonstrating higher carbon corrosion resistance, with uniform gas distribution resulting in better performance stability. It is worth mentioning that both pristine samples, show very small peak power density decrease between 60 and 100% RH, which suggests that the optimized GDL configuration presented in the first part, might be implemented on other carbon types.

REFERENCES

[1] Birol F. World Energy Outlook. International Energy Agency 2020:23–8.

[2] Looney B. Statistical Review of World Energy, 2020 | 69th Edition. Bp 2020;69:66.

[3] Sugawara E, Nikaido H. EIA energy outlook 2020. US Energy Information Agency 2019;58:7250–7.

[4] Xu Y, Ramanathan V, Victor DG. Global warming will happen faster than we think. Nature 2018;564:30–2. https://doi.org/10.1038/d41586-018-07586-5.

[5] Sorgulu F, Dincer I. A renewable source based hydrogen energy system for residential applications. International Journal of Hydrogen Energy 2018;43:5842–51. https://doi.org/10.1016/j.ijhydene.2017.10.101.

[6] Barbir F, Yazici S. Status and development of PEM fuel cell technology. International Journal of Energy Research 2008. https://doi.org/10.1002/er.1371.

[7] Suha Yazici M. Hydrogen and fuel cell activities at UNIDO-ICHET. International Journal of Hydrogen Energy 2010;35:2754–61. https://doi.org/10.1016/j.ijhydene.2009.04.072.

[8] IRENA IREA. Hydrogen : a Renewable Energy Perspective - Report prepared for the 2nd Hydrogen Energy Ministerial Meeting in Tokyo, Japan. 2019.

[9] Economy I– IP for H and FC in the. Green Hydrogen Summit – Chile 2020 Panel on " Coopetition ": Navigating international cooperation and competition International Government-Led Collaborations on Hydrogen Historical Context 2020.

[10] Abdel-Baset T, Benjamin T, Borup R, Martin KE, Garland N, Hirano S, et al. The. US Deparment of Energy (DOE). Energy Efficiency and Renewable Energy https://energy.gov/eere/fuelcells/doe-technical-targets-polymer-electrolyte-membrane-fuel-cell-components 2017:30. https://doi.org/10.2172/1220127.

[11] Ministerial CE. Clean Energy Ministerial n.d. http://www.cleanenergyministerial.org/.

[12] Ambition H, Peninsula I, Ambition H, Ambition H, Ambition H, Ambition H, et al. PRESS RELEASE 30 energy players initiate an integrated value chain to deliver green hydrogen across Europe at the price of fossil fuels 2022.

[13] Kim M, Lim JW, Kim KH, Lee DG. Bipolar plates made of carbon fabric/phenolic composite reinforced with carbon black for PEMFC. Composite Structures 2013;96:569–75. https://doi.org/10.1016/j.compstruct.2012.09.017.

[14] Austrlian Government Chief Scientist. Hydrogen for Australia's future 2018:59.

[15] Staffell I, Scamman D, Velazquez Abad A, Balcombe P, Dodds PE, Ekins P, et al. The role of hydrogen and fuel cells in the global energy system. Energy and Environmental Science 2019;12:463–91. https://doi.org/10.1039/c8ee01157e.

[16] Hoffman P. Hydrogen-the optimum chemical fuel. Applied Energy 1994;47:183–99. https://doi.org/10.1016/0306-2619(94)90078-7.

[17] Mazloomi K, Gomes C. Hydrogen as an energy carrier : Prospects and challenges. Renewable and Sustainable Energy Reviews 2012;16:3024–33. https://doi.org/10.1016/j.rser.2012.02.028.

[18] Sengodan S, Lan R, Humphreys J, Du D, Xu W, Wang H, et al. Advances in reforming and partial oxidation of hydrocarbons for hydrogen production and fuel cell applications. Renewable and Sustainable Energy Reviews 2018;82:761–80. https://doi.org/10.1016/j.rser.2017.09.071.

[19] Simpson AP, Lutz AE. Exergy analysis of hydrogen production via steam methane reforming 2007;32:4811–20. https://doi.org/10.1016/j.ijhydene.2007.08.025.

[20] Speight JG. Handbook of Industrial Hydrocarbon processes. 2011. https://doi.org/10.1016/B978-0-7506-8632-7.10012-X.

[21] Stenberg V, Rydén M, Mattisson T, Lyngfelt A. Exploring novel hydrogen production processes by integration of steam methane reforming with chemical-looping combustion (CLC-SMR) and oxygen carrier aided combustion (OCAC-SMR). International Journal of Greenhouse Gas Control 2018;74:28–39. https://doi.org/10.1016/j.ijggc.2018.01.008.

[22] Hickman DA, Schmidt LD. The role of boundary layer mass transfer in partial oxidation selectivity. Journal of Catalysis 1992;136:300–8. https://doi.org/10.1016/0021-9517(92)90063-N.

[23] Dissanayake D, Rosynek MP, Kharas KCC, Lunsford JH. Partial oxidation of methane to carbon monoxide and hydrogen over a Ni/Al2O3 catalyst. Journal of Catalysis 1991;132:117–27. https://doi.org/10.1016/0021-9517(91)90252-Y.

[24] Steinberg M, Cheng HC. Modern and prospective technologies for hydrogen production from fossil fuels. International Journal of Hydrogen Energy 1989;14:797–820. https://doi.org/10.1016/0360-3199(89)90018-9.

[25] Bartels JR, Pate MB, Olson NK. An economic survey of hydrogen production from conventional and alternative energy sources. International Journal of Hydrogen Energy 2010;35:8371–84. https://doi.org/10.1016/j.ijhydene.2010.04.035.

[26] Sánchez-Bastardo N, Schlögl R, Ruland H. Methane Pyrolysis for CO2-Free H2 Production: A Green Process to Overcome Renewable Energies Unsteadiness.

Chemie-Ingenieur-Technik 2020;92:1596–609. https://doi.org/10.1002/cite.202000029.

[27] Thangalazhy-Gopakumar S, Adhikari S, Gupta RB, Tu M, Taylor S. Production of hydrocarbon fuels from biomass using catalytic pyrolysis under helium and hydrogen environments. Bioresource Technology 2011;102:6742–9. https://doi.org/10.1016/j.biortech.2011.03.104.

[28] Chisholm G, Cronin L. Hydrogen From Water Electrolysis. Elsevier Inc.; 2016. https://doi.org/10.1016/B978-0-12-803440-8/00016-6.

[29] Jorg A, Balzer C, Louis J. SHELL HYDROGEN STUDY ENERGY OF THE FUTURE ? 2017.

[30] Nazir H, Louis C, Jose S, Prakash J, Muthuswamy N, Buan MEM, et al. Is the H2 economy realizable in the foreseeable future? Part I: H2 production methods. International Journal of Hydrogen Energy 2020;45:13777–88. https://doi.org/10.1016/j.ijhydene.2020.03.092.

[31] Obstawski P, Bakoń T, Czekalski D. Comparison of solar collector testing methods—theory and practice. Processes 2020;8:1–29. https://doi.org/10.3390/pr8111340.

[32] Thomas S, Zalbowitz M. Fuel Cells - Green Power n.d.

[33] Abdin Z, Mérida W. Hybrid energy systems for off-grid power supply and hydrogen production based on renewable energy: A techno-economic analysis. Energy Conversion and Management 2019;196:1068–79. https://doi.org/10.1016/j.enconman.2019.06.068.

[34] Nguyen T, Abdin Z, Holm T, Mérida W. Grid-connected hydrogen production via large-scale water electrolysis. Energy Conversion and Management 2019;200:112108. https://doi.org/10.1016/j.enconman.2019.112108.

[35] Züttel A. Hydrogen storage methods. Naturwissenschaften 2004;91:157–72. https://doi.org/10.1007/s00114-004-0516-x.

[36] Zohuri B. Hydrogen energy: Challenges and solutions for a cleaner future. Hydrogen Energy: Challenges and Solutions for a Cleaner Future 2018:1–283. https://doi.org/10.1007/978-3-319-93461-7.

[37] IEA. The Future of Hydrogen n.d. https://www.iea.org/reports/the-future-of-hydrogen.

[38] Dybkjaer I. Ammonia Production Processes. Ammonia 1995:199–327. https://doi.org/10.1007/978-3-642-79197-0_6.

[39] Farmasi PB. Petroleum Refining. 2017.

[40] Javadli R, Klerk A. Desulfurization of heavy oil. Applied Petrochem Research 2012;1:3–19. https://doi.org/10.1007/s13203-012-0006-6.

[41] Dalena F, Senatore A, Basile M, Knani S, Basile A, Iulianelli A. Advances in methanol production and utilization, with particular emphasis toward hydrogen generation via membrane reactor technology. Membranes 2018;8. https://doi.org/10.3390/membranes8040098.

[42] Spiegel C. Designing and Building Fuel Cells n.d.

[43] Dincer I, Acar C. ScienceDirect Smart energy solutions with hydrogen options. International Journal of Hydrogen Energy 2018;43:8579–99. https://doi.org/10.1016/j.ijhydene.2018.03.120.

[44] Bizon N. ScienceDirect Improving the PEMFC energy efficiency by optimizing the fueling rates based on extremum seeking algorithm. International Journal of Hydrogen Energy 2014;39:10641–54. https://doi.org/10.1016/j.ijhydene.2014.04.194.

[45] Chen Z, Dodelet J. Materials for High-Temperature Fuel Cells Fuel Cell Science and Engineering High Energy Density Lithium Batteries Principles and Applications of Lithium Secondary Batteries Electrocatalysis of Direct Methanol Fuel Cells Electrochemical Technologies for En. n.d.

[46] Zhao T, Xu C. Direct Methanol Fuel Cell : Overview Performance and Operational Conditions. Encyclopedia of Electrochemical Power Sources 2009.

[47] U.S Department of Energy. Fuel Cell Handbook. Fifth. 2000.

[48] Smitha B, Sridhar S, Khan AA. Solid polymer electrolyte membranes for fuel cell applications — a review 2005;259:10–26. https://doi.org/10.1016/j.memsci.2005.01.035.

[49] Haile SM. Fuel cell materials and components ଌ 2003;51:5981–6000. https://doi.org/10.1016/j.actamat.2003.08.004.

[50] Mehta V, Cooper JS. Review and analysis of PEM fuel cell design and manufacturing 2003;114.

[51] B. E, R. H. Mass Transport Limitations in Proton Exchange Membrane Fuel Cells and Electrolyzers. Mass Transfer - Advanced Aspects 2011. https://doi.org/10.5772/20349.

[52] Jordan LR, Shukla AK, Behrsing T, Avery NR, Muddle BC, Forsyth M. E € ect of di € usion-layer morphology on the performance of polymer electrolyte fuel cells operating at atmospheric pressure 2000:641–6.

[53] Neergat M, Shukla AK. Effect of diffusion-layer morphology on the performance of solid-polymer-electrolyte direct methanol fuel cells 2002;104:289–94.

[54] Park G, Sohn Y, Yang T, Yoon Y, Lee W, Kim C. Effect of PTFE contents in the gas diffusion media on the performance of PEMFC 2004;131:182–7. https://doi.org/10.1016/j.jpowsour.2003.12.037.

[55] U.S Department of Energy. Multi-Year Research, Development, and Demonstration Plan 2017;2015:1–58.

[56] Cho J, Oh H, Park J, Min K, Lee E, Jyoung J. ScienceDirect Effect of the micro porous layer design on the dynamic performance of a proton exchange membrane fuel cell. International Journal of Hydrogen Energy 2013;39:459–68. https://doi.org/10.1016/j.ijhydene.2013.10.041.

[57] Litster S, Mclean G. PEM fuel cell electrodes 2004;130:61–76. https://doi.org/10.1016/j.jpowsour.2003.12.055.

[58] Ramasamy RP, Kumbur EC, Mench MM, Liu W, Moore D, Murthy M. Investigation of macro- and micro-porous layer interaction in polymer electrolyte fuel cells 2008;33:3351–67. https://doi.org/10.1016/j.ijhydene.2008.03.053.

[59] Paganin VA, Ticianelli EA, Gonzalez ER. Development and electrochemical studies of gas diffusion electrodes for polymer electrolyte fuel cells 1996;26:297–304.

[60] Tan Z, Jia L, Zhang Z. A Study on the Transport Process in Gas Diffusion Layer of Proton Exchange Membrane Fuel Cells 2011;20:449–53. https://doi.org/10.1007/s11630-011-0494-1.

[61] Chu H, Yeh C, Chen F. Effects of porosity change of gas diffuser on performance of proton exchange membrane fuel cell 2003;123:1–9.

[62] Song JM, Cha SY, Lee WM. Optimal composition of polymer electrolyte fuel cell electrodes determined by the AC impedance method 2001;94:78–84.

[63] Zhang F, Advani SG, Prasad AK. Performance of a metallic gas diffusion layer for PEM fuel cells 2008;176:293–8. https://doi.org/10.1016/j.jpowsour.2007.10.055.

[64] Chen R, Zhao TS. A novel electrode architecture for passive direct methanol fuel cells 2007;9:718–24. https://doi.org/10.1016/j.elecom.2006.11.004.

[65] Yu EH, Scott K. Direct methanol alkaline fuel cell with catalysed metal mesh anodes 2004;6:361–5. https://doi.org/10.1016/j.elecom.2004.02.002.

[66] Tang Y, Zhou W, Pan M, Chen H, Liu W, Yu H. Porous copper fiber sintered felts : An innovative catalyst support of methanol steam reformer for hydrogen production 2008;33:2950–6. https://doi.org/10.1016/j.ijhydene.2008.04.006.

[67] Shao Z, Lin W, Zhu F, Christensen PA, Zhang H, Yi B. A tubular direct methanol fuel cell with Ti mesh anode 2006;160:1003–8. https://doi.org/10.1016/j.jpowsour.2006.02.047.

[68] Oedegaard A, Hebling C, Schmitz A, Møller-holst S, Tunold R. Influence of diffusion layer properties on low temperature DMFC 2004;127:187–96. https://doi.org/10.1016/j.jpowsour.2003.09.015.

[69] Yi P, Peng L, Lai X, Li M, Ni J. Investigation of sintered stainless steel fiber felt as gas diffusion layer in proton exchange membrane fuel cells. International Journal of Hydrogen Energy 2012;37:11334–44. https://doi.org/10.1016/j.ijhydene.2012.04.161.

[70] Yang C, Chiu S, Lin C. Electrochemical performance of an air-breathing direct methanol fuel cell using poly (vinyl alcohol)/ hydroxyapatite composite polymer membrane 2008;177:40–9. https://doi.org/10.1016/j.jpowsour.2007.11.010.

[71] Pozio A, Sil RF, Francesco M De, Giorgi L. Nafion degradation in PEFCs from end plate iron contamination 2003;48:1543–9. https://doi.org/10.1016/S0013-4686(03)00026-4.

[72] Antunes RA, Cristina M, Oliveira L, Ett G, Ett V. Corrosion of metal bipolar plates for PEM fuel cells : A review. International Journal of Hydrogen Energy 2010;35:3632–47. https://doi.org/10.1016/j.ijhydene.2010.01.059.

[73] Benziger J, Nehlsen J, Blackwell D, Brennan T, Itescu J. Water flow in the gas diffusion layer of PEM fuel cells 2005;261:98–106. https://doi.org/10.1016/j.memsci.2005.03.049.

[74] Hussaini IS, Wang CY. Measurement of relative permeability of fuel cell diffusion media 2010;195:3830–40. https://doi.org/10.1016/j.jpowsour.2009.12.105.

[75] Sasikumar G, Ryu H. Comparison of electrode backing materials for polymer electrolyte membrane fuel cells. Journal of the Korean Electrochemical Society 2003;6:183–6.

[76] Stampino P, Omati L, Dotelli G. Electrical Performance of PEM Fuel Cells With Different Gas Diffusion Layers. Journal of Fuel Cell Science and Technology 2013;8:1–5. https://doi.org/10.1115/1.4003630.

[77] Williams M V, Soc JE, Williams M V, Begg E, Bonville L, Kunz HR. Characterization of Gas Diffusion Layers for PEMFC Characterization of Gas Diffusion Layers for PEMFC 2004. https://doi.org/10.1149/1.1764779.

[78] Wang Y, Wang C, Chen KS. Elucidating differences between carbon paper and carbon cloth in polymer electrolyte fuel cells 2007;52:3965–75. https://doi.org/10.1016/j.electacta.2006.11.012.

[79] Antolini E. Recent developments in polymer electrolyte fuel cell electrodes 2004:563–76.

[80] Staiti P, Lucia S, Calabria R. Influence of electrodic properties on water management in a solid polymer electrolyte fuel cell 1992;22:663–7.

[81] Bevers D, Rogers R, Bradke M. Examination of the influence of PTFE coating on the properties of carbon paper in polymer electrolyte fuel cells. Journal of Power Sources 1996;63:193–201.

[82] Prasanna M, Ha HY, Cho EA, Hong S, Oh I. Influence of cathode gas diffusion media on the performance of the PEMFCs 2004;131:147–54. https://doi.org/10.1016/j.jpowsour.2004.01.030.

[83] Lim C, Wang CY. Effects of hydrophobic polymer content in GDL on power performance of a PEM fuel cell. Electrochimica Acta 2004;49:4149–56. https://doi.org/10.1016/j.electacta.2004.04.009.

[84] Lin G, Nguyen T. Effect of Thickness and Hydrophobic Polymer Content of the Gas Diffusion Layer on Electrode Flooding Level in a PEMFC Guangyu Lin and Trung Van Nguyen service Effect of Thickness and Hydrophobic Polymer Content of the. Journal of the Electrochemical Society 2005;152:A1942–8. https://doi.org/10.1149/1.2006487.

[85] Park S, Lee J, Popov BN. Effect of PTFE content in microporous layer on water management in PEM fuel cells 2008;177:457–63. https://doi.org/10.1016/j.jpowsour.2007.11.055.

[86] Gostick JT, Ioannidis MA, Fowler MW, Pritzker MD. Electrochemistry Communications On the role of the microporous layer in PEMFC operation. Electrochemistry Communications 2009;11:576–9. https://doi.org/10.1016/j.elecom.2008.12.053.

[87] Qi Z, Kaufman A. Improvement of water management by a microporous sublayer for PEM fuel cells 2002;109:1–9.

[88] Atiyeh H, Karan K, Peppley B, Phoenix A, Halliop E, Pharoah J. Experimental investigation of the role of a microporous layer on the water transport and performance of a PEM fuel cell. Journal of Power Sources 2007;170:11–121.

[89] Tseng C, Lo S. Effects of microstructure characteristics of gas diffusion layer and microporous layer on the performance of PEMFC. Energy Conversion and Management 2010;51:677–84. https://doi.org/10.1016/j.enconman.2009.11.011.

[90] Fu X, Ruan J, Zhang R, Hu S. Effect of the Microporous Layer Structure and Hydrophobicity on the Performance of Direct Methanol Fuel Cells Effect of the Microporous Layer Structure and Hydrophobicity on the Performance of Direct Methanol Fuel Cells 2018. https://doi.org/10.12783/dteees/ICPEEE2018/23368.

[91] Park S, Lee J, Popov BN. Effect of carbon loading in microporous layer on PEM fuel cell performance 2006;163:357–63. https://doi.org/10.1016/j.jpowsour.2006.09.020.

[92] Nam J, Lee K, Hwang G, Kim C, Kaviany M. Microporous layer for water

morphology control in PEMFC. International Journal of Heat and Mass Transfer 2009;52:2779–91. https://doi.org/10.1016/j.ijheatmasstransfer.2009.01.002.

[93] Wang M, Medina S, Pfeilsticker JR, Pylypenko S, Ulsh M, Mauger SA. Impact of Microporous Layer Roughness on Gas-Diffusion- Electrode-Based Polymer Electrolyte Membrane Fuel Cell Performance 2019:7–11. https://doi.org/10.1021/acsaem.9b01871.

[94] Mathur VK, Crawford J. 4 . Fundamentals of Gas Diffusion Layers in PEM Fuel Cells 2003;400.

[95] Cindrella L, Kannan AM, Lin JF, Saminathan K, Ho Y, Lin CW, et al. Gas diffusion layer for proton exchange membrane fuel cells — A review 2009;194:146–60. https://doi.org/10.1016/j.jpowsour.2009.04.005.

[96] Arvay A, Yli-rantala E, Liu C, Peng X, Koski P, Cindrella L, et al. Characterization techniques for gas diffusion layers for proton exchange membrane fuel cells e A review. Journal of Power Sources 2012;213:317–37. https://doi.org/10.1016/j.jpowsour.2012.04.026.

[97] Kong CS, Kim D, Lee H, Shul Y, Lee T. Influence of pore-size distribution of diffusion layer on mass-transport problems of proton exchange membrane fuel cells 2002;108:185–91.

[98] Fishman Z, Bazylak A. Heterogeneous Through-Plane Porosity Distributions for Treated Heterogeneous Through-Plane Porosity Distributions for Treated PEMFC GDLs. Journal of Electrochemical Society 2011;158:B841–5. https://doi.org/10.1149/1.3594578.

[99] Kandlikar SG, Garofalo ML, Lu Z. Water Management in A PEMFC : Water Transport Mechanism and Material Degradation in Gas Diffusion Layers ~ 2011:814–23. https://doi.org/10.1002/fuce.201000172.

[100] Tanuma T. Effect of Properties of Hydrophilic Microporous Layer (MPL) on PEFC Performance Effect of Properties of Hydrophilic Microporous Layer (MPL) on. Journal of Electrochemical Society 2017;164:F499–503. https://doi.org/10.1149/2.0371706jes.

[101] Simon C, Kartouzian D, David M, Wilhelm F, Gasteiger HA. Impact of Microporous Layer Pore Properties on Liquid Water Transport in PEM Fuel Cells : Carbon Black Type and Perforation Impact of Microporous Layer Pore Properties on Liquid Water Transport in PEM Fuel Cells : Carbon Black Type and Perforation. Journal of Electrochemical Society 2017;164:F1697–711. https://doi.org/10.1149/2.1321714jes.

[102] Kitahara T, Konomi T, Nakajima H. Microporous layer coated gas diffusion layers for enhanced performance of polymer electrolyte fuel cells 2010;195:2202–11. https://doi.org/10.1016/j.jpowsour.2009.10.089.

[103] Nam JH, Kaviany M. Effective diffusivity and water-saturation distribution in single- and two-layer PEMFC diffusion medium. International Journal of Heat and Mass Transfer 2003;46:4595–611. https://doi.org/10.1016/S0017-9310(03)00305-3.

[104] Weber AZ, Newman J. Effects of Microporous Layers in Polymer Electrolyte Fuel Cells. Journal of The Electrochemical Society 2005;152:A677. https://doi.org/10.1149/1.1861194.

[105] Jiao K, Zhou B. Effects of electrode wettabilities on liquid water behaviours in PEM fuel cell cathode 2008;175:106–19. https://doi.org/10.1016/j.jpowsour.2007.09.048.

[106] Omrani R, Shabani B. ScienceDirect Gas diffusion layer modifications and treatments for improving the performance of proton exchange membrane fuel cells and electrolysers : A review. International Journal of Hydrogen Energy 2017:1–22. https://doi.org/10.1016/j.ijhydene.2017.09.132.

[107] Wargo EA, Schulz VP, Çeçen A, Kalidindi SR, Kumbur EC. Resolving macro- and micro-porous layer interaction in polymer electrolyte fuel cells using focused ion beam and X-ray computed tomography. Electrochimica Acta 2013;87:201–12. https://doi.org/10.1016/j.electacta.2012.09.008.

[108] Hiramitsu Y, Sato H, Hori M. Prevention of the water flooding by micronizing the pore structure of gas diffusion layer for polymer electrolyte fuel cell. Journal of Power Sources 2010;195:5543–9. https://doi.org/10.1016/j.jpowsour.2010.03.039.

[109] Passalacqua E, Squadrito G, Lufrano F, Patti A, Giorgi L, Conversion EE. E € ects of the di € usion layer characteristics on the performance of polymer electrolyte fuel cell electrodes 2001:449–54.

[110] Zhan Z, Xiao J, Li D, Pan M, Yuan R. Effects of porosity distribution variation on the liquid water flux through gas diffusion layers of PEM fuel cells 2006;160:1041–8. https://doi.org/10.1016/j.jpowsour.2006.02.060.

[111] Kannan AM, Cindrella L, Munukutla L. Functionally graded nano-porous gas diffusion layer for proton exchange membrane fuel cells under low relative humidity conditions. Electrochimica Acta 2008;53:2416–22. https://doi.org/10.1016/j.electacta.2007.10.013.

[112] Chen F, Chang M, Hsieh P. Two-phase transport in the cathode gas diffusion layer of PEM fuel cell with a gradient in porosity 2008;33:2525–9. https://doi.org/10.1016/j.ijhydene.2008.02.077.

[113] Feser JP, Prasad AK, Advani SG. On the relative influence of convection in serpentine flow fields of PEM fuel cells 2006;161:404–12. https://doi.org/10.1016/j.jpowsour.2006.04.129.

[114] Ismail MS, Hughes KJ, Ingham DB, Ma L, Pourkashanian M. Effect of PTFE loading of gas diffusion layers on the performance of proton exchange membrane fuel cells running at high-ef fi ciency operating conditions 2013:1592–9. https://doi.org/10.1002/er.

[115] Lufrano F, Passalacqua E, Squadrito G, Patti A, Giorgi L, Casaccia CR, et al. Improvement in the di € usion characteristics of low Pt-loaded electrodes for PEFCs 1999:445–8.

[116] Giorgi L, Antolini E, Pozio A, Passalacqua E, Casaccia CR, Anguillarese V, et al. In ¯ uence of the PTFE content in the di € usion layer of low-Pt loading electrodes for polymer electrolyte fuel cells 1998;43:3675–80.

[117] Park SB, Kim S, Park Y Il, Oh MH. Fabrication of GDL microporous layer using PVDF for PEMFCs. Journal of Physics: Conference Series 2009;165:1–4. https://doi.org/10.1088/1742-6596/165/1/012046.

[118] Jordan LR, Shukla AK, Behrsing T, Avery NR, Muddle BC, Forsyth M. Diffusion layer parameters influencing optimal fuel cell performance 2000:250–4.

[119] Antolini E, Passos RR, Ticianelli EA. Effects of the carbon powder characteristics in the cathode gas diffusion layer on the performance of polymer electrolyte fuel cells 2002;109:477–82.

[120] Park S, Popov BN. Effect of cathode GDL characteristics on mass transport in PEM fuel cells. Fuel 2009;88:2068–73. https://doi.org/10.1016/j.fuel.2009.06.020.

[121] Meng H, Wang C. Electron Transport in PEFCs 2004:358–67. https://doi.org/10.1149/1.1641036.

[122] Gamburzev S, Appleby AJ. Recent progress in performance improvement of the proton exchange membrane fuel cell (PEMFC) 2002;107:5–12.

[123] Bruchi F, Srinivasan S. Operating Proton Exchange Membrane Fuel Cells Without External Humidification of the Reactant Gases Fundamental Aspects. Journal of Electrochemical Society 1997;144:2767–72.

[124] Zhou T, Liu H. Effects of the electrical resistances of the GDL in a PEM fuel cell. Journal of Power Sources 2006;161:444–53. https://doi.org/10.1016/j.jpowsour.2006.04.106.

[125] Mishra V, Yang F, Pitchumani R. Measurement and Prediction of Electrical Contact Resistance Between Gas Diffusion Layers and Bipolar Plate for Applications to PEM Fuel Cells. Transactions of the ASME 2004;1:2–9. https://doi.org/10.1115/1.1782917.

[126] Radhakrishnan V, Haridoss P. Effect of cyclic compression on structure and properties of a Gas Diffusion Layer used in PEM fuel cells. International Journal of Hydrogen Energy 2010;35:11107–18.

https://doi.org/10.1016/j.ijhydene.2010.07.009.

[127] Stuckey PA, Lin JF, Kannan AM. Gas Diffusion Layers for Proton Exchange Membrane Fuel Cells Using In situ Modified Carbon Papers with Multi-walled Carbon Nanotubes Nanoforest 2010:369–74. https://doi.org/10.1002/fuce.200900141.

[128] Wilson M, Gottesfeld S. Thin-film catalyst layers for polymer electrolyte fuel cell electrodes. Journal of Applied Electrochemistry 1992;22:1–7.

[129] Athanasaki G, Wang Q, Shi X, Chauhan N, Vimala V. ScienceDirect Design and development of gas diffusion layers with pore forming agent for proton exchange membrane fuel cells at various relative humidity conditions. International Journal of Hydrogen Energy 2020;46:6835–44. https://doi.org/10.1016/j.ijhydene.2020.11.187.

[130] Chun JH, Jo DH, Kim SG, Park SH, Lee CH, Kim SH. Improvement of the mechanical durability of micro porous layer in a proton exchange membrane fuel cell by elimination of surface cracks. Renewable Energy 2012;48:35–41. https://doi.org/10.1016/j.renene.2012.04.011.

[131] Kandlikar SG, Lu Z, Lin TY, Cooke D, Daino M. Uneven gas diffusion layer intrusion in gas channel arrays of proton exchange membrane fuel cell and its effects on flow distribution 2009;194:328–37. https://doi.org/10.1016/j.jpowsour.2009.05.019.

[132] Nitta I, Hottinen T, Himanen O, Mikkola M. Inhomogeneous compression of PEMFC gas diffusion layer Part I . Experimental 2007;171:26–36. https://doi.org/10.1016/j.jpowsour.2006.11.018.

[133] Hiramitsu Y, Sato H, Hosomi H, Aoki Y, Harada T, Sakiyama Y, et al. Influence of humidification on deterioration of gas diffusivity in catalyst layer on polymer electrolyte fuel cell. Journal of Power Sources 2010;195:435–44. https://doi.org/10.1016/j.jpowsour.2009.07.035.

[134] Wood DL, Borup RL. during Long-Term PEMFC Operation 2010. https://doi.org/10.1149/1.3454740.

[135] Bosomoiu M, Tsotridis G, Bednarek T. Study of effective transport properties of fresh and aged gas diffusion layers. Journal of Power Sources 2015;285:568–79. https://doi.org/10.1016/j.jpowsour.2015.03.132.

[136] Arif M, Cheung SCP, Andrews J, Andrews J. fuel cells : A simulation study supported by experiment . the gas diffusion layer on mass transport losses in PEM fuel cells : A simulation study supported 2020. https://doi.org/10.1021/acs.energyfuels.0c02596.

[137] Ha T, Cho J, Park J, Min K, Kim H, Lee E, et al. Experimental study on carbon

corrosion of the gas diffusion layer in polymer electrolyte membrane fuel cells. International Journal of Hydrogen Energy 2011;36:12436–43. https://doi.org/10.1016/j.ijhydene.2011.06.098.

[138] Thomas A, Maranzana G, Didierjean S, Dillet J, Lottin O. ScienceDirect Thermal and water transfer in PEMFCs : Investigating the role of the microporous layer. International Journal of Hydrogen Energy 2014;39:2649–58. https://doi.org/10.1016/j.ijhydene.2013.11.105.

[139] Lapicque F, Belhadj M, Bonnet C, Thomas Y. Review article A critical review on gas diffusion micro and macroporous layers degradations for improved membrane fuel cell durability 2016;336:40–53. https://doi.org/10.1016/j.jpowsour.2016.10.037.

[140] Yuan XZ, Li H, Zhang S, Martin J, Wang H. A review of polymer electrolyte membrane fuel cell durability test protocols. Journal of Power Sources 2011;196:9107–16. https://doi.org/10.1016/j.jpowsour.2011.07.082.

[141] Wang A, Liu W, Ren N, Zhou J, Cheng S. Key factors affecting microbial anode potential in a microbial electrolysis cell for H2 production. International Journal of Hydrogen Energy 2010;35:13481–7. https://doi.org/10.1016/j.ijhydene.2009.11.125.

[142] Lim SJ, Park GG, Park JS, Sohn YJ, Yim SD, Yang TH, et al. Investigation of freeze/thaw durability in polymer electrolyte fuel cells. International Journal of Hydrogen Energy 2010;35:13111–7. https://doi.org/10.1016/j.ijhydene.2010.04.079.

[143] Kim S, Mench MM. Physical degradation of membrane electrode assemblies undergoing freeze/thaw cycling: Micro-structure effects. Journal of Power Sources 2007;174:206–20. https://doi.org/10.1016/j.jpowsour.2007.08.111.

[144] Wu J, Yuan XZ, Martin JJ, Wang H, Yang D, Qiao J, et al. Proton exchange membrane fuel cell degradation under close to open-circuit conditions. Part I: In situ diagnosis. Journal of Power Sources 2010;195:1171–6. https://doi.org/10.1016/j.jpowsour.2009.08.095.

[145] Cho J, Ha T, Park J, Kim H, Min K, Lee E, et al. Analysis of transient response of a unit proton-exchange membrane fuel cell with a degraded gas diffusion layer. International Journal of Hydrogen Energy 2011;36:6090–8. https://doi.org/10.1016/j.ijhydene.2011.02.060.

[146] Chen G, Zhang H, Ma H, Zhong H. Electrochemical durability of gas diffusion layer under simulated proton exchange membrane fuel cell conditions. International Journal of Hydrogen Energy 2009;34:8185–92. https://doi.org/10.1016/j.ijhydene.2009.07.085.

[147] Park J, Oh H, Ha T, Lee Y Il, Min K. A review of the gas diffusion layer in proton

exchange membrane fuel cells: Durability and degradation. Applied Energy 2015;155:866–80. https://doi.org/10.1016/j.apenergy.2015.06.068.

[148] Reiser CA, Bregoli L, Patterson TW, Yi JS, Yang JD, Perry ML, et al. A reverse-current decay mechanism for fuel cells. Electrochemical and Solid-State Letters 2005;8:273–6. https://doi.org/10.1149/1.1896466.

[149] Wong KH, Kjeang E. Macroscopic In-Situ Modeling of Chemical Membrane Degradation in Polymer Electrolyte Fuel Cells. Journal of The Electrochemical Society 2014;161:F823–32. https://doi.org/10.1149/2.0031409jes.

[150] Katzel J, Arlt T, Klages M, Hausmann J, Markotter H, Messerschmidt M, et al. Effect of ageing of gas diffusion layers on the water distribution in fl ow fi eld channels of polymer electrolyte membrane fuel cells. Journal of Power Sources 2016;301:386–91. https://doi.org/10.1016/j.jpowsour.2015.10.004.

[151] Arlt T, Klages M, Messerschmidt M, Scholta J. In fl uence of arti fi cially aged gas diffusion layers on the water management of polymer electrolyte membrane fuel cells analyzed with in-operando synchrotron imaging. Energy 2016. https://doi.org/10.1016/j.energy.2016.10.061.

[152] Liu W, Zuckerbrod D. DETECTION OF HYDROGEN PEROXIDE IN PEM FUEL CELLS. The Electrochemical Society 2004;502:492–502. https://doi.org/10.1149/200421.0492PV.

[153] Fairweather J, Mukundan R, Fenton J, Borup R. In Situ and Ex Situ Characterization of Carbon Corrosion in PEMFCs. ECS Transactions 2010;33:433–46.

[154] Spernjak D, Fairweather J, Mukundan R, Rockward T, Borup RL. In fl uence of the microporous layer on carbon corrosion in the catalyst layer of a polymer electrolyte membrane fuel cell. Journal of Power Sources 2012;214:386–98. https://doi.org/10.1016/j.jpowsour.2012.04.086.

[155] Zhan Z, Xiao J, Zhang Y, Pan M, Yuan R. Gas diffusion through differently structured gas diffusion layers of PEM fuel cells 2007;32:4443–51. https://doi.org/10.1016/j.ijhydene.2007.03.041.

[156] Lee HK, Park JH, Kim DY, Lee TH. A study on the characteristics of the diffusion layer thickness and porosity of the PEMFC. Journal of Power Sources 2004;131:200–6. https://doi.org/10.1016/j.jpowsour.2003.12.039.

[157] El-Kharouf A, Mason TJ, Brett DJL, Pollet BG. Ex-situ characterisation of gas diffusion layers for proton exchange membrane fuel cells. Journal of Power Sources 2012;218:393–404. https://doi.org/10.1016/j.jpowsour.2012.06.099.

[158] Liu M. In-Situ Characterization of Electrode Reactions in Solid Oxide Fuel Cells. ECS Proceedings Volumes 2003;2003–07:1132–46.

https://doi.org/10.1149/200307.1132pv.

[159] Watt I. The Principles and Practice of Electron Microscopy. vol. 61. 1986. https://doi.org/10.1086/415260.

[160] Huhtamäki T, Tian X, Korhonen JT, Ras RHA. Surface-wetting characterization using contact-angle measurements. Nature Protocols 2018;13:1521–38. https://doi.org/10.1038/s41596-018-0003-z.

[161] Lawrence M, Jiang Y. Porosity, Pore Size Distribution, Micro-structure. 2017. https://doi.org/10.1081/e-ess3-120042734.

[162] Zhang J, Zhang H, Wu J, Zhang J. PEM Fuel Cell Fundamentals. 2013. https://doi.org/10.1016/B978-0-444-53688-4.00001-2.

[163] Mench MM, Wang C, Thynell ST. An Introduction to Fuel Cells and Related Transport Phenomena. 2000.

[164] Sousa R, Gonzalez ER. Mathematical modeling of polymer electrolyte fuel cells. Journal of Power Sources 2005;147:32–45. https://doi.org/10.1016/j.jpowsour.2005.03.191.

[165] Barbir F. Pem Fuel Cells: Theory and Practice (2nd Edition). Elsevier 2012:543.

[166] Kim J, Lee S, Srinivasan S, Chamberlin CE. Modeling of Proton Exchange Membrane Fuel Cell Performance with an Empirical Equation. Journal of The Electrochemical Society 1995;142:2670–4. https://doi.org/10.1149/1.2050072.

[167] Liu J, Yang C, Liu C, Wang F, Song Y. Design of Pore Structure in Gas Diffusion Layers for Oxygen Depolarized Cathode and Their Effect on Activity for Oxygen Reduction Reaction 2014.

[168] Zhang S, Yuan X, Wang H, Me W, Zhu H, Shen J, et al. A review of accelerated stress tests of MEA durability in PEM fuel cells 2009;34:388–404. https://doi.org/10.1016/j.ijhydene.2008.10.012.

[169] Yang Y, Zhou X, Li B, Zhang C. Recent progress of the gas diffusion layer in proton exchange membrane fuel cells: Material and structure designs of microporous layer. International Journal of Hydrogen Energy 2021;46:4259–82. https://doi.org/10.1016/j.ijhydene.2020.10.185.

[170] Liu H, George MG, Messerschmidt M, Zeis R, Kramer D, Scholta J, et al. Accelerated Degradation of Polymer Electrolyte Membrane Fuel Cell Gas Diffusion Layers I . Methodology and Surface Characterization 2017;164:0–8. https://doi.org/10.1149/2.0071707jes.

[171] Rodney L, Alan D. Carbon Corrosion in PEM Fuel Cells during Drive Cycle Operation. ECS Transactions 2016;25325.

[172] Passalacqua E, Lufrano F, Squadrito G, Patti A, Giorgi L. Nafion content in the catalyst layer of polymer electrolyte fuel cells : effects on structure and performance 2001;46:799–805.

[173] Lin JH, Chen WH, Su SH, Su YJ, Ko TH. Washing experiment of the gas diffusion layer in a proton-exchange membrane fuel cell. Energy and Fuels 2008;22:2533–8. https://doi.org/10.1021/ef800116c.

[174] Lin G, Van Nguyen T. Effect of thickness and hydrophobic polymer content of the gas diffusion layer on electrode flooding level in a PEMFC. Journal of the Electrochemical Society 2005;152. https://doi.org/10.1149/1.2006487.

[175] Pasaogullari U, Wang CY. Liquid Water Transport in Gas Diffusion Layer of Polymer Electrolyte Fuel Cells. Journal of The Electrochemical Society 2004;151:A399. https://doi.org/10.1149/1.1646148.

[176] Wang XL, Zhang HM, Zhang JL, Xu HF, Tian ZQ, Chen J, et al. Micro-porous layer with composite carbon black for PEM fuel cells 2006;51:4909–15. https://doi.org/10.1016/j.electacta.2006.01.048.

[177] Lobato J, Cañizares P, Rodrigo MA, Úbeda D, Pinar FJ, Linares JJ. Optimisation of the Microporous Layer for a Polybenzimidazole-Based High Temperature PEMFC – Effect of Carbon Content 2010:770–7. https://doi.org/10.1002/fuce.200900175.

[178] Nanadegani FS, Lay EN, Sunden B. Effects of an MPL on water and thermal management in a PEMFC. International Journal of Energy Research 2019;43:274–96. https://doi.org/10.1002/er.4262.

[179] Larbi B, Alimi W, Chouikh R, Guizani A. Effect of porosity and pressure on the PEM fuel cell performance. International Journal of Hydrogen Energy 2012;38:8542–9. https://doi.org/10.1016/j.ijhydene.2012.11.022.

[180] Passalacqua E, Squadrito G, Lufrano F, Patti A, Giorgi L. Effects of the diffusion layer characteristics on the performance of polymer electrolyte fuel cell electrodes. Journal of Applied Electrochemistry 2001;31:449–54. https://doi.org/10.1023/A:1017547112282.

[181] U.S. Department of Energy. DoE Procedures For Performing PEM Single Cell Testing 2009:70.

[182] Shen Q, Hou M, Yan X, Liang D, Zang Z, Hao L, et al. The voltage characteristics of proton exchange membrane fuel cell (PEMFC) under steady and transient states. Journal of Power Sources 2008;179:292–6. https://doi.org/10.1016/j.jpowsour.2007.12.049.

[183] Kannan AM, Menghal A, Barsukov I V. Gas diffusion layer using a new type of graphitized nano-carbon PUREBLACK® for proton exchange membrane fuel

cells. Electrochemistry Communications 2006;8:887–91. https://doi.org/10.1016/j.elecom.2006.03.041.

[184] Owejan JE, Yu PT, Makharia R. Mitigation of Carbon Corrosion in Microporous Layers in PEM Fuel Cells. ECS Transactions 2019;11:1049–57. https://doi.org/10.1149/1.2781018.

[185] Young AP, Stumper J, Gyenge E. Characterizing the Structural Degradation in a PEMFC Cathode Catalyst Layer: Carbon Corrosion. Journal of The Electrochemical Society 2009;156:B913. https://doi.org/10.1149/1.3139963.

[186] Stevens DA, Hicks MT, Haugen GM, Dahn JR. Ex Situ and In Situ Stability Studies of PEMFC Catalysts. Journal of The Electrochemical Society 2005;152:A2309. https://doi.org/10.1149/1.2097361.

[187] Ball SC, Hudson SL, Thompsett D, Theobald B. An investigation into factors affecting the stability of carbons and carbon supported platinum and platinum/cobalt alloy catalysts during 1.2 V potentiostatic hold regimes at a range of temperatures. Journal of Power Sources 2007;171:18–25. https://doi.org/10.1016/j.jpowsour.2006.11.004.

[188] Babu SK, Brien TO, Workman MJ, Wilson M, Borup R. Editors ' Choice — Diffusion Media for Cation Contaminant Transport Suppression into Fuel Cell Electrodes Editors ' Choice — Diffusion Media for Cation Contaminant Transport Suppression into Fuel Cell Electrodes 2021. https://doi.org/10.1149/1945-7111/abde82.

[189] Noto H, Kondo M, Otake Y, Kato M. Development of fuel cell hybrid vehicle by Toyota -durability-. SAE Technical Papers 2009. https://doi.org/10.4271/2009-01-1002.

[190] Spernjak D, Fairweather J, Mukundan R, Rockward T, Borup RL. Influence of the microporous layer on carbon corrosion in the catalyst layer of a polymer electrolyte membrane fuel cell. Journal of Power Sources 2012;214:386–98. https://doi.org/10.1016/j.jpowsour.2012.04.086.

[191] Decker EL, Frank B, Suo Y, Garoff S. Physics of contact angle measurement. Colloids and Surfaces 1999;156:177–89.

[192] Lin F, Li D, Neumann W. Effect of Surface Roughness on the Dependence of Contact Angles on Drop Size. Journal of Colloid and Interface Science 1993;159:86–95.

[193] Antolini E. Formation, microstructural characteristics and stability of carbon supported platinum catalysts for low temperature fuel cells. Journal of Materials Science 2003;38:2995–3005. https://doi.org/10.1023/A:1024771618027.

[194] Kangasniemi KH, Electrochem J, Soc E, Kangasniemi KH, Condit DA, Jarvi TD.

Characterization of Vulcan Electrochemically Oxidized under Simulated PEM Fuel Cell Conditions Characterization of Vulcan Electrochemically Oxidized under Simulated PEM Fuel Cell Conditions 2004. https://doi.org/10.1149/1.1649756.

[195] Gruver GA. The Corrosion of Carbon Black in Phosphoric Acid 1974;1:1719–20.

[196] Wood D, Borup RL. Durability Aspects of Gas-Diffusion and Microporous Layers. Polymer Electrolyte Fuel Cell Durability, 2009, p. 159–95.

[197] Wood D, Davey J, Atanassov P, Borup R. PEMFC Component Characterization and Its Relationship to Mass-Transport Overpotentials during Long-Term Testing. ECS Transactions 2006;3:753–63. https://doi.org/10.1149/ma2006-02/8/641.

[198] Auer E, Freund A, Pietsch J, Tacke T. Carbons as supports for industrial precious metal catalysts. Applied Catalysis A: General 1998;173:259–71. https://doi.org/10.1016/S0926-860X(98)00184-7.

[199] Barsukov I V, Gallego MA, Doninger JE. Novel materials for electrochemical power sources — introduction of 2006;153:288–99. https://doi.org/10.1016/j.jpowsour.2005.05.077.

[200] Maass S, Finsterwalder F, Frank G, Hartmann R, Merten C. Carbon support oxidation in PEM fuel cell cathodes. Journal of Power Sources 2008;176:444–51. https://doi.org/10.1016/j.jpowsour.2007.08.053.

[201] Yu HM, Ziegler C, Oszcipok M, Zobel M, Hebling C. Hydrophilicity and hydrophobicity study of catalyst layers in proton exchange membrane fuel cells. Electrochimica Acta 2006;51:1199–207. https://doi.org/10.1016/j.electacta.2005.06.036.

[202] Lee C, Walter M. Gas diffusion layer durability under steady-state and freezing conditions. Journal of Power Sources 2007;164:141–53. https://doi.org/10.1016/j.jpowsour.2006.09.092.

[203] Owejan JE, Makharia R. Mitigation of Carbon Corrosion in Microporous Layers in PEM Fuel Cells. The Electrochemical Society 2007;11:1049–57.

[204] Zhang X, Yang Y, Zhang X, Guo L, Liu H. INCREASE OF MASS TRANSPORT LOSS IN POROUS MEDIA CAUSED BY CARBON CORROSION IN PEM FUEL 2018:9–11.

[205] Liu H, Soc JE, Liu H, George MG, Messerschmidt M, Zeis R. Accelerated Degradation of Polymer Electrolyte Membrane Fuel Cell Gas Diffusion Layers Cell Gas Diffusion Layers. Journal of Electrochemical Society 2017;164:F695–703. https://doi.org/10.1149/2.0071707jes.

[206] George MG, Liu H, Muirhead D, Banerjee R, Ge N, Shrestha P, et al. Accelerated Degradation of Polymer Electrolyte Membrane Fuel Cell Gas Diffusion Layers.

Journal of The Electrochemical Society 2017;164:F714–21. https://doi.org/10.1149/2.0091707jes.

[207] Baek SM, Koh SG, Kim KN, Kang JH, Nam JH, Kim CJ. A numerical study on the performance of polymer electrolyte membrane fuel cells due to the variation in gas diffusion layer permeability. Journal of Mechanical Science and Technology 2011;25:457–67. https://doi.org/10.1007/s12206-010-1229-z.

[208] Oh HS, Lim KH, Roh B, Hwang I, Kim H. Corrosion resistance and sintering effect of carbon supports in polymer electrolyte membrane fuel cells. Electrochimica Acta 2009;54:6515–21. https://doi.org/10.1016/j.electacta.2009.06.028.

[209] Mohanta PK, Regnet F, Jörissen L. Graphitized Carbon: A promising stable cathode catalyst support material for long term PEMFC applications. Materials 2018;11. https://doi.org/10.3390/ma11060907.

APPENDIX A

SAMPLE AND RH SELECTION

I. Sample and RH selection (see section 6.1)

A series of GDL samples with identical carbon substrate and carbon loading of 3 ± 0.15 mg.cm^{-2} were prepared, and their fuel cell performances were evaluated. The MPL configurations are shown in Figure I and the PEG content is summarized in Table A. The MEAs with various GDL samples were evaluated at 50, 60, 80 and 100 % RH conditions. As seen from the Figures II and III, all the samples exhibited identical fuel cell performances at 50, 60 and 80 % RH conditions. Optimum membrane hydration plays an important role on the PEMFC performance and durability. The fuel cell performances of the all the MEAs were lower due to flooding, while sample 2 remained unchanged at 100 % RH, in both H_2/O_2 and H_2/air. Based on the very weak performance of the MEA with the commercial GDL sample at 50 % RH, 60 % RH was selected as the lowest RH value for the fuel cell performance and durability evaluation operation, hence fuel cell performance comparison would be possible under identical operating conditions.

Table A. GDL configurations

GDL Sample	Number of MPL layers	PEG wt%
1	1	0
2	1	30
3	2	(a) 0 and (b) 30
4	2	(a) 20 and (b) 30
5	3	(a) 10, (b) 20 and (c) 30
6	4	(a) 0, (b) 10, (c) 20 and (d) 30
7	1	40

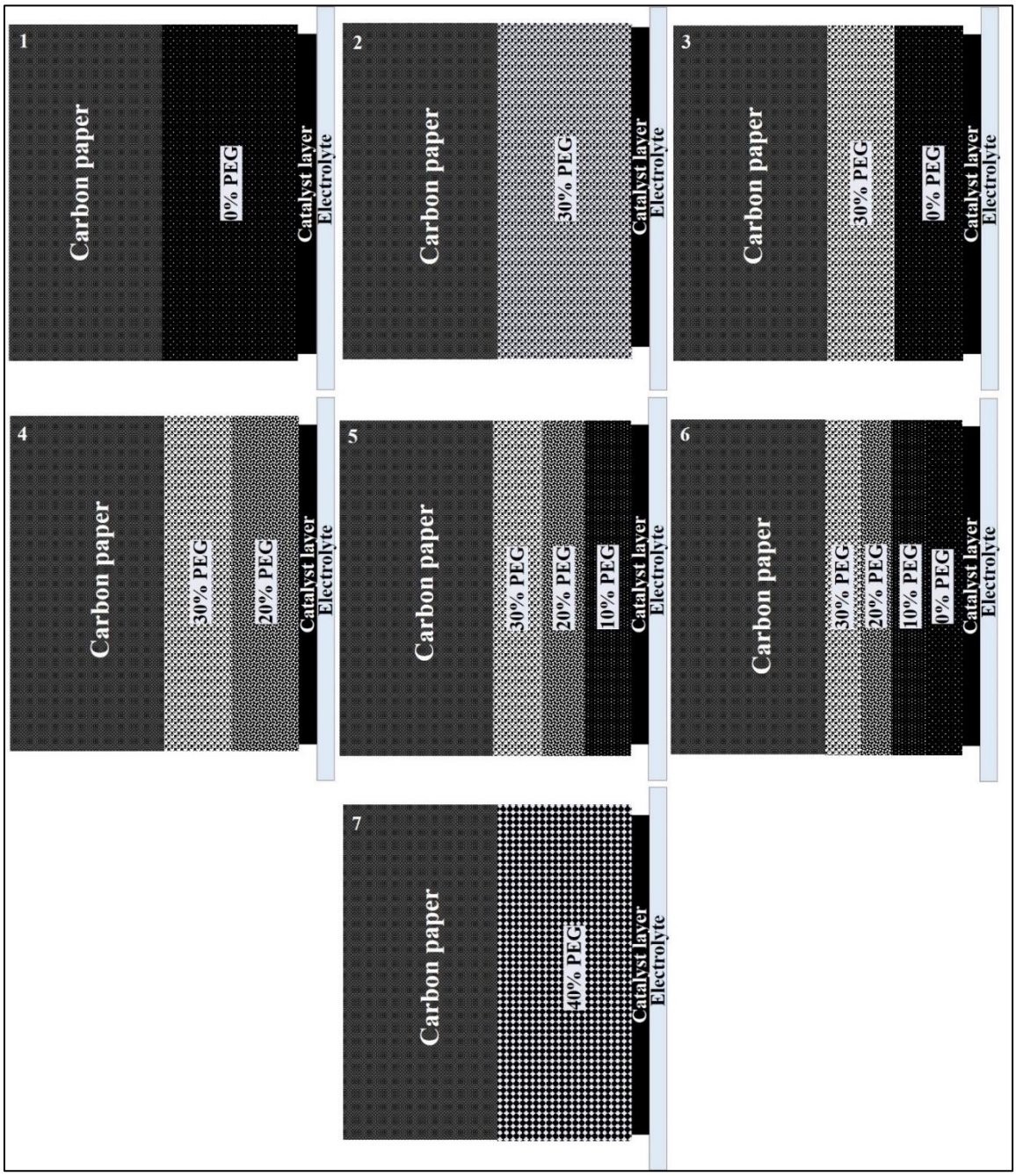

Figure I. Configuration of gas diffusion layer samples 1 - 7.

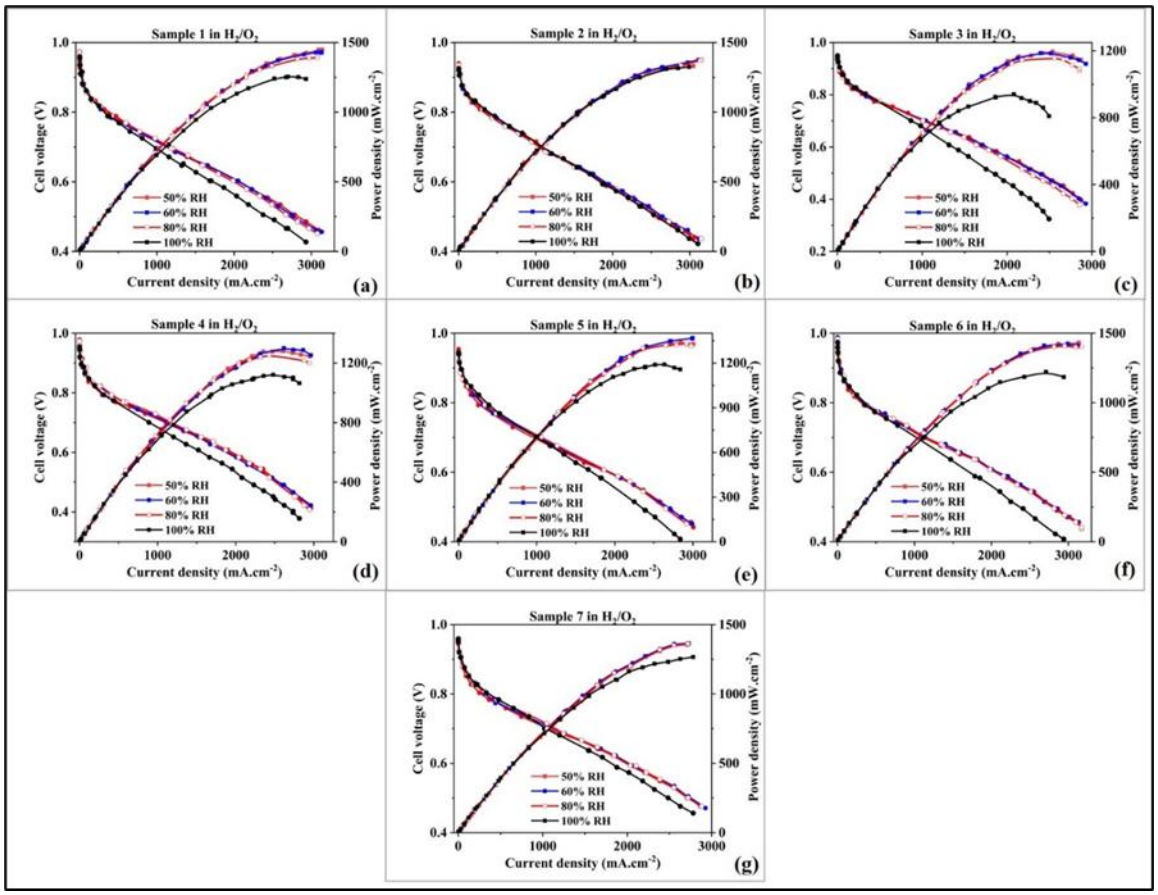

Figure II. Fuel cell performance at 70 ^{o}C in H_2/O_2 for fabricated GDL samples 1-7.

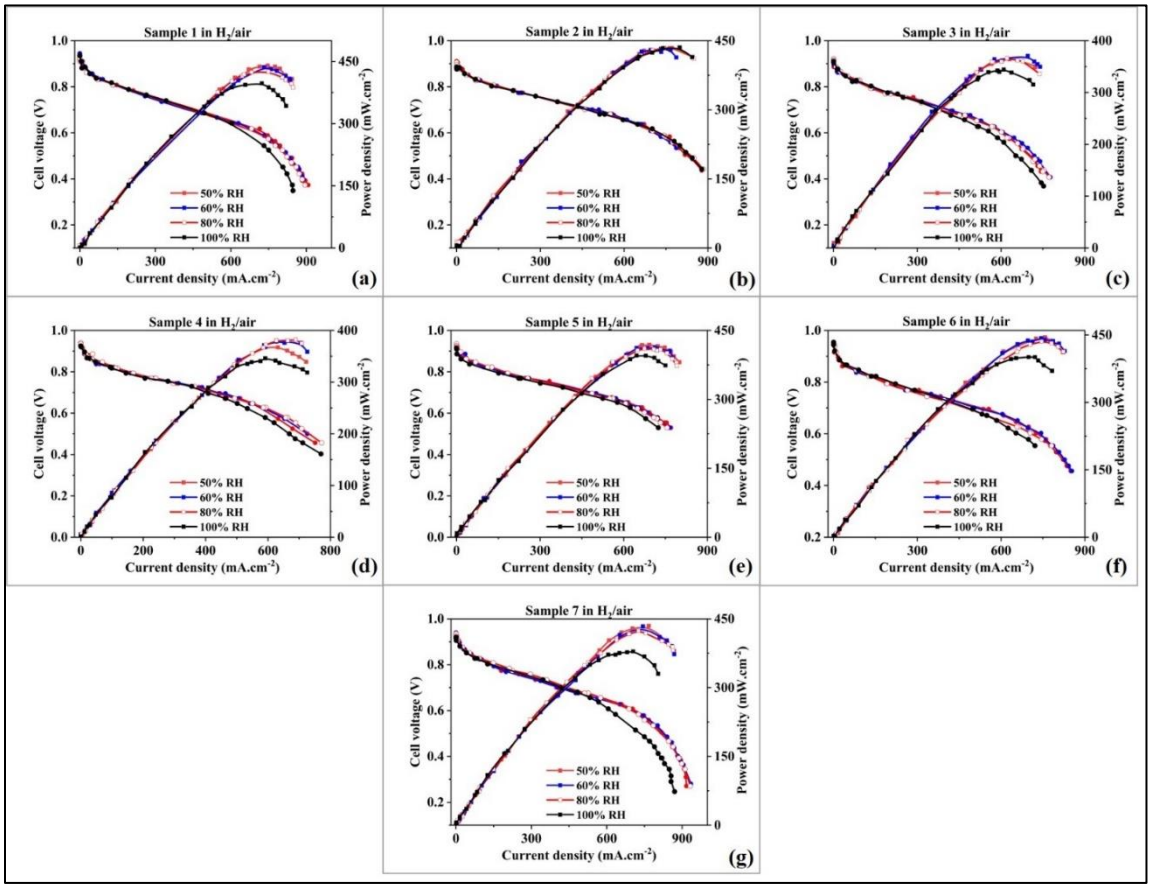

Figure III. Fuel cell performance at 70 ^{o}C in H_2/air for fabricated GDL samples 1-7.

The peak power densities for all fabricated GDLs in H_2/O_2 and H_2/air are shown in Fig IV. The three samples with the highest peak power densities in both H_2/O_2 and H_2/air were selected for further evaluation (samples 1, 2 and 6). The three best performing samples, along with the commercial GDL were characterized for contact angle, pore size distribution, porosity and cross-section and surface morphology and the results are presented in the main thesis (see section 6.1).

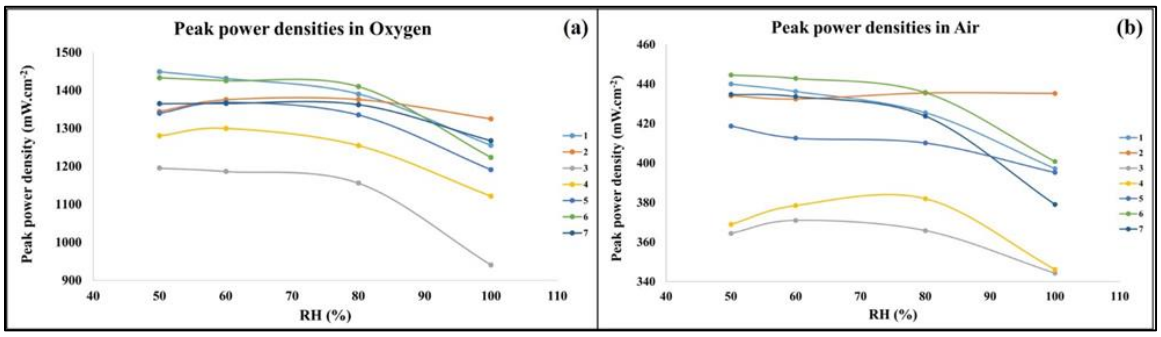

Figure IV. Peak power densities of fabricated GDLs at various RH in (a) H_2/O_2 and (b) H_2/air.

II. Sample selection (see section 6.2)

PUREBLACK® GDL configuration with 30% PEG as pore forming agent demonstrated high and stable performance during fuel cell operation at 70 ^oC at 60 and 100% RH in both H_2/O_2 and H_2/air, hence it was selected for degradation by two methods of accelerated stress tests, with warm water and warm 30% solution of hydrogen peroxide, in order to evaluate the characteristics after degradation and durability of the MPL in water dissolution and carbon corrosive environment. The fuel cell performance and characteristics of the PUREBLACK® GDLs were then compared to VULCAN® with similar configuration (30% PEG) and commercial GDLs, aged in the same conditions. Table B summarizes the GDL samples and time intervals chosen for the ASTs.

Table B. List of samples from ASTs

Carbon	**PUREBLACK® (PB)**		**VULCAN® (VL)**		**Commercial (COM)**	
AST	**Hydrogen Peroxide**	**Water**	**Hydrogen Peroxide**	**Water**	**Hydrogen Peroxide**	**Water**
Time intervals	PB0	PB250	VL0	VL250	COM0	COM250
	PB8	PB500	VL8	VL500	COM8	COM500
	PB16	PB750	VL16	VL750	COM16	COM750
	PB24	PB1000	VL24	VL1000	COM24	COM1000

The fuel cell peak power densities at all time intervals for the PUREBLACK®, VULCAN® and commercial GDL samples are shown in Figures V for water and VI for hydrogen peroxide ASTs using H_2/O_2 and H_2/air, respectively at 60 and 100 % RH.

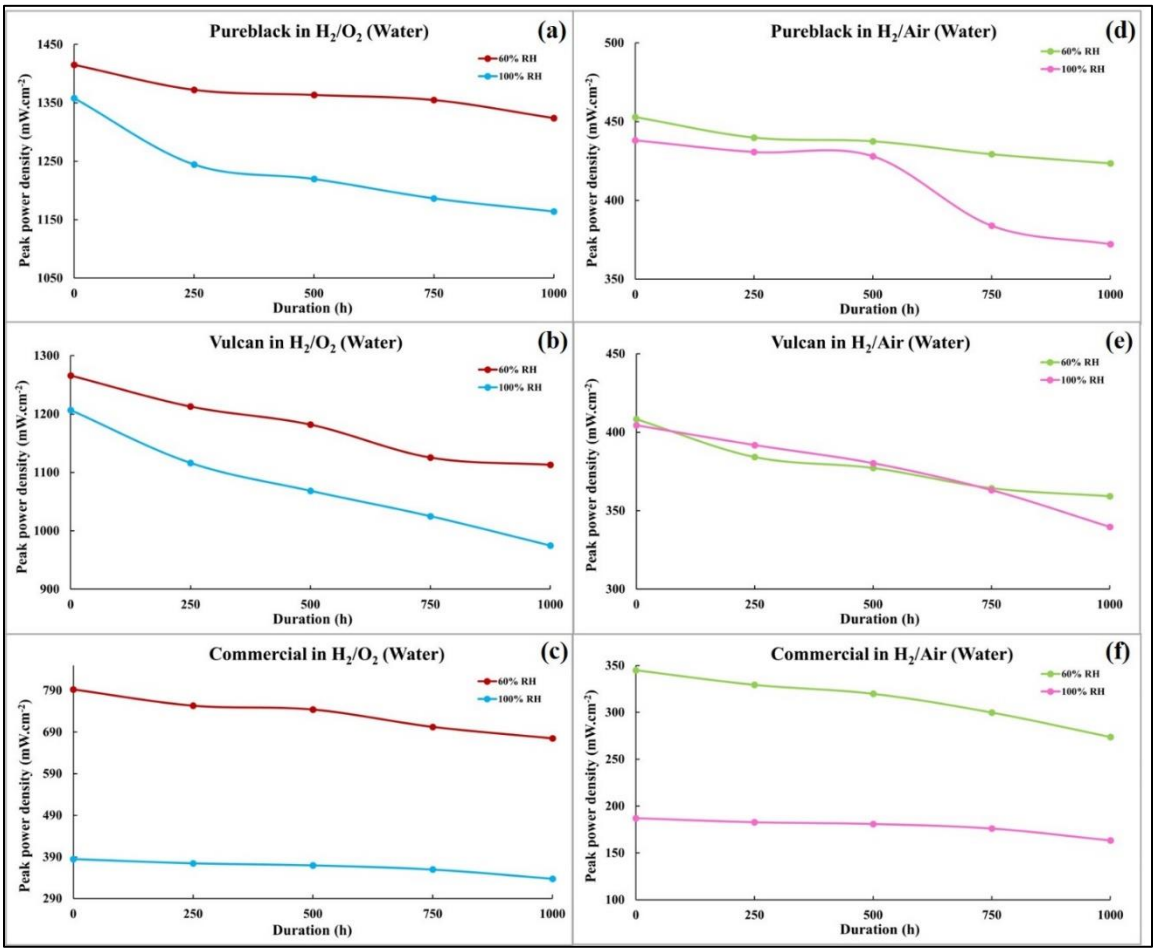

Figure V. Peak power densities for aged samples in water using (a)-(c) H_2/O_2 and (d)-(f) H_2/air.

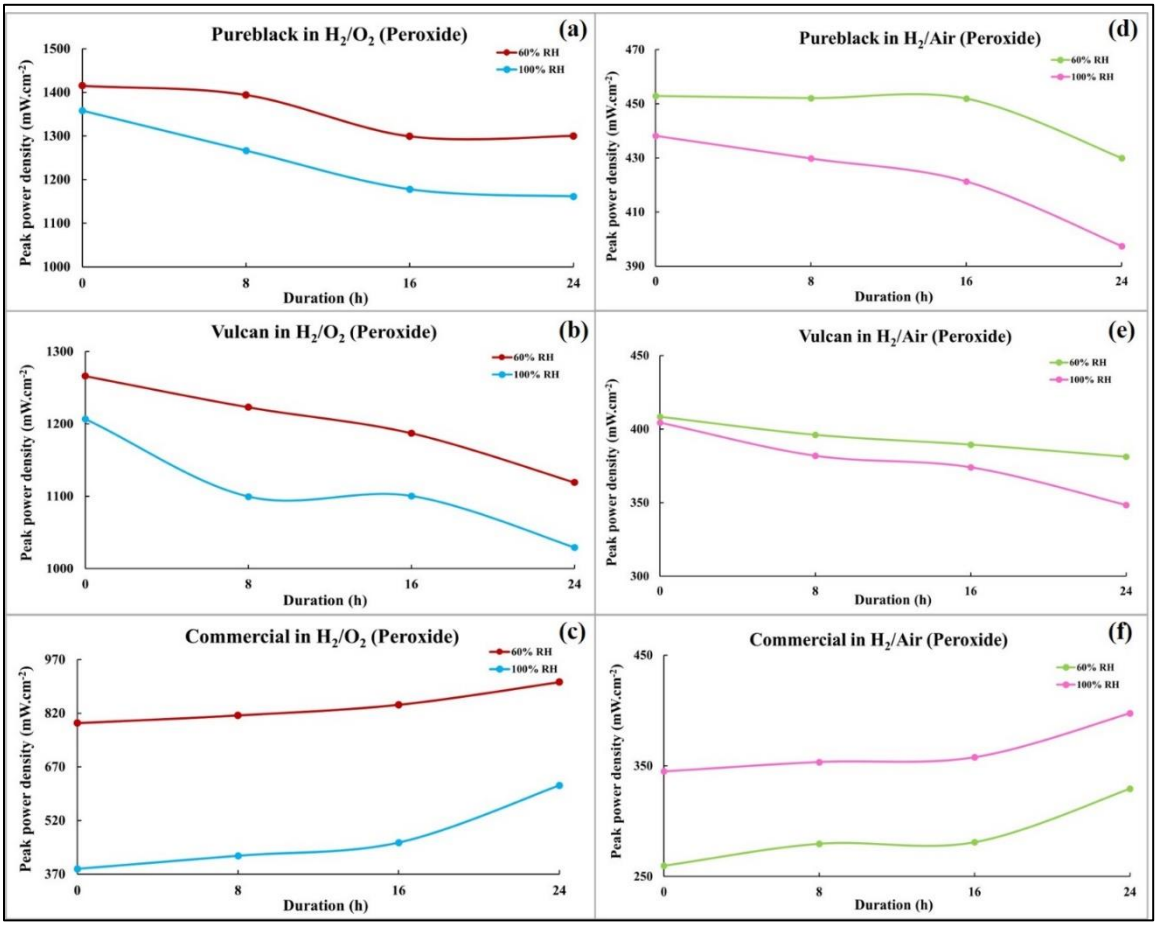

Figure VI. Peak power densities for aged samples in hydrogen peroxide using (a)-(c) H_2/O_2 and (d)-(f) H_2/air.

As seen in Figures V and VI, all the samples demonstrated lower peak power densities due to the carbon corrosive environment of water and hydrogen peroxide. However, the commercial GDLs show an increase in peak power densities, when aged in hydrogen peroxide, which can be attributed to unstable performance due to its weak structural characteristics, hence this sample was rejected.

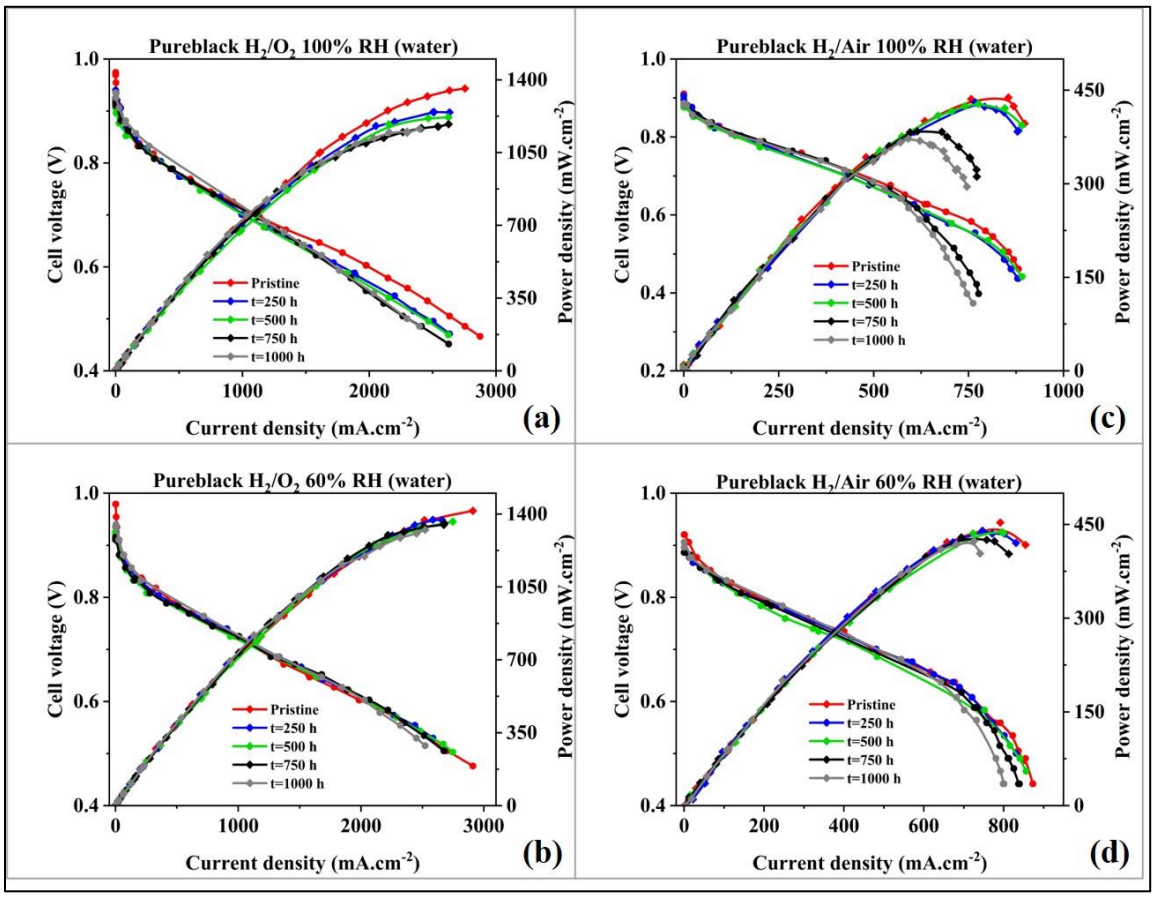

Figure VII. Fuel cell performance for PUREBLACK® GDL aged in water using H_2/O_2 at (a) 100%, (b) 60% RH and H_2/air at (c) 100% and (d) 60% RH.

Figures VII and VIII show the fuel cell performance during the ASTs for PUREBLACK® GDLs. There is a noticeable performance loss when the system is operating at high relative humidity conditions, however this loss is minimized when the RH drops to 60% for both AST methods. Furthermore, it can be seen that the maximum performance loss in both AST methods for PUREBLACK® increases with time (1000 h for water and 24 h for hydrogen peroxide).

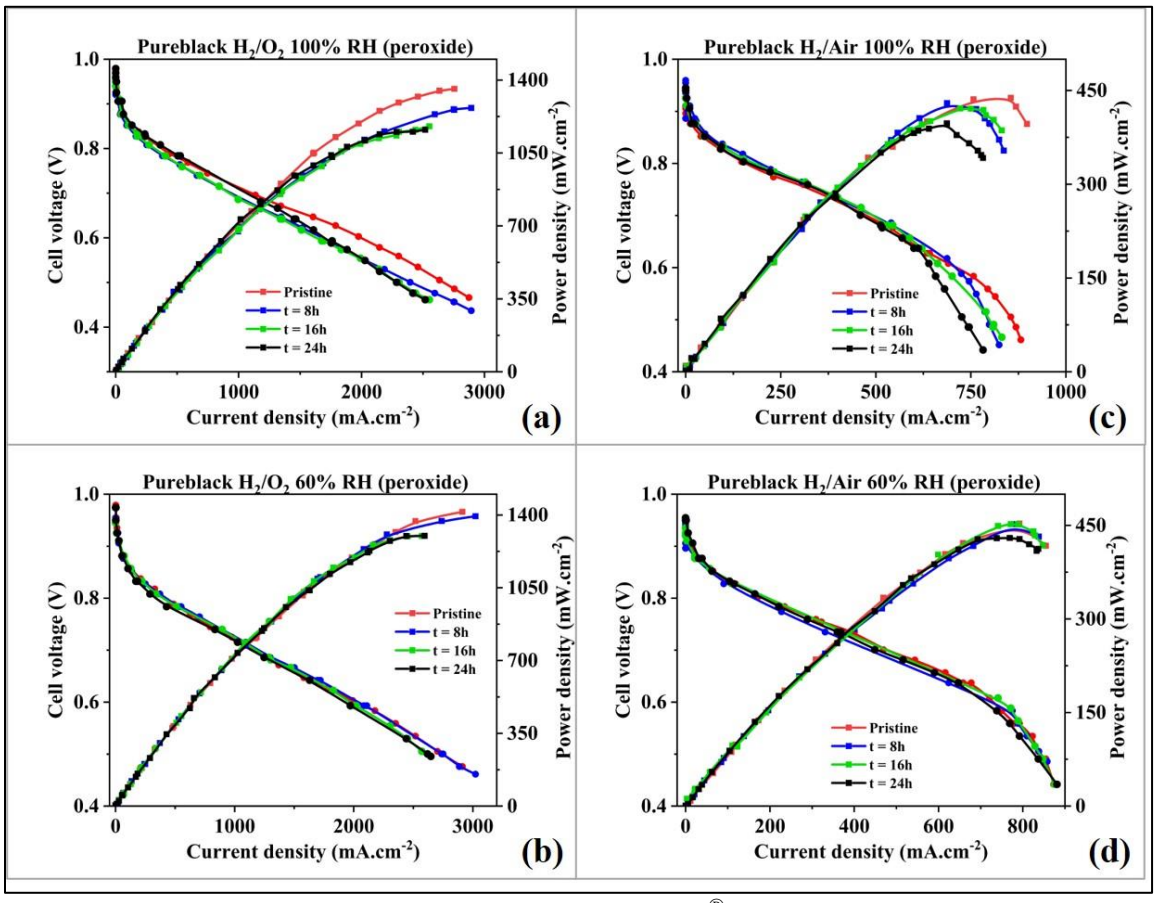

Figure VIII. Fuel cell performance for PUREBLACK® GDL aged in hydrogen peroxide using H_2/O_2 at (a) 100%, (b) 60% RH and H_2/air at (c) 100% and (d) 60% RH.

The corresponding fuel cell performance during ASTs for VULCAN® is shown in Figures IX and X for water and hydrogen peroxide, respectively. Similar to PUREBLACK®, the performance loss in VULCAN® GDLs is greater at high RH conditions and decreases when the RH drops, and the percentage loss is increasing with AST time. However, it appears that the loss of performance in dry conditions for VULCAN® is higher than the PUREBLACK®. Therefore, PUREBLACK® and VULCAN® pristine and most degraded samples in both AST methods (1000 h in water and 24 h in hydrogen peroxide) were selected for further characterization.

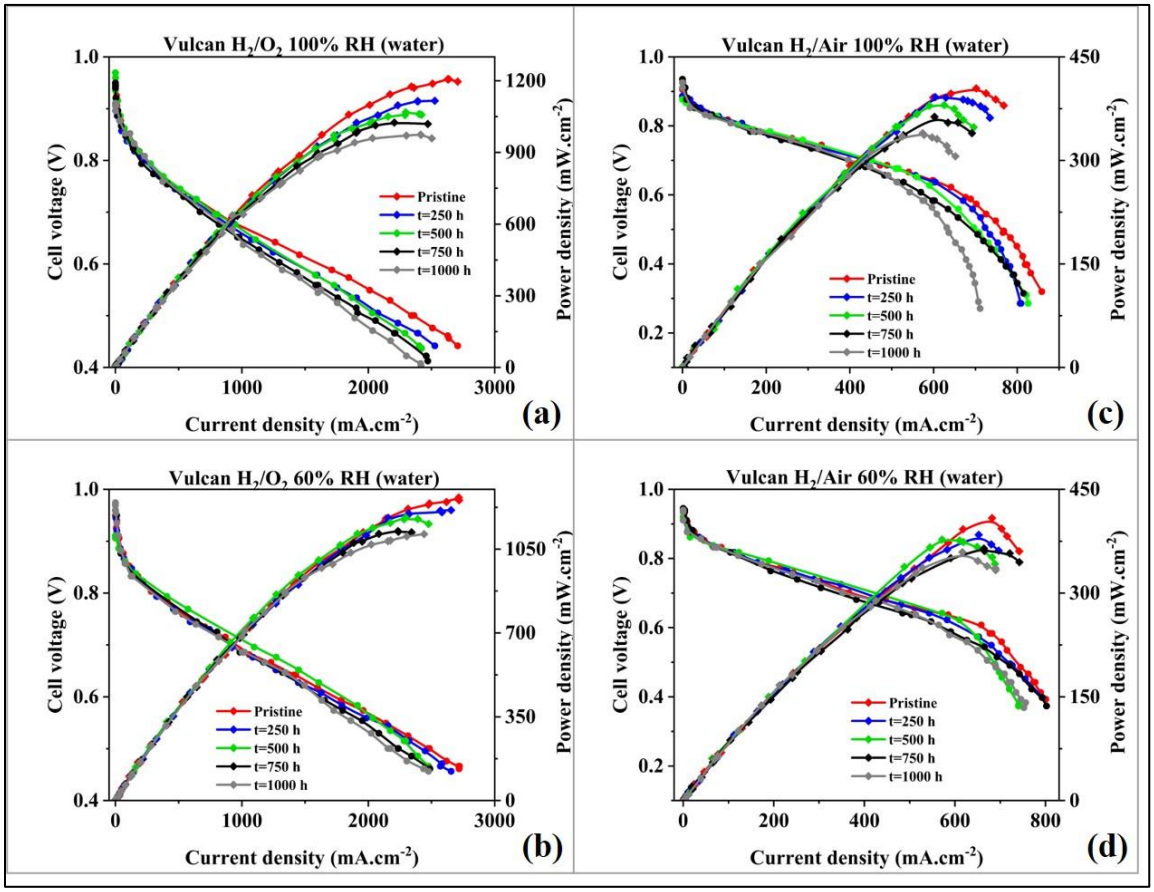

Figure IX. Fuel cell performance for VULCAN® GDL aged in water using H_2/O_2 at (a) 100%, (b) 60% RH and H_2/air at (c) 100% and (d) 60% RH.

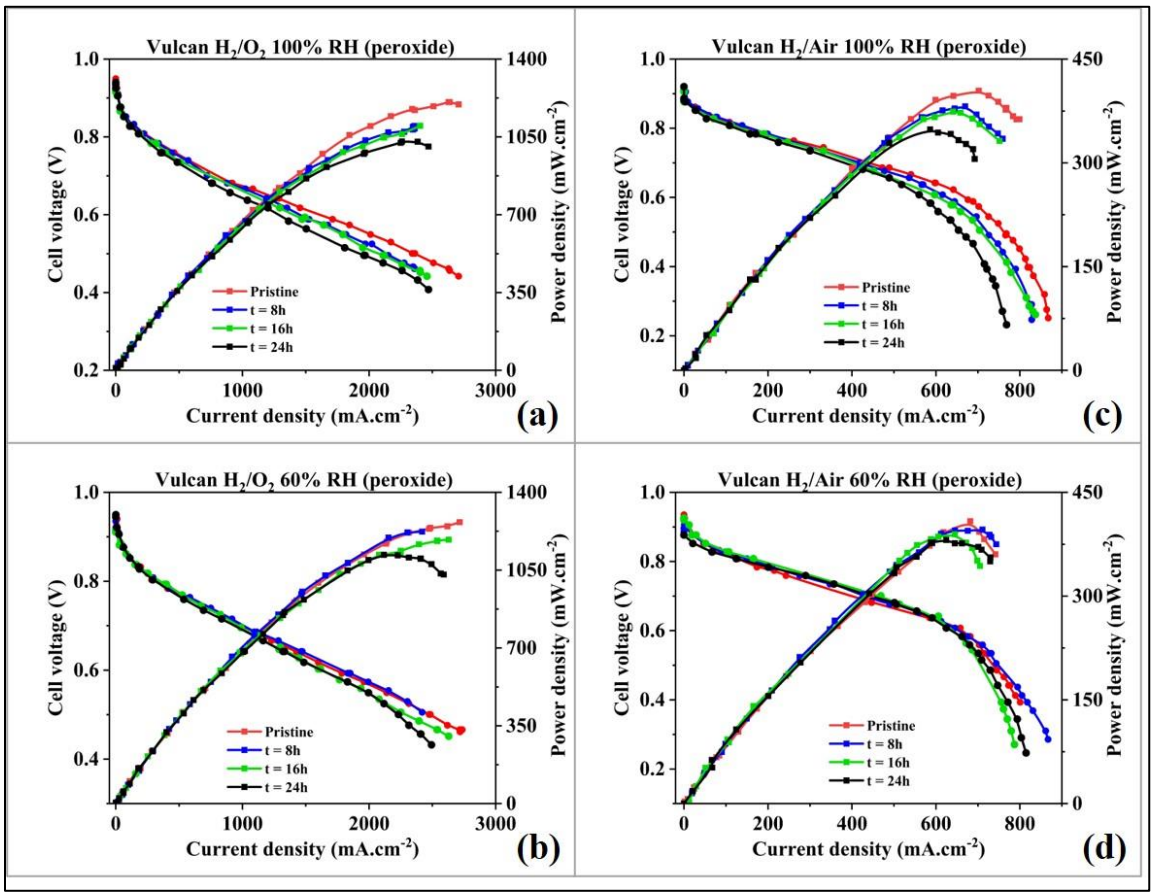

Figure X. Fuel cell performance for VULCAN® GDL aged in hydrogen peroxide using H_2/O_2 at (a) 100%, (b) 60% RH and H_2/air at (c) 100% and (d) 60% RH.